Universidad de **Valladolid**

Escuela Técnica Superior de Ingenieros de Telecomunicación

Tesis de Máster

Máster Universitario en Investigación en Tecnologías de la Información y las Comunicaciones

Fiber consistency measures on brain tracts from digital streamline, stochastic and global tractography

Autor:

Gonzalo Barrio Arranz

Tutor:

Dr. Santiago Aja Fernández

Valladolid, September 11, 2012

Título:	Fiber consistency measures on brain tracts from digital streamline, stochastic and global tractography
Autor:	Gonzalo Barrio Arranz
Tutor:	Dr. Santiago Aja Fernández
Departamento:	LPI

Tribunal

Presidente:	Dr.
Vocal:	Dr.
Secretario:	Dr.

Fecha:	
Calificación:	

Resumen del TFM

La tractografía es el proceso que se emplea para estimar la estructura de las fibras nerviosas del interior del cerebro *in vivo* a partir de datos de Resonancia Magnética (MR). Existen varios métodos de tractografía, que generalmente se dividen en locales y globales. Los primeros intentan reconstruir cada fibra por separado, mientras que los segundos intentan reconstruir todas las estructuras neuronales a la vez, buscando una configuración que mejor se ajusta a los datos proporcionados.

Dichos métodos globales han demostrado ser más precisos y fiables que los métodos de tractografía local, para datos sintéticos. Sin embargo hasta la fecha no hay estudios que definan la relación entre los parámetros de adquisición de la MR y los resultados de tractografía estocástica o global con datos reales.

Esta tésis de Master pretende mostrar la influencia de ciertos parámetros de adquisición como el factor de difusión de las secuencias de adquisición, el espaciado entre voxels o el número de gradientes en la variabilidad de las tractografías obtenidas.

Palabras clave

RM, RMTD, Tractografía, Estocástica, Global, Análisis de Imagen Médica

Abstract

Tractography is the process used to estimate the structure of the nervous fibers in the interior of the brain *in vivo* from magnetic resonance data (MR). There are several methods of tractography, which are usually divided into local and global. The first attempt to reconstruct each fiber separately, while the latter try to reconstruct all the neural structures at the same time, looking for a configuration that best fits the provided data.

Global methods have proven to be more accurate and reliable than local methods for synthetic data.

However to date there are no studies that define the relationship between MR acquisition parameters and the results of stochastic or global tractography with real data.

This Master thesis is intended to show the influence of some parameters of acquisition as the factor of dissemination of sequences of acquisition, the spacing between voxels or the number of gradients in the variability of the obtained tractographies.

Keywords

MRI, DTMRI, Tractography, Stochastic, Global, Medical Image Analysis

Agradecimientos

Gracias a Ola Friman, Marco Reisert y Valeri Kiselev por su código.

Contents

List of Figures

Chapter 1

Introduction

1.1 Basis of MRI and tractography

Magnetic Resonance Imaging (MRI) is a medical imaging technique used to visualize the internal structures of the body *in vivo*. MR images are extremely rich in information due to the great number of parameters that have influence on each voxel value. One of its main features is that we can use it to differentiate between tissue types, and it has been very successfully as a diagnostical tool, but it is not an adequate tool to study the intricacies of the structure of the nervous tissues.

Diffusion Tensor Imaging (DTI) can solve this limitation [1]. DTI is a MRI method that maps the diffusion process of the water molecules, providing information about the diffusion of water at each voxel. Molecular diffusion in tissues is not free, and reflects interactions with many obstacles around it. For example, the neural axons of white matter in the brain or muscle fibers in the heart have an internal fibrous structure. Water will then diffuse more rapidly in the direction parallel to the fibers, and more slowly perpendicular to it, therefore revealing details about tissue architecture, either healthy or diseased.

Some neurological diseases are associated with abnormalities that can be detected an measured with DTI

1.1.1 Basis of DTI mathematical model

Each voxel contains information about the local characteristics of diffusion. Normally, this information is modeled as a 2nd order tensor, using measurements from at least six different directions.

Modeling diffusion as a tensor has certain mathematical advantages, they are rotationally invariant (their values does not change when the coordinate system used to describe them is rotated); the diffusion tensor is positive definite, thus all of its eigenvalues are positive. Each eigenvalue represents the magnitude of diffusion in the direction of the eigenvector associated with that eigenvalue.

The 2nd order tensor can be described as an ellipsoid, whose major and minor axis are formed by the eigenvectors and associated eigenvalues of the tensor. The eigenvector associated with the largest eigenvalue is sometimes referred to as the principal diffusion direction.

1.1.2 Basis of tractography

But the tensor and its eigenvalues and eigenvectors are a multidimensional structure and is not useful to visualize the interior of the brain. A popular technique used to visualize these diffusion tensors is to extract fiber tracts which summarize the diffusion information across many voxels. This technique is known as tractography.

Several methods exist for performing tractography:

- The most common method is to generate fiber tracks that follow the direction of maximal water diffusion of the voxels they pass through. This method is known as streamline tractography[22]. Streamline tractography has relatively low computational cost and is very useful for visualization of DTI data. However, it does not provide information about the uncertainty of the generated tracks, and limits the regions that streamlining tractography can reach as the majority of streamline tractography algorithms stop at highly isotropic regions, where the main direction is not well defined.

- Stochastic tractography [38] provides a measure of confidence of the estimated fiber tracks, by performing tractography under a probabilistic framework. They can generate tracts that momentarily pass through regions of low anisotropy because they integrate local fiber orientation uncertainty into the uncertainty of the entire tract.
- Global tractography methods try to reconstruct the fibers simultaneously by finding the configuration that describes best the measured data. Global tracking promises a better stability with respect to noise and imaging artifacts.
  The fibers are reconstructed from small line segments that get bind together during the optimization phase. Their orientation and number are adjusted simultaneously to match the data.
  The main problem of global methods is a very long computation time, often unacceptable in the clinical setting.

Together, DTI and tractography can help us to study the structure of the brain and to obtain quantitative measures of diffusion within its tissues. They work particularly well in defining and characterizing white matter structures. it exists a growing interest in the last decades in using magnetic resonance diffusion imaging to provide information on anatomical connectivity in the brain by measuring the diffusion of water in white matter tracts. Among the measures, the most commonly derived from diffusion data is fractional anisotropy (FA), which quantifies local tract directionality and integrity.

But while DT-MRI tractography can produce striking images of the brain anatomy, it suffers from a number of problems:

- Brain tractography lacks of a neuroanatomical white matter "gold standard". Currently it does not exist a definitive validation standard for in vivo images.
- Lack of reliability within the same data-set. For many tractography algorithms, specially for the simple streamline methods, their estimations are very dependent on seedpoint placement. Also, there can be differences based on the initialization position. The propagation of fibers through a noisy diffusion tensor field may result in deviation from the true fiber and therefore may lead to erroneous connection estimates. The errors in the diffusion tensor and, consequently, the major eigenvector are an unknown function of the measurement noise, tensor eigenvalues, tensor encoding set, and tensor field geometry. There can be even computer-dependent bias.
- Problems resolving the crossing or meeting of different fiber bundles

In summary, obtaining reliable data and drawing meaningful and robust inferences from them, with diffusion MRI, can be challenging. The effects of the acquisition parameters on the quantifying diffusion indexes, have been profusely studied; some papers such as Wakana et al.[71] have studied the effects of streamline reproducibility intersubjects and intrasession, and Zhan et al.[73] have studied the effects of some acquisition parameters onto streamline connectivity but the effects of the acquisition parameters into the reproducibility of different tractography algorithms have not been properly studied.

1.2 Objectives

One of the ultimate goals for all tractography techniques is to define quantitative and reproducible parameters for measuring anatomical connectivity. The main objective of this Master's thesis is to study the reproducibility of the fiber tracks and the variability created by the acquisition parameters onto the reconstructed fiber tracks for different tractography methods. To evaluate which of the the major technical factors of DTI that affect image quality also have effect in the track results; with a special focus on the b-values, the number and orientations of diffusion-weighted acquisitions, voxel spacing as well as the fiber tracking parameters

1.3 Phases and methods

The following phases are followed for the writing of this Master thesis:

1 Reading literature on the scope of the project; as a contact intake with the properties and essential concepts.

2 Study of existing algorithms currently used in the state-of-the-art tractography.

3 Development of experiments on tractography using those different algorithms and an extensive data set of brain images.

1.4 Structure of this memory

This report has been structured in seven chapters:

- Chapter 2 establishes the basis of our experiments.
- Chapter 3 discusses the theoretical concepts and general ideas behind MRI and the DT-MRI, and gives an state of the art of the the mathematical models used to characterize the diffusion and its use along the main existing tractography methods and algorithms.
- Chapter 4 details the materials and methods used in the experiments, explaining the parameters and configurations employed.
- Chapter 5 explains the additions created for the Saturn software (Software Application of Tensor Utilities for Research in Neuroimaging) specifically for this Master thesis.
- Chapter 6 collects the results obtained for the tractography experiments and discuses them.
- Chapter 7 finally details the conclusions of this work and possible future lines of investigation.

Appendix A contains a publication related to Master thesis. Appendix B and C contains tables with data employed for the experiments.

Chapter 2

Study plan

The objective of this study is to understand how the acquisition parameters of the MR can influence the tractography results. In order to accomplish this, we want to compare tractography reconstructions of different parts of the brain, created with different tractography methods, from several volume data acquired with three combinations of three different acquisition parameters.

In order to compare the tracks, we plan to check two different factors: The count of correctly extracted tracks and the mean profiles extracted from the fibers. There are many potential sources of variation in quantitative DTI parameters. Therefore, is important to be consistent in data acquisition, reconstruction, and processing across subjects in clinical DTI research.

2.1 Objectives for data processing

One of the major sources of variability of the track estimation, in addition to noise and lack of spatial resolution, comes from the fact that fiber tracks have to be started from certain user-selected ROIs to identify specific white matter tracts. This fact can be avoided by seeding every voxel in the entire 3D volume containing the head, and thereby generating all the white matter streamlines in one computation. Then, we can extract specific tracks by using manually placed ROIs and spatial designed filters. This process is known as whole brain tractography.

Whole brain tractography as two main advantages over the more simple user-selected ROI points. First is an automatic process; second, it may find some tracks that are missed by ROI-based seeding; third, the large number of fibers created can compensate small error estimation that accumulates along each step of the tractography and finally it can produce a better balance of streamline density along the delineated tract. On the flip side, it has great requirements of computation time, memory and disk space.

2.1.1 Tractography algorithms

We plan to compare two local tractography algorithms and one global: The streamline tractography proposed by Mori et al.[22], a bayesian probabilistic algorithm implemented by Friman et al.[38]. and a global reconstruction algorithm implemented by Reisert et al.[56].

2.1.2 Profile extraction from fiber tracts

Profiles of each fiber are extracted based from their points, limited from a max distance to a preestablished model. Mean values and standard deviation of the tensor values are computed and stored. Tract based measurements are more robust and reproducible than voxel-wise measures, in both intrasession and intersession measurements, according to Farrel et al.[70]

2.1.3 ROI definition and spatial filtering

After the whole brain tractography we will extract specific tracks of interest by using manually placed ROIs and spatial designed filters. In highly isotropic regions, the main direction is not well defined, and many streamline algorithms will stop the estimation tracts in that zone. Unfortunately, isotropic voxels occur throughout the

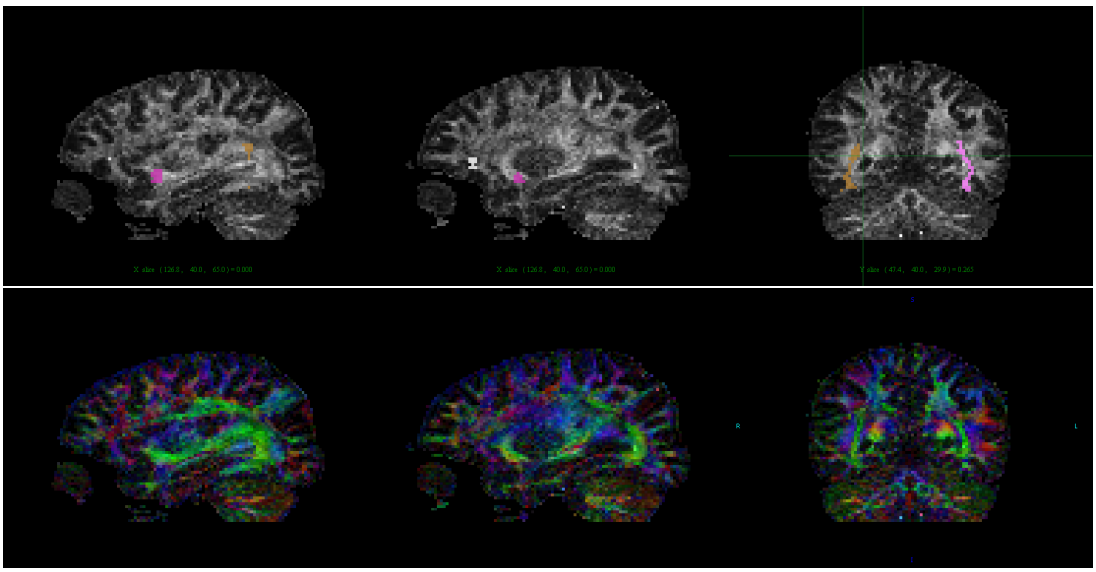

Figure 2.1: ROIs defining IOFF spatial filter.

brain, even in regions with highly coherent fibers, due to noise, distortions in the DTI data or insufficient spatial resolution which result in partial volume effects. To avoid highly isotropic regions, our experiments are centered on highly anisotropic and well known regions of the brain.

For this work, we are interested in four major white matter structures, the Inferior Occipitofrontal Fasciculus (IOFF), the Corpus Callosum (CC), the Cingulum (Cing) and the Corticospinal tract (CST). These are highly studied brain zones, with a high number of connections and a very defined main orientation.

Inferior occipito-frontal fasciculus (ioff)

This white matter structure crosses the brain along the Anterior to Posterior axis. Connects the ipsilateral frontal and occipital lobes; ipsilateral frontal and posterior parietal and temporal lobes; intermingles with uncinate fasciculus. Its main function is the integration of auditory and visual association cortices with prefrontal cortex. It is also related with the language learning.

On the RGB viewer, these fibers are easy to identify (they are marked in green in the fig. refIOFF) as they cross the brain from the Anterior to the Posterior part of the brain. Two groups of three ROIs are defined to filter the the left and right IOFF fibers:

- First, from the Sagittal view on the left hemisphere, we define a small patch over the middle occipital surcus (a hook shaped curve on the Parietal region). This is shown on the fig. 2.1.3 (right).
- Then, again from the Sagittal view, define the other two regions, on the Central and the Anterior regions, as can be seen on the fig. 2.1.3 (center and left).
- Changing to the Coronal view, we search the ROIs that we have defined and complete them. This is shown on the fig. 2.1.3 (left, center and right).
- We repeat these three steps for the other side of the brain.

Cingulum

The cingulum is a circonvolution or gyrus in the medium area of the brain. This structure connects the prefrontal cortex and other portions of frontal lobe to other posterior structures including temporal lobe and hippocampus. Its disruption is usually related in Alzheimer's disease and vascular dementia. The ROIs for the cingulum are defined from the Sagittal and the Axial view. On the RGB viewer, the Cingulum tracts can be clearly seen near the medial longitudinal fissure, in blue and green, around the Corpus Callosum in red.

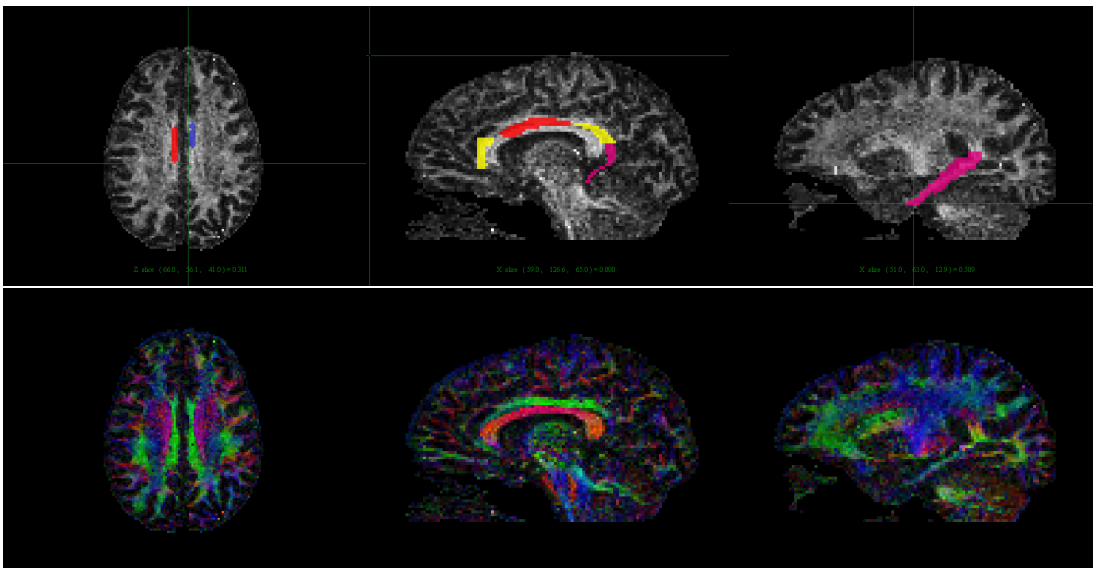

Figure 2.2: ROIs defining Cingulum spatial filter.

- First, from the Axial view, we define the first region on the just over the Corpus Callosum (shown on the fig. 2.1.3 left).
- The second ROI is defined form the Sagittal view; at the same level of the previous ROI, both at the front and the back of the Corpus Callosum limits (seen the fig. 2.1.3 (center)).
- The third ROI follows the inferior part of the gyrus. The ROI does not follow the same straight direction of the superior part, but turn outwards to the temporal lobe. This ROI can be seen on the fig. 2.1.3 (right).
- Finally, from the Axial view, we must search the previously defined ROIs and complete them.

Corticospinal tract

This region connects the cerebral motor cortex to medulla, then descends into contralateral spinal cord. The corticospinal tract conducts impulses from the brain to the spinal cord. It contains mostly motor axons. The corticospinal tract is made up of two separate tracts in the spinal cord: the lateral corticospinal tract and the anterior corticospinal tract. If injured, induces motor deficiencies and hemiparesis. The corticospinal tract originates from pyramidal cells in layer V of the cerebral cortex. About half of its fibres arise from the primary motor cortex. Other contributions come from the supplementary motor area, premotor cortex, somatosensory cortex, parietal lobe, and cingulate gyrus. The average fiber diameter is in the region of 10 micrometers.

These ROIs are defined from the Axial and Coronal views. The Corticospinal Tract can be seen on the RGB viewer in blue, from the base of the spinal cord to the blue-green at the somatosensor cortex:

- The first ROI is defined from the Axial view, covering all the base of one side of the medulla(as is shown on the fig. 2.1.3 left).
- The second ROI is first defined on the Coronal view; at the same Anterior to Posterior level that the previous ROI. This new ROI must be situated at the height of the internal capsule. Then, from the Axial view, we complete the ROI of the fiber tract. An example can be seen on the fig. 2.1.3 (center).
- The third ROI is first defined from the Coronal view at the same A-P level of the previous ROIs, and covers all the motor area of the cortex. The figure 2.1.3 right shows an example.
- Finally, we repeat these three steps for the other side of the brain.

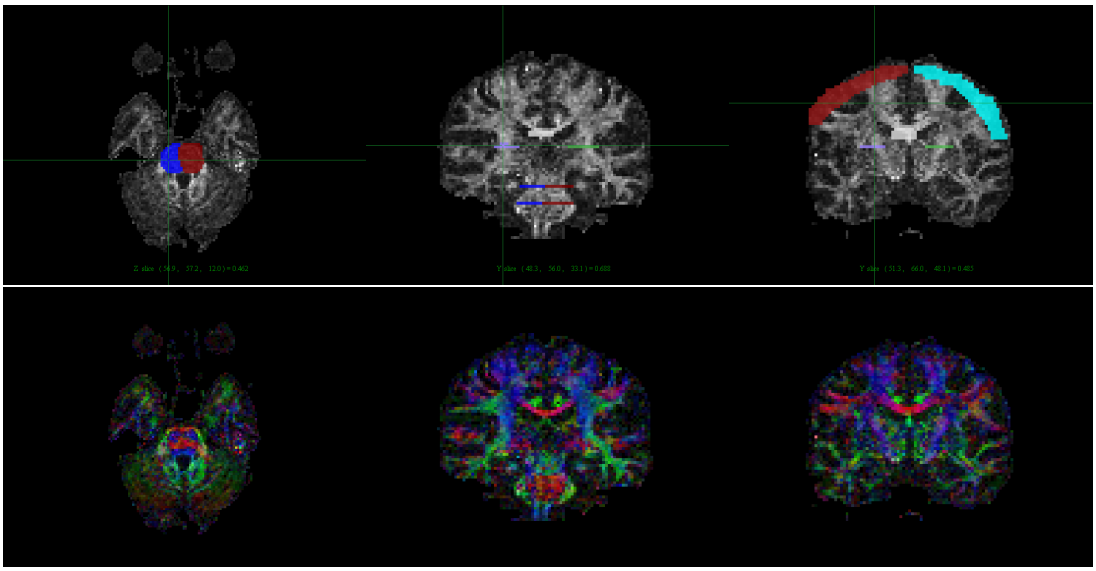

Figure 2.3: ROIs defining CST spatial filter.

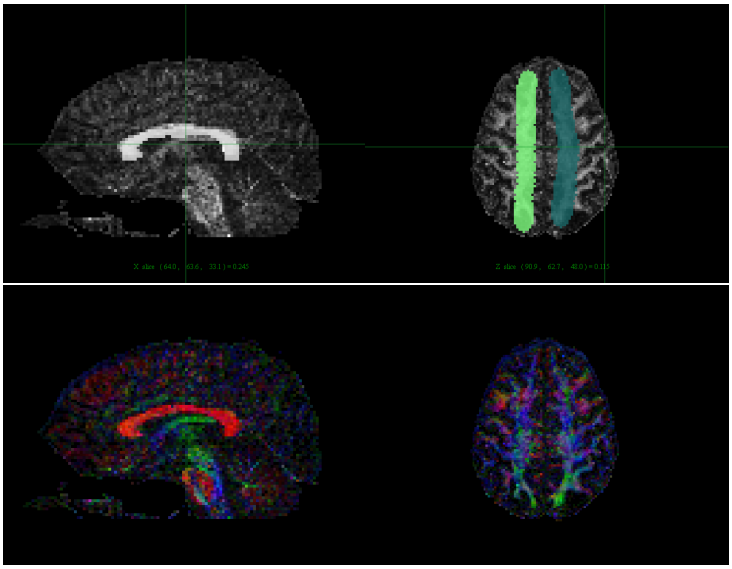

Figure 2.4: ROIs defining CC spatial filter.

Corpus Callosum

The Corpus Callosum is the largest fiber bundle in the brain. It connects the neocortical areas between both cerebral hemispheres; most are mirror image of each other. It is related to interhemispheric sensorimotor function and auditory connectivity.

The CC is a wide, flat bundle of neural fibers beneath the cortex in the eutherian brain at the longitudinal fissure. It connects the left and right cerebral hemispheres and facilitates interhemispheric communication. It is the largest white matter structure in the brain, consisting of 200-250 million contralateral axonal projections.

The ROIs for the Corpus Callosum are defined from the Sagittal and the Axial views. The Corpus Callosum can be seen on the RGB viewer in red at the level of the interhemispheric fissure, turning to blue up to the superior and parietal cortex. The protocol used to define the ROIs is this:

- The first ROI is defined from the Sagittal view, at the center of the brain, at the level of the interhemispheric fissure,. The Corpus Callosum is the big red zone that goes between the brain hemispheres from left to right (as is shown on the fig. 2.1.3 left).
- The second ROI and third ROI are defined form the Axial view; one over the right and one over the left hemisphere, way up the level of the superior frontal lobe and the paracentral lobe. An example can be seen on the fig. 2.1.3 (right).

Chapter 3

State of Art

3.1 Diffusion Weighted Imaging (DWI)

Diffusion Weighted Imaging (DWI) is a non invasive technique of Magnetic Resonance (MR) that provides information about the the diffusion of water molecules in the brain. This technique appeared first in the late 1980s and it is used to study the local characteristics of water molecules inside organic tissues *in vivo*.

Its physical basis is the assumption that the phase of the electrons of the water molecules inside the biological tissues respond at intense magnetic fields (for example, in a typical T1-weighted image water molecules are excited with a strong homogeneous magnetic field). In T2-weighted images, contrast is produced by measuring the loss of synchrony between the water protons. When water is in an environment where it can freely tumble, relaxation times tends to take longer. Using this data, we can create an image that differentiates between tissue types due to their relaxation time.

Unfortunately, MRI images do not provide much information about the orientation of the neural tracts within each voxel; information we could use to determine the connectivity between different regions of gray matter.

These interactions are orientation-dependent, meaning that the diffusion in parts of the brain has directionality. The influence of several magnetic fields from different orientations is useful for determining structures in the brain that restrict the flow of water in one direction, such as the myelinated axons of nerve cells. As the Figure 3.1 shows, the myelin cover and the neurofilaments are oriented structures that cause the perpendicular diffusion coefficient, $D(\perp)$, to be smaller than the parallel diffusion coefficient $D(\|)$. Knowing the main structure and

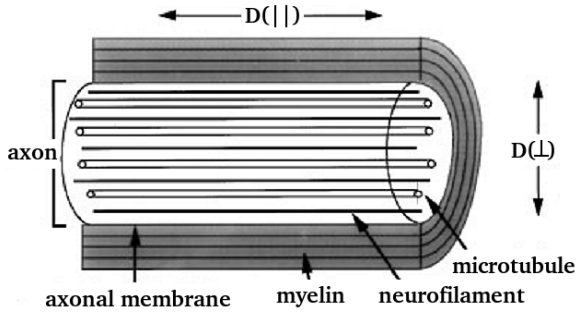

Figure 3.1: Schematic view of a myelinated axon [13].

connectivity of the brain, and differences between health and pathological tissues can give us a great insight of the neural diseases and of the brain itself.

3.2 Diffusion Tensor Imaging (DTMRI)

Diffusion Tensor MRI (DTMRI) is a special technique of MRI that can be used to produce neural tract images with useful structural information. Instead of using a homogeneous magnetic field, varies its intensity linearly

by a pulsed field gradient. Since precession of the protons is proportional to the magnet strength (b-value), they move at different rates, resulting in dispersion of the phase and signal loss. Then, another gradient pulse is applied (with the same direction and opposite magnitude) to refocus or rephase the spins. Protons that have moved between pulses due to Brownian diffusion reduce the signal measured by the MRI machine. Therefore each DWI provides information about the magnitude of diffusion in one particular direction. Using from six to, sometimes, hundreds of measurements is possible to generate a single resulting calculated image data set [1].

In DTI, each voxel is defined by its rate of diffusion and its preferred direction of diffusion. These properties are described by a 3×3 symmetric tensor with six uniques coefficients.

The properties of each voxel of a single DTI image is usually calculated by vector or tensor math from six or more different diffusion weighted acquisitions, each obtained with a different orientation of the diffusion sensitizing gradients.

Under noise-free conditions, the diffusion tensor is related to the DWI intensity by this equation:

$$S_i = S_0 e^{-b_i g_i^T D g_i} \tag{3.1}$$

where D is the diffusion tensor, S_i is the DWI intensity, S_0 is the baseline intensity, g_i and b_i are the gradient directions and diffusion weighting factor respectively. The diffusion tensor is positive definite, so all of its eigenvalues are positive. Each eigenvalue represents the magnitude of diffusion in the direction of the eigenvector associated with that eigenvalue. The eigenvector associated with the largest eigenvalue is also called the principal diffusion direction (PDD). Some anisotropy coefficients that can be derived from the tensor information, such as Fractional Anisotropy (FA) and others, can be used in clinical studies [3].

The single diffusion constant is the simplest model that we can use to characterize water diffusion, assuming that the system has isotropic structures. Its main advantage (simplicity, as it only needs six parameters to be estimated) can also be its main weakness. The tensor model may oversimplify the underlying anatomy,so it is important to interpret results derived from the tensor model with care. For these reasons, there is an increasing interest in high order models that can capture and display the DWI information.

Ultimately, clinical researchers are often interested in the global neural fiber bundles. These span through multiple voxels, limiting the usefulness of localized studies. The directional information can be exploited at a higher level of structure by following neural tracts through the brain. This process is called tractography.

Most of the current techniques in DWI tractography can be divided into two major components: **local modeling of the diffusion propagator** at each voxel, and **fiber tracking algorithms** integrating this local information into streamlines representing fiber tracts. Advanced tractography algorithms and high-order models are key concepts in the study of neural structures and its connectivity; and both are highly related to each other. In the next sections we will describe them in detail.

3.3 Low and high-order diffusion models

The role of the modeling techniques is to reconstruct the diffusion propagator from DWI data; converting the diffusion weighted signal into a quantity able to characterize the number and orientation of the fiber tracts at each voxel.

Some methods try to simplify the reconstruction of the diffusion propagator; either on the spatial domain or on the q-space acquisition domain. The first works under the assumption of Gaussian anisotropic diffusion and is simpler; the second provides a less parametrized representation of the diffusion propagator. More complex models use composited acquisitions, like the multiple-tensor model and the ball-and-stick model.

Also, another class of methods directly aims to the reconstruction of the distribution of fiber orientations, e.g., by spherical deconvolution.

3.3.1 Spatial model approaches

Simple diffusion tensor model

The most commonly used is the diffusion tensor (DT) [1]. It requires as few as six DW images to characterize each voxel (although usually up to twenty five are taken). First fits a Gaussian model for voxel wise diffusion, and assumes that only one main direction exists within each voxel. Data is sampled on a 3D Cartesian lattice.

DT assumes that diffusion model is a mean zero trivariate Gaussian distribution.

$$p(x) = \left((4\pi t)^3 det(D)\right)^{-\frac{1}{2}} exp\left(-\frac{x^T D^{-1} x}{4t}\right) \tag{3.2}$$

D is the diffusion tensor and t the diffusion time.

$$D = \begin{pmatrix} D_{xx} & D_{xy} & D_{xz} \\ D_{yx} & D_{yy} & D_{yz} \\ D_{zx} & D_{zy} & D_{zz} \end{pmatrix} \tag{3.3}$$

DTI is popular due to the simplicity of the model and of the imaging acquisition. Also is compatible with clinical conditions. However, it can only characterize one fiber compartment per voxel; this simplification is not always a good representation of fiber orientation and can lead to difficult interpretations in complex regions.

Several alternatives have been proposed to overcome the DT limitation, most of them are based on high angular resolution diffusion imaging (HARDI), which uses several tens to a few hundreds of DWI.

3.3.2 Q-space model approaches

Methods based on q-space provide an estimate of the angular dependence of the spin propagator, by exploiting its Fourier relationship with the DWI signal measured as a function of the q-vector [2]. The estimated spin propagator corresponds to the probability that a random water molecule will have a particular displacement over the diffusion time. In these models the fiber orientation are taken from the spin propagator by identifying the directions along which the probability of displacement is highest.

A common criticism of the q-space methods is the violation of the Narrow Pulse Approximation (the assumption that the spins move an insignificant distance during the gradient pulse itself). Q-space formalism is only strictly valid if this condition is true, and for the *i*n vivo cases, this requires DW gradient pulse durations of 1 ms or less. Unfortunately, on current clinical systems, the required diffusion weighting cannot be obtained with such short pulse durations due to the limited gradient amplitudes available. However, it has been shown that with longer DW gradient pulses, the spin displacements obtained reflect the difference between the spin's time-averaged positions during each DW gradient pulse. This will cause an underestimation of quantitative measurements of displacement, but importantly will not necessarily affect the estimated orientations, and indeed may be beneficial[4],[5].

Another criticism of q-space is the fact that the directions with the highest probability of displacement are relatively broad and overlap significantly. While not necessarily a problem itself, closely aligned fiber orientations will be blurred together and will thus be identified as a single orientation; this can lead to a bias in the estimated fiber orientations [6].

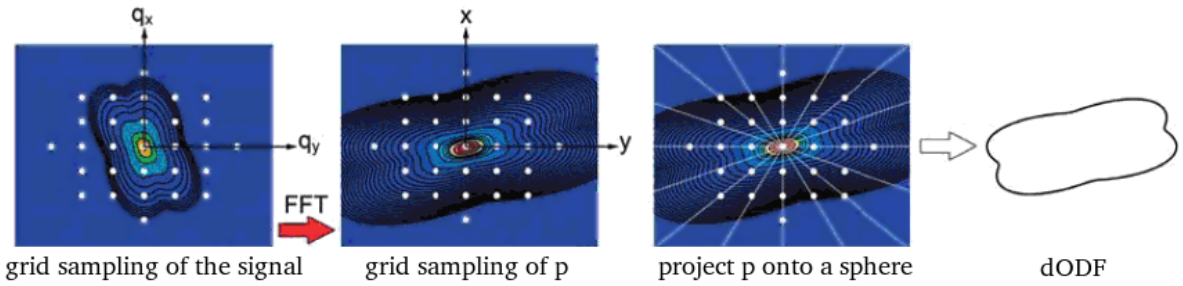

Figure 3.2: ODF estimation with DSI [48].

Diffusion Spectrum Imaging (DSI)

DSI is the direct application of q-space in 3D. It reconstructs a discrete representation of p directly from a 3D Cartesian grid in q-space, from which it is trivial to perform the required 3D Fourier transform. We can compute

the diffusion orientation density function (ODF) from p as:

$$ODF(\hat{x}) = \int_0^{\inf} p(\alpha\hat{x})dx \tag{3.4}$$

where $\hat{x}$ is a unit vector in the direction of x. The reconstruction gives the values of p on a grid of displacement.

Fiber orientations are identified by reducing the 3D spin propagator to its 2D radial projection and finding the peaks of its ODF. $ODF(\hat{x})$ is computed numerically by interpolating the grid representations of p:

For a 3D vector $\vec{u}$ with $|u| = 1$, we define

$$ODF(u) = \int p(\rho u)\rho^2 d\rho \tag{3.5}$$

where $\rho = |r|$, $\rho^2 d\rho$ is the 3D volume element and the integral is computed as a discrete sum over a range of voxels in diffusion r-space. The ODF can have multiple pairs of equal and opposite peaks, each pair provides a distinct fiber orientation estimation. The figure 3.5 shows the procedure: on the left panel, the white spots shows the points in which we acquire the measurements; the second panel shows p, the Fourier Transform of the signal, together with the grid displacement vectors at which the FFT provides the value of p. To obtain the ODF we interpolate the grid of samples of p and integrate along radial lines.

The main disadvantages of DSI are:

- Requires a large amount of data (the complete Cartesian sampling of q-space), at least one order of magnitude greater than DT.
- Lengthy acquisition (requires large pulsed field gradients to satisfy the Nyquist condition for diffusion in nerve tissue).

This measurement scheme is not practical if we are only interested on the angular structure (much of the information in the measures contributes only to the radial structure of p).

Q-Ball Imaging (QBI)

An alternative approach to DSI, based on sampling on a spherical shell (or combination of shells) in diffusion wavevector space, as seen in figure 3.3.2,. Uses shorter acquisition times and requires less data than DSI. It approximates the ODF using a spherical tomographic inversion called the Funk-Radon transform (also known as the spherical Radon transform). The value of the transformation of a spherical function at a point $\hat{x}$ is the integral

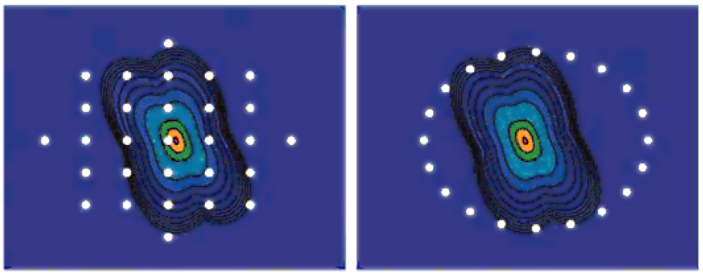

Figure 3.3: Illustration of the grid sampling and the spherical sampling acquisition protocols [48].

of the function over the circle $C(x)$ perpendicular to $\hat{x}$ at a fixed radius in q-space. Is model-independently and it can resolve multiple intravoxel fiber orientations without any assumptions on the diffusion process such as Gaussianity or multi-Gaussianity [11]. Then, at each voxel, directions of maximum diffusion are defined as local maxima of its ODF. QBI is acquired with low to intermediate q values to ensure adequate Signal to Noise Ratio (SNR). This introduces some blurring into the ODF. Larger q-values reduce the blurring but at the expense of SNR and or scan time. Higher spherical harmonic orders have been shown to increase the sensitivity of the q-ball reconstruction to fiber populations crossing at small angles. However, this comes at the expense of increased error in measured fiber orientation.

Persistant Angular Structure (PAS)

In [12], Jansons et al. define, for the HARDI data, a statistic called the (radially) persistent angular structure (PAS). It is a representation of the relative mobility of particles in each direction. Spins are assumed to diffuse a fixed distance with an angular distribution given by the PAS. The spherical samples in the q-space of the 3D Fourier transform can be taken as the probability density function of particle displacements.

It is a computationally intensive method. The non linear optimization and numerical integration make the PAS much slower than QBI or deconvolution methods, so normally a maximum entropy constraint is defined to operate on low b-value data and to improve the stability of the results and the velocity of its estimation.

Both QBI and PAS compute functions of the sphere that reflect the angular structure of the particle displacement density. The peaks of these functions provide estimates of fiber orientations.

Diffusion Orientation Transform (DOT)

Like PAS, it gives an estimation of a spin propagator at any given radius. The 3D Fourier transform is made tractable by assuming a mono exponential radial dependence for the DW signal. ODF is not a radial projection of the spin propagator, but corresponds to the amplitude of the spin propagator for a chosen displacement R_0. This provides increased separation between various fiber orientations when using larger values of R_0.

3.3.3 Mixture model approaches

Mixture models assume that the DW signal for a particular combination of fiber orientations is the weighted sum of each population's contribution to the signal.

Estimating the fiber orientations becomes a matter of fitting the model to the given DW data.

This requires two conditions: first, there is a negligible exchange of water molecules between fiber populations at diffusion time (according to [13] exchange effects can only become significant if fibers from different bundles interdigitate at micron scale) and second, fibers must share at least some of the DWI characteristics, which makes possible to reduce the complexity of the model and increase the stability of the reconstruction (this can go from assuming axial symmetry of diffusion to stating that the diffusion signal is identical for all fiber bundles). These assumptions may seem excessive, but these parameters have a relative weak effect on anisotropy and the estimated orientation will not be affected by it.

Mixture models can be improved with constraints: i.e. those based in prior knowledge of the fiber distribution (like the constraint of non negative volume fractions [9]) or a maximum entropy constraint (that favors a distribution of fiber orientations with a few well defined peaks [10]).

Multi tensor model

A natural extension of the DT model. Assumes that the DWI signal is created from a mixture of compartments each described by its own diffusion tensor. The signal $S(g)$ is predicted as the combination of several Gaussian models:

$$S_(\mathbf{g}) = S_0 \sum_{i=1}^{n} f_i e^{b\mathbf{g}^\mathbf{T} D_i \mathbf{g}} \tag{3.6}$$

where n is the number of compartments, S_0 is the non diffusion-weighted signal, b is the diffusion weighting, and g is the diffusion-sensitizing gradient. The sum of f_i is equal to one. There are particles displacements in n distinct compartments, between which no exchange of particles occurs. It is assumed that the number of distinct fiber populations is known. A full n-tensor model has $7n - 1$ degrees of freedom, but additional constraints are imposed in practice. Usually, by assuming equal eigenvalues on all D_i, or imposing axial symmetry ($l_2 = l_3$). For practical considerations of noise, most works normally uses a maximum of $n = 2$ (losing accuracy if it fits a model with $n \geq 2$).

A weakness of this strategy stems from the potential failures of the fitting process. Fitting multi-tensor models requires nonlinear optimization, usually done by descent-type algorithms or local maxima. The QBI approach, which converts directly the diffusion data into a fiber ODF, overcomes this difficulty.

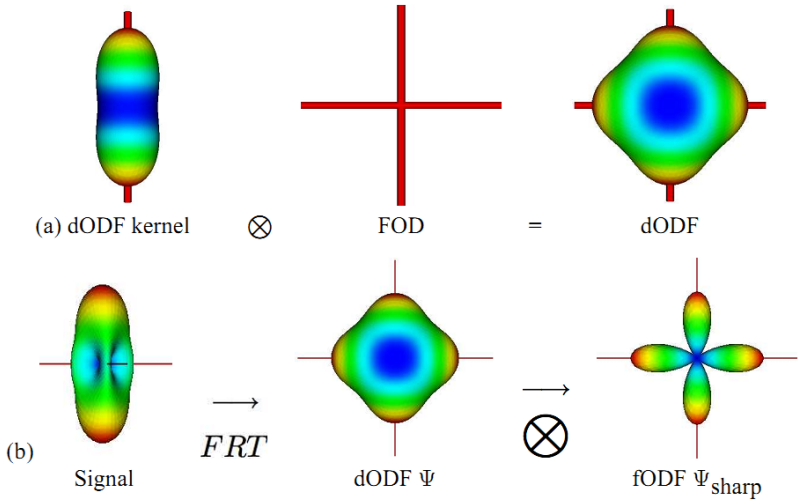

Figure 3.4: Spherical convolution / deconvolution. In a) the convolution between diffusion ODF (dODF) kernel and the fiber orientation distribution (FOD) produces a smooth dODF. In b) the Funk Radon transform (FRT) of the simulated HARDI signal produces a soomth dODF; which is transformed into a sharp fiber ODF by a deconvolution with the ODF kernel of a) [20].

Combined Hindered and Restricted Model of Diffusion (CHARMED)

CHARMED is strongly related to multitensor models. It is formed by one extra axonal compartment (characterized by a single diffusion tensor) and n intra-axonal compartments (corresponding to n fiber populations).

It is characterized by a model of restricted diffusion within cylinders. Requires a more complete 3D q-space acquisition to discriminate between both models. In CHARMED, the data is acquired from multiple q-values per DW orientation, and multiple orientations. Also this model requires a large maximum q-value (accomplished by increasing echo acquisition time . By contrast, most high-order models employs the HARDI strategy: acquiring a large number of DW directions with a constant b or q-value. This allows to focus on the angular part of the DW signal and to select the most appropriate diffusion weighting to maximize contrast to noise per unit of scan-time [14].

Ball and stick model

This model assumes that all D_i have equal eigenvalues (completely isotropic) and the remaining "stick" compartments are perfectly linear (the second and third eigenvalues are zero $l_2 = l_3 = 0$). For n fiber terms, this leads to $k = n + 1$ compartments and $3n + 1$ degrees of freedom. We consider the model up to $n = 3$. Fitting the ball-and-stick model can theoretically be formulated as a deconvolution problem with a discrete ODF

Spherical Deconvolution model(SD)

A generalization of previous methods: SD assumes a distribution, rather than a discrete number, of fiber populations. The summation becomes an integral over the distribution so it takes account for an infinite number of fiber populations. The method assumes that the diffusion signal $S(\theta, \phi)$ is the convolution of the ODF.

It tries to reconstruct directly the distribution of fiber orientations. This requires an explicit model of the diffusion properties of a single fiber (convolution kernel), and its results are more easily interpretable.By assuming a particular convolution kernel (representing the DW signal for single fiber orientation) the fiber orientation distribution can be estimated by a constrained spherical deconvolution.

$$S_(\theta, \phi) = \int_0^{2\pi} \int_0^{\pi} ODF(\theta', \phi') R(\gamma') sin(\theta') d\theta' d\phi' \tag{3.7}$$

where γ' is the angle between directions given by (θ, ϕ) and (θ', ϕ'). Typically, $S(\theta, \phi)$ and $R(\gamma)$ are estimated from the data and modeled in spherical harmonics and rotational harmonics, respectively. This reduces spherical deconvolution to simple scalar division, and yields $ODF(\theta, \phi)$.

Some implementations differ in the convolution kernel employed (some assume a DT model [15], and some measure it directly from the data [16]). They also differ in the constraints of the solution (some implementations introduce a non negativity constraint [16] and others a maximum entropy term [10]).

SD, like DSI and QBI, can be expressed as linear matrix operations, so their computation times can be kept very short. Linear spherical deconvolution is extremely fast and does not require pre-specification of an expected number of fibers. On the other hand, multi-tensor models offer higher accuracy for applications like multi-fiber streamline tractography.

3.4 Tractography: Basics

In the brain, the white matter consist in axons that form bundles which connect different regions of the brain. Fiber tractography algorithms take the local diffusion information and integrate them into tracks that aim to represent the neural fibers tracts. Many prominent tracts are large enough to be delineated by DTI and to estimate connections between adjacent voxels.

Tractography is the only tool we currently have to visualize white matter neural tracts *in vivo* and non invasive, providing us information of the white matter architecture and connections.

The most simplest implementation for performing tractography is the numerical integration between neighboring image voxels that are thought to belong to the same white matter fiber tract. Typically, it starts from a preassigned voxel called the "seeding voxel". Integration continues examining the directional consistency between the principal eigenvectors of the two neighboring voxels and between the fiber direction and the vector connecting the two voxels. The angle θ between two vectors a and b can be calculated with the inner product:

$$cos(\theta) = \frac{\vec{ab}}{|\vec{ab}|} \tag{3.8}$$

Knowing the angular relationships, tractography continues choosing those with angles smaller than a prespecified threshold. Then process steps up to the next voxel before reaching a determined stop criteria. An example of this can be seen in the figure 3.4

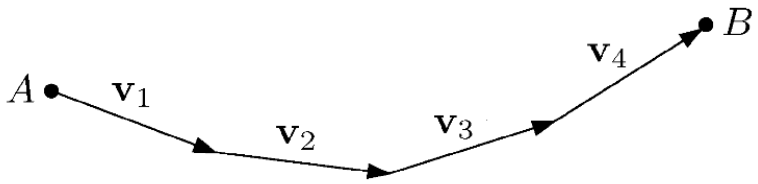

Figure 3.5: Fiber path composed by a track of vectors [38].

The definition of the voxel neighborhood can be extended from the simplest case of $3 \times 3 \times 3$ to, for instance, $5 \times 5 \times 5$. This extension would allow a jump if an underlying voxel contains an erroneously estimated fiber direction (due to fiber crossing or noise contamination), at the expense of computational complexity. The optimal choice of the voxel neighborhood definition depends of the spatial resolution and the width of the fiber tracts under consideration.

3.4.1 Deterministic algorithms

Deterministic algorithms, also called streamline tractography, are based on line propagation techniques to delineate the white matter pathways. The simplest tractography algorithms: they only follow the most probable direction at each voxel. They rely on these basic points:

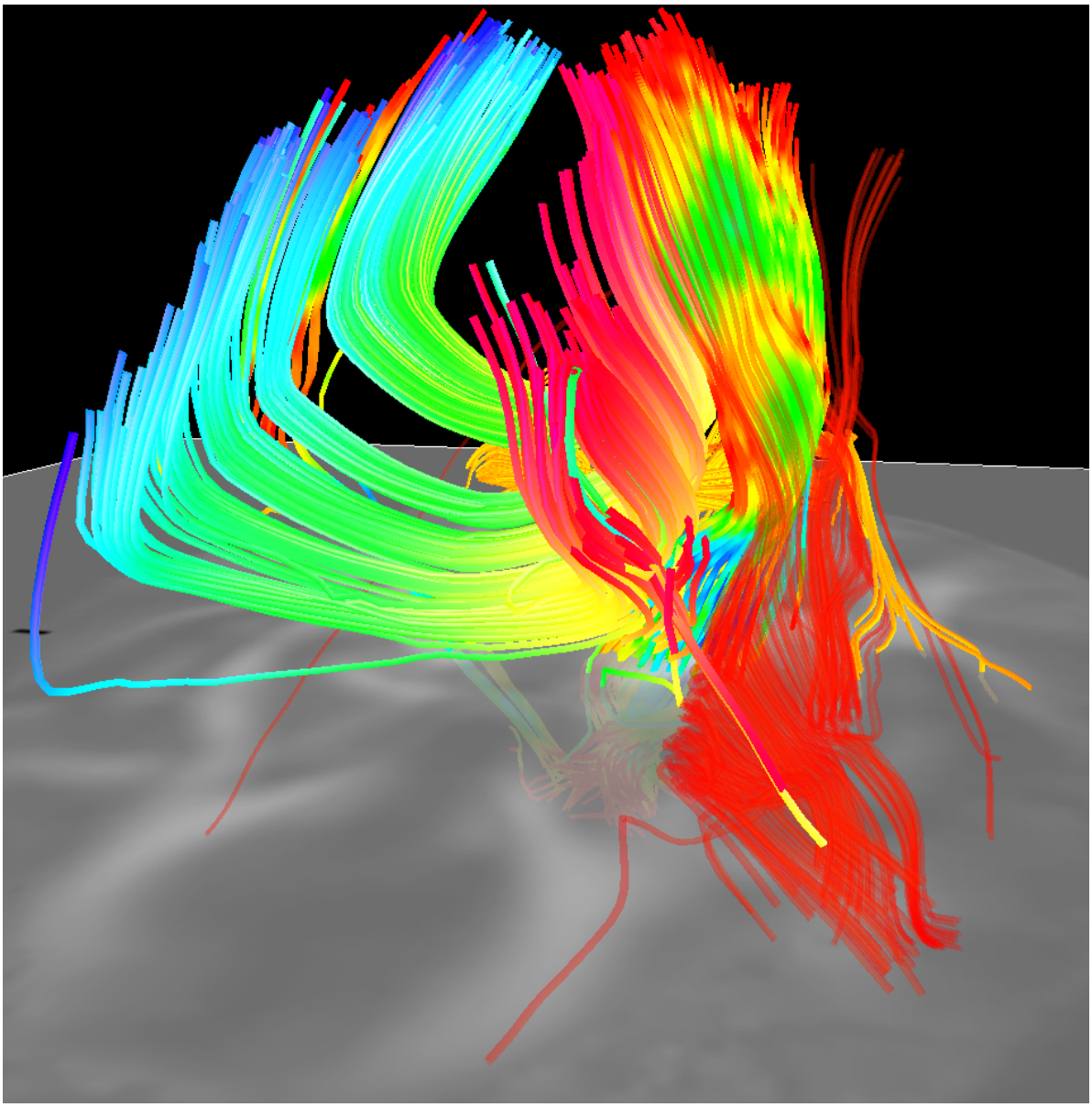

Figure 3.6: An example of deterministic tractography.

- Seed point: It is necessary the identification of a suitable starting position to initiate the algorithm. In brain tractography, the selection of anatomically appropriate regions is critical. Small changes in the starting position can lead to very different results. Usually this part is manually performed by an operator although other methods exists like the brute force method (in which tracking is initiated from all the voxels in the data in combination with tract editing methods to identify tracts of interest) or the fMRI method (peak activation areas of functional MRI data is used as a starting point, allowing for correlational analysis between structural and functional connectivity).
- Step size: Distance between successive steps. Most algorithms work with a fixed value, although some use a variable length. The radius of curvature of the tract is strongly dependent on the step size. A small step size allows the algorithm to follow more closely the curvature of the tracts, at the expense of a bigger computational load.
- Track propagation. The algorithms try to estimate the white matter fiber direction based on the DW data around each point. The algorithm can advance from the starting position along the estimated orientation. Then, the orientation of the new position is reestimated until a termination criteria is achieved. We will expand this point later.
- Termination criteria. Most common criteria is a threshold based on a measure of anisotropy (typically, if the value of fractional anisotropy at a voxel is below 0.15, the track is terminated) [17]. There are two reasons for this. First, in regions with low anisotropy, the major eigenvector of the diffusion tensor will tend to be poorly estimated and sensitive to noise; and second, anisotropy tends to be high in white matter and low in gray matter, a sudden drop in anisotropy is likely to coincide with the gray/white matter boundary, where tracts are generally assumed to start and end.

  The second most common criteria is based on the local curvature of the track: if the angle between the directions of two subsequent steps is above certain threshold (typically 90 degrees), the track is stopped. A sudden change in direction of the track is likely to be caused by data artifacts. This also reduces the number of tracks that "rebound" or turn around and return to the seeding point.

  Other proposed criteria are a measure of the coherence of the fiber orientations within the neighboring voxels [22], or the use of a binary mask of permitted and forbidden regions.

Another point usually mentioned on tractography is tract edit. Tract editing is a refinement method. Consists of defining regions through which the tract of interest is known to pass. Tracks that enter these regions are considered anatomically plausible, and all other tracks are discarded. It is also possible to define regions through which the tract is known not to pass and discard any tracks that enter these regions. These methods are very powerful for removing spurious findings, but they require expert anatomical knowledge. While tract editing can reduce the number of false negatives, it can also reduce the number of true positives. Also, these techniques are not suited to exploratory studies, where connections may not be known a priori.

Methods of track propagation

Normally it is assumed that the major eigenvector of the diffusion tensor can give a good estimation of the fiber orientation within each imaging voxel. For deterministic algorithms, track propagation depends on two factors: the interpolation method used to estimate the tensor values and the propagation algorithm employed.

- Interpolation methods: The simplest method is nearest-neighbor interpolation: at any point, the quantity of interest (usually the whole tensor) used is approximated to that of the nearest voxel value. Most algorithms use tri-linear interpolation, whereby is calculated as a weighted sum from the 8 voxels nearest to the point of interest [17]. Other perform tri-linear interpolation on the raw DW signals themselves, and recompute the major eigenvector based on this data. Another approach is to interpolate the elements of the diffusion tensor themselves [19, 20, 21].
- Propagation algorithms: These algorithms aim to represent the white matter fiber tracts as 3D space curves, calculating new steps at each time.
  - Fiber Assignment by Continuous Tracking (FACT) algorithm: The most basic propagation algorithm, each new step is integrated tangent to the main eigenvector direction. Presented by Basser et al. [1], employs an Euler integration procedure. Euler method is is accurate only to a first-order, so it is susceptible to large accumulated errors and numerical instabilities. Some algorithms use an adaptative step size to control the amount of error introduced in each step.

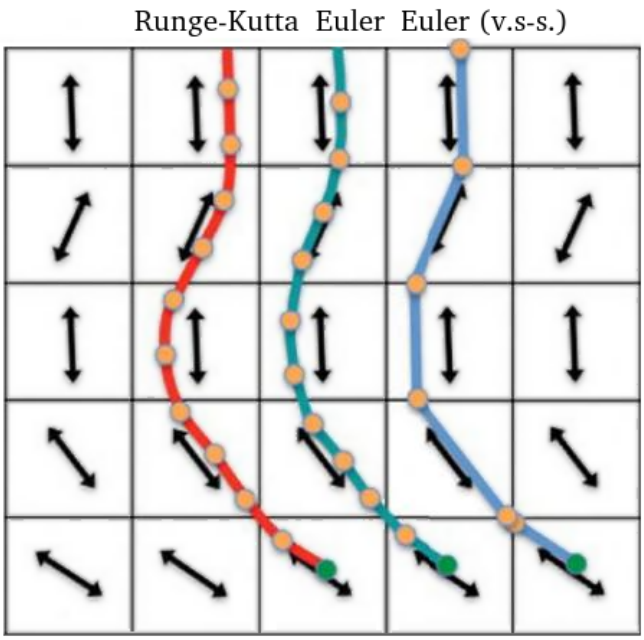

Figure 3.7: Three track propagation algorithms. From left to right: Runge-Kutta, Euler and Euler with variable step-size.

More advanced versions employs a fourth order Runge Kutta integrator, for it can achieve better estimations in highly curved regions minimizing the integration error per step.

Mori et al. [22] developed a more complex variation, which alters the propagation direction at the voxel boundary interfaces. It uses variable step sizes, depending upon the length of the trajectory needed to pass through a voxel.

– Tensor Deflection methods (TEND): An approach, proposed by Weinstein et al. [23] and Lazar et al [24] to resolve ambiguities in complex regions using the entire diffusion tensor information, instead of just the major eigenvector direction.

  It works with a combination of the direction of the incoming vector and the outcoming vector weighted by the linearity index of diffusion and some user-defined parameters. For example, if the incoming vector coincides with one of the tensor eigenvectors, the propagation direction will not be deviated.

  TEND is less sensitive to both measurement noise and lower tensor anisotropy than STT. However, TEND will underestimate the trajectory curvature for curved pathways, as it limits the curvature of the deflection. This error is cumulative, but can be reduced by using smaller step sizes. Consequently, with TEND there is a tradeoff between lower error in straight sections and higher errors in curved sections.

Examples of deterministic algorithms

In [25], Fillard et al. present a comparative study of several deterministic tractography algorithms with different modeling methods against real phantom data.

- Multitensor methods: Ramirez et al. [26] defines a mixture of single and 2-tensor models (when a tensor has a much larger importance than the other, the 2-tensor approach is dropped), the next propagation direction is chosen as the closest to the previous direction among all available candidate directions given the single or 2-tensor model.

Malcolm et al. [27] also propose a tractography 2-tensor model. Each step follows the tensor whose PDD is the closest to the previous direction. However, instead of using least-squares to fit the tensor parameters directly, it uses an unscented Kalman filter to make an estimation given the results of previous positions along the fiber. Nevertheless, the tractography algorithm employed is the bottleneck of the method as errors may accumulate during the reconstruction, which may eventually lead to erroneous pathways.

- Q-Space methods: Sakaie et al. [28] employs a fast PAS calculation with a simple FACT algorithm. Each next step direction is defined by the local maxima of the ODF (subject to angular and magnitude thresholding). This method is not appropriate to use in crossing regions. According to [25] high angular resolution and noise immunity of the persistent angular structure are not sufficient to compensate for shortcomings of simple streamline tractography in the presence of complex fiber geometries.
- Spherical deconvolution: In [29], Goh et al. present a FOD based method. Tensor values and ODF are estimated using a probability density constraint and a spatial regularity prior. The constraint enforces the ODF to be positive, while the spatial prior ensures the resulting field to be spatially smooth, and the method is consequently robust to noise. Tracking algorithm is a simple first-order integration method, by detecting ODF maxima with a threshold over the sphere.

  Descoteaux et al. [30] method estimates the FOD with a SD and a constrained regularization method. This is specially noise sensitive; the simple streamline tracking used can be mislead by erroneous FOD maxima, especially in crossing regions.

  The method of Jeurissen et al. [31] also implements the constrained SD to estimate the FOD. Given that data with low angular contrast and low SNR makes the estimated fiber orientations very susceptible to noise contamination, the estimation method applies an adaptive anisotropic Gaussian filter to increase SNR. Then, the FOD maxima is extracted using a Newton optimization method. Tracking is ended when FOD peak intensities are beneath a threshold or a maximum angle is exceeded.

  With SD, the denoising process seems to overcome the decreased precision of the fiber spatial positions induced by the diminished resolution; SNR should not always be sacrificed at the profit of spatial resolution

These methods are highly dependent on the accuracy of the ODF estimation. In conclusion, multi tensor based methods perform better than single tensor methods in crossing regions.

For high SNR datasets, diffusion models such as ODF can correctly model the underlying fiber distribution and can be used in conjunction with streamline tractography. In high SNR and simple regions, the single-DT model is still able to correctly characterize numerous fiber bundles. For medium or low SNR datasets, a prior on the spatial smoothness of either the diffusion model or the fibers is recommended for correct modeling of the fiber distribution and obtain proper tractography results.

Limitations of deterministic algorithms

There are several issues with most of the previously mentioned tractography algorithms. These problems can be summed up in a small list:

- Using only the principal eigenvector means that the information of the second and the third eigenvectors is entirely excluded.
- The directional consistency criteria favors tracks without sharp turning angles. Some tracts are known to show prominent directional turning, such as the Meyer loop, and can present difficulties to the algorithms.
- Placement of the seed voxels. Small differences in starting point can lead to very different results. To study the number of tracts passing through certain regions of interest, one can preassign seed voxels manually and follow the diffusion through it or, alternatively, can place the seed voxels globally within the entire brain region. The later, also called "brute force approach", detects all possible tracts within the range at the expense of huge computation time. Tracts that do not pass through the designated regions of interest are filtered out.

3.4.2 Probabilistic algorithms

Noise in DW measurements introduces uncertainty in the model estimation, these errors accumulates along the fiber track and can lead to completely different connections.

Deterministic algorithms don't provide information about the accuracy of the estimated track. Probabilistic tractography tries to provide a confidence interval of the reconstructed pathways.

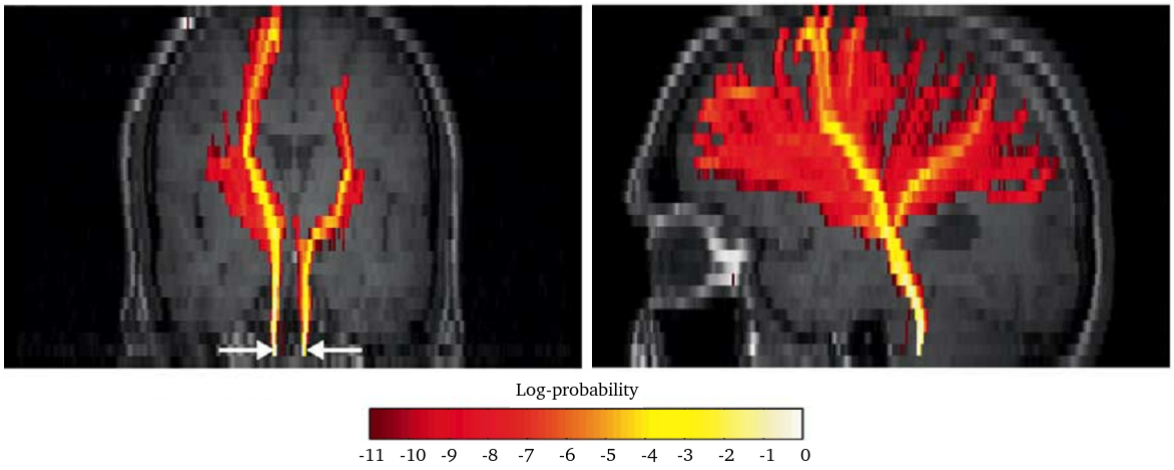

Figure 3.8: An example of probabilistic tractography [38].

Most probabilistic approaches are derived from deterministic streamlines and therefore share many of their characteristics and limitations. The main difference lies in the main direction estimation: the direction for the next step is not unique but chosen from a range of likely orientations; probabilistic algorithms estimates orientation at random from the local probability density function (PDF).

Starting from a seed point, the track is propagated with each step selected at random. After a large number of samples, is possible to compute the probability of the dominant streamline.

The ratio between the total number of pathways and the number of pathways that reach a determined voxel infers how likely is that such pathway could have arisen by chance alone, or how reproducible is the pathway through the data. Repeating the same process a large number of times introduces uncertainty at each estimation of the fiber orientation.

It is important to distinct between precision (the reproducibility of the result) and accuracy (difference between the measured and the true data). Probabilistic tracking results give an indication of the precision of the tracking but give no indication about its accuracy. An example of probabilistic tractography can be seen in the figure 3.4.2

Characterization of the fiber orientation PDF

A key aspect these algorithms is the characterization of the fiber orientation PDF. Ideally it should provide an estimate of the fiber orientation and its uncertainty, based on the given data and its noise. There are a great number of methods, such as:

- Heuristic functions on the DT shape: Parker et al.[32] present a framework that estimates the uncertainty based on the orientation of the tensor ellipsoid. The direction of the next step is decided by interpolating the twenty-six nearest neighbours tensor values; each tensor rotated by a frame of reference chosen at random from a specific shape model. Two models can be used, a 0^{th} order model based on the anisotropy of the tensor; and a 1^{st} order model, based on the relative magnitudes of the second and third eigenvectors.
- Bootstrap methods: An extremely powerful nonparametric statistical procedure for determining the uncertainty of a given statistic. It works by randomly selecting individual measurements (in this case individual diffusion-weighted images) from a set of repeated measurements, thus generating many bootstrap samples. Each bootstrap sample provides a random estimate of a given statistic. By generating a sufficient number of the bootstrap replicates one obtains a measure of uncertainty or, in some cases, the PDF of the given statistic.

  Some bootstrap methods are variations of the deterministic methods, like Jones et al.[33], which defines a single pathway (propagated parallel to the PDD from a seed point) iterated a large number of times to produce a maximum visitation count that shows the most highly reproducible trajectory.

  Other approaches rely on a priori assumptions about the error distribution. The overall variability in the trajectory of reconstructed tracts is determined not only by the uncertainty in the vector field (which would

determine the likelihood of going off track) but also by the characteristics of the surrounding tissue (like the FA index).

In the wild bootstrap method of Jones et al.[34], and large number of tensor volumes are generated by first fitting the diffusion tensor using linear least squares and then computing the residuals to the fitted model. Then, tracks are created with a simple Runge-Kutta algorithm through all the volumes. This data is used to create a "cone of uncertainty" at each vertex. This method allows to apply bootstrap methodologies to data which was not explicitly acquired with multiple repeat data sets. When comparing these estimations with those obtained from Monte Carlo simulations, no difference is found in the median values. However, a substantially larger dispersion can be observed.

There are four main approaches to computing bootstrap confidence intervals: normal approximation, percentile, bias-corrected percentile, and percentile-t [34].

- Bayesian inference methods: Diffusion tensor model assumes a local 3D Gaussian diffusion profile, so diffusion goes along only on the dominant direction. Bayesian techniques allows for the application of prior constraints on parameters in the model where such constraints are sensible.

  The output of these algorithms is a set of nodes describing the maximum likelihood pathway through the DTI data, with no measure of confidence on the location of this pathway.

  There are two general approaches to fit a parametrized model to data:

  The first is to look for the set of parameters which best fit the data. This is called a point estimate of the parameters. A special case of this is Maximum Likelihood Estimation (MLE), where we look for the set of parameters which maximize the probability of seeing this realization of the data given the model and its parameters.

  The second approach is to associate a PDF with the parameters. This distribution is called the posterior distribution on the parameters given the data.

- Other methods:

  Random walk method: Koch et al.[35] propose a Monte-Carlo simulation that determines the probability of a jump in a particular direction from a given voxel based on the local value of the diffusion tensor components and the adjacent voxels.

  Graph theories approaches: In [35] Iturria et al. present a method for characterizing anatomical connections between brain gray matter areas. First, voxels are modeled as nodes of a non-directed graph, with the weight of an arc linking two neighbor nodes is estimated by the intravoxel white matter orientational distribution function. Secondly, an iterative algorithm is used to solve the most probable path problem between any two nodes. Third, for assessing anatomical connectivity between K gray matter structures, the previous graph is redefined as a K + 1 partied graph by partitioning the initial nodes set in K non-overlapped gray matter subsets and one subset clustering the remaining nodes.

Examples of probabilistic algorithms

Grouped on its basis of characterization of the uncertainty of the fiber orientation:

- Heuristic functions: Tournier et al.[36] propose the Front Evolution Tractography algorithm (FRET), in which the each new step is expressed in terms of a front emanating from the seed point. A child front is generated from the parent point, which describes the local evolution of the front. The child front is made up of the set of points obtained by stepping away from the parent point by step size along the directions sampled. At each iteration, many child fronts are generated and merged to form the surface of the main front. For the next iteration, each point on the new surface will be used to generate a child front. ODF function dictates the evolution of the front and contains all the assumptions made. The likelihood index is defined by the magnitude of the main eigenvector and a combination of anisotropy indexes.
- Bayesian inference: In [37] Behrens et al. present an online Bayesian method for assessing the most appropriate number of fiber orientations for the data at each voxel. Automatic relevance determination (ARD) is a model selection technique that fits data to the model, but ensures that parameters that are not supported by the data, do not contribute to the likelihood. It is different from other normally used techniques, that fit different models to the data separately, and compare them on the basis of a metric reflecting data fit and model complexity. This is achieved by placing a prior distribution on a parameter in a Bayesian model, which will force that parameter to take the value zero if, and only if, there is no evidence in the data for its existence. This prior distribution can take a number of forms. However, the

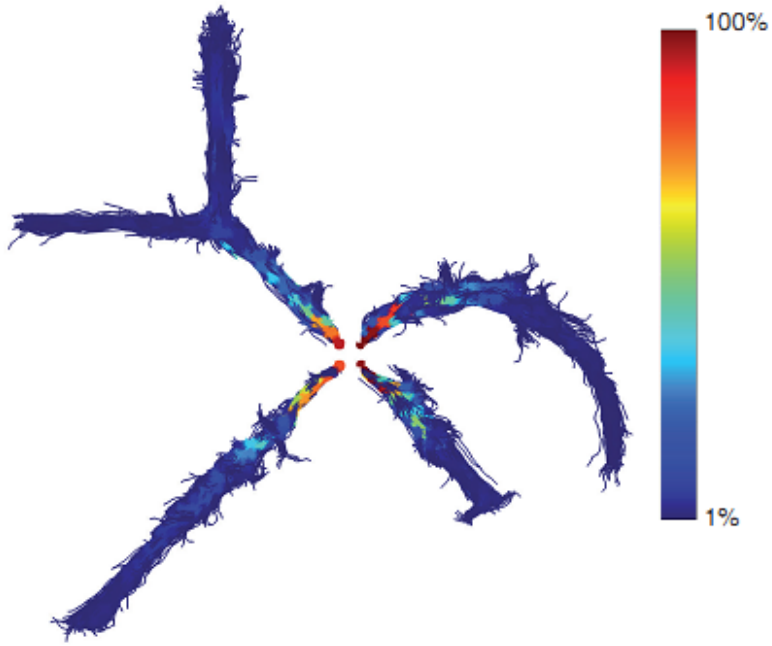

Figure 3.9: Synthetic data of five equal FA paths. There is a bias that favors shortest, straightest paths [47].

most common of these is a Gaussian distribution with mean zero, but unknown variance. ARD only requires a single model to be fit to the data (as opposed to fitting every candidate model and comparing).

Friman et al. [38] describe a Bayesian approach for deriving probability density functions of the local fiber orientation, and an associated theorem that facilitates the estimation of the parameters in this model. The probability of a fiber going from a to b can be found by summing the probabilities for all paths of all lengths between these areas, to diminish computation complexity, it is estimated as a Monte Carlo method. It is assumed that the prior distribution can be factorized (meaning that prior knowledge about the nuisance parameters in each point of integration is independent of both the previous step direction and prior knowledge about the next step direction). Also, is assumed that the diffusion measurements do not depend on the previous step direction. Modeling and estimation are carried out at two levels: a global level and a local level. At the global level, estimates the probability that a fiber seeded in a point or area A reaches and area B; at a local fiber orientation is estimated from the diffusion data, and uncertainty enters in this process due to image noise and complex fiber architectures.

In [39], Wedeen et al. describe the PDF with DSI.The PDF is estimated from these ODF by projection of the data in the radial direction. The directions of maximum diffusion are defined as local maxima of the ODF projection that produces least curvature for the incoming path.

In the method of Berman et al. [40], the orientations of fiber populations within a voxel are defined by the local maxima of the ODF, subject to angular and magnitude thresholds. Maxima are located with an iterative gradient ascent routine that identifies peaks.

Limitations of the probabilistic algorithms

They can be summarized in:

- Distance bias: The voxels closer to the seed region are more likely to be reached than farther voxels; therefore is common to find short, anatomically implausible tracks with higher probability values than more distant, biologically relevant connections, as figure 3.4.2 shows. Length and shape of the tract alone influences tracking accuracy and precision and, therefore, will influence any connectivity measure derived

from probabilistic tractography. Furthermore, if a fiber system branches the total number of reconstructed streamlines will be divided reducing the connectivity index [14].

- Dependence of the data acquisition protocol: Estimations made with higher quality data (higher SNR, larger number of DW directions, etc.), can lead to more precise and less spread tracking results. This leads to a greater density of tracks reaching the connected region, and hence to a greater probability of connection.
- Complex tract configurations: If the tract of interest has a specially complex configuration, (as if branches to or merges from multiple directions) there will be a reduction of the ratio of fibers that reach its target. Each destination will be assigned a lower probability value that it corresponds.

3.4.3 Global optimization algorithms

Deterministic and probabilistic tractography algorithms are local methods: they try to construct fibers independently path-by-path, instead of reconstructing tracts one by one; each fiber does not have influence on the others. With global methods, long pathways are estimated in small successive steps by following the local distribution of fiber directions; the basic principle is analogous to curve fitting. Often the global methods start by performing modeling, first for a predetermined geometric smoothness of the fiber tracts; then the shortest or the most suitable path is searched so that a general agreement with the principal eigenvectors can be reached. The balance between tract smoothness and tensor consistency is balanced iteratively by a predefined energy and penalty variables. Compared with local methods, global methods are a lot more slow that the deterministic ones but are also more robust. They can give a more precise estimations and seem to be well-adapted in real, noisy situations, as the entire neural pathway is the parameter to be optimized.

Examples of global optimization algorithms

In [41], Reisert et al. propose a global tractography method. Each segment of a fiber is a parameter to be optimized (they try to associate with neighboring segments to form longer chains of low curvature while modeling the diffusion weighted data at best). Each segment contributes as a single isotropic Gaussian model, which eventually results in a mixture of Gaussian in each voxel. The behaviour of each segment is controlled by an interaction between line elements and by an increasing match to the measured data.

Each fiber segment is described by a continuous spatial position $x \in Re^3$ and an orientation $n \in S_2$ by the tuple $X_i = (x_i, n_i)$, and each connection between endpoints is described by $E = (X_1^{\alpha_1}, X_2^{\alpha_2})$. The parameter $\alpha = -, +$ defines the direction along the segment.

The aim of the optimization is to maximize the a-posteriori probability, $P(M|D)$ with respect to M; which is equivalent to finding the minimum of its total energy, $E(M) = E_{int}(M) + E_{ext}(M, D)$.

$$P(M) = e^{-E_{int}(M)/T} \tag{3.9}$$

$$P(M|D) = e^{-E_{ext}(M,D)/T} \tag{3.10}$$

The internal energy term, E_{int}, controls the behaviour of line segments, in particular driving them to build long fibers. Each segment can make connections with both of its endpoints. If two segments are connected, they feel a certain attraction force such that they stay nearby and keep their orientations similar; they do not attract other segments. The internal energy is a sum over all connections:

$$E_{int}(M) = \sum_{(X_1^{\alpha_1}, X_2^{\alpha_2}) \in \epsilon} U_{con}(X_1^{\alpha_1}, X_2^{\alpha_2}) \tag{3.11}$$

where ϵ is the set of all connections, and $U_{con}(X_1^{\alpha_1}, X_2^{\alpha_2})$ is the interaction potential, composed by the squared distances from the endpoints of the segments to the midpoint of the line connecting both, as seen in figure 3.4.3.

$$U_{con}(X_1^{\alpha_1}, X_2^{\alpha_2}) = \frac{1}{l^2}(|||x_1 + \alpha_1 l n_1 - \bar{x}|||^2 + |||x_2 + \alpha_2 l n_2 - \bar{x}|||^2) - L \tag{3.12}$$

$\bar{x}$ is the midpoint and the bias L is a connection likeliness. Large $L > 0$ imply a high likeliness that two segments link together.

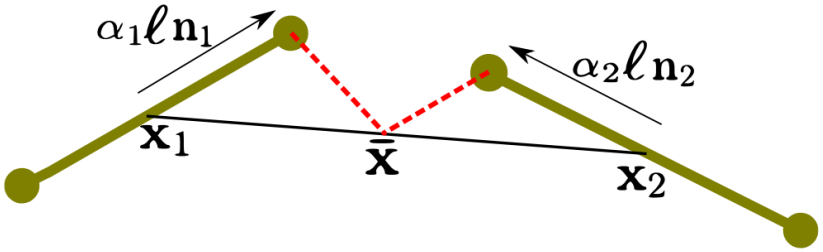

Figure 3.10: Two line segments (given by midpoints x_1, x_2 and orientations n_1, n_2) and the elements for constructing their internal energy. The red dotted lines indicate the distances whose sum of square defines the internal energy [56].

The external energy term, E_{ext}, expresses the similarity of the model with respect to the data.

$$\rho_M(x,n) = w \sum_{X_i} \rho_{X_i}(x,n) \tag{3.13}$$

where w is the weight with which each segment contributes. The external energy is the L_2-norm of the meanless signal difference:

$$E_{ext}(M,D) = |||\rho_M^{'} - D^{'}|||^2_{L_2(\mathbb{R}^3 \times S_2)} \tag{3.14}$$

The energy E_{ext} forces the model to be close to the measurement in anisotropic areas where the data interpretation is unambiguous, while the segments in isotropic areas do not affect the energy as long as they are isotropically distributed.

The method uses a Metropolis-Hastings sampler to draw samples from the posterior distribution.

$$P(M,D) \propto P(D|M)P(M) \propto e^{-E(M)/T} \tag{3.15}$$

As more low is the temperature T, more like is that the sample from $P(M|D)$ corresponds to minima of $E(M)$. For an undetermined number of iterations, a segment choose certain state M transitions randomly according to a proposal distribution p^{prop}. This modification is accepted if the so-called Green's ratio R is above 1, where R is:

$$R = \frac{P(M'|D)p^{prop}(M'|M)}{P(M|D)p^{prop}(M'|M)} \tag{3.16}$$

After a certain number of iterations the resulting chain of states follows the desired distribution. There are two stopping criteria: the ratio of the connections versus the number of segments, and the distribution of fiber length. Once both have converged to a kind of stable state the iteration is stopped.

The proposal splits into three different types, each with a certain probability: segment creation/deletion (p_{birth},p_{pdeath}), segment moves (p_{shift},$p_{optimize}$) and segment connections (p_{fiber}).

The absence of any boundary conditions minimizes the dependence on the operator and keeps the necessary user interaction low.

The results of this method vary according to certain parameters such as width ρ and orientation sharpness c. They both control the expected number of fibers of the reconstruction. A small choice for ρ results in a high number of reconstructed fibers. The segment length l controls the expected curvature of the fibers. Large l imply low curvature and vice versa. Usually values of $2\rho < l$ are taken. The connection bias L is the likelihood that two segments become connected. Large values lead to 'curly' reconstructions with lots of false positive connections, while small L result in rather short fibers. The weight w is the parameter which controls the expected number of segments. For low values, the reconstruction needs more segments to 'explain' the same signal portion. Reasonable values of w tend to be within $0.2stdev < w < 0.5stddev$ of the data, according to Reisert et al. [41].

The interplay of w, ρ and c is the most crucial part for obtaining good results.

3.4.4 Other tractography algorithms

Fast marching algorithms

The process of passage from one vector to another is modeled similar to the propagation of a water wave from the seed point: new points are generated from each point of the front, along a connectivity matrix; which is used to select a subset of pathways of connection.

The speed of the wavefront toward all directions is determined by the colinearity of the principal eigenvectors in the neighbour voxels, following the direction of the maximum propagation speed. More advanced algorithms can modify the propagation speed by the magnitude of the eigenvalues or resolve fiber crossing regions.

For example, in Parker et al.[42], the rate at which the front propagates is linked to the information contained in the main eigenvector field or to its embedded connectivity information (given by scalar product of the normal to the front in each position to weight propagation if is pointing towards).

Fiber tracking via fluid mechanics analogy

The information of the diffusion tensor is included by a modeling process based on the Navier Stokes equation, simulating an artificial fluid flowing through the data volume. The most likely connection paths between pre-assigned points are estimated by the gradient of the vector flow (a metric derived from the fluid velocity vector field).

Algorithms with a priori anatomic knowledge: Previous algorithms are based only on directional consistency or tract smoothness. First applies a global searching procedure to find anatomic connections, which are used to guide the subsequent fiber tracking process.

This method can improve the tracking accuracy, especially in the region of complex fiber crossing. On the other hand, normal anatomy cannot be extrapolated to pathological situations, although some studies used anatomic templates constructed from a specific group of patients to assist tractography. [43].

3.5 Limits of neural tractography

Most of the advancements in this field in the last decade have been in modeling the source of the signal variation in the presence of complex regions; leading to new modeling techniques, such as DSI, Q-Ball or SD. As tractography is the only tool currently available to study the connectivity of the brain in vivo, we must ask ourselves how far can these methods be relied on and what are their limitations to represent tissue connectivity.

These limitations can be summarized as:

- Directional consistency: The main parameter for fiber tracking; all the tracking algorithms use it as the major constraint. It risks having bias in favor of connecting fibers with similar orientations, highly curved fibers such as the Meyer loop may be easily missed meanwhile incidental consistency can lead to identify spurious tracts with no actual anatomic existence. This is also complicated by complex architecture (like twisting or branching or kissing or crossing zones) or the presence of noise. The estimation of the PDD shows high accuracy if the diffusion tensors has high FA values (and are less prone to noise influences), but if the first eigenvalue is not much larger than the second eigenvalue, the angular deviation from the true value could become rather large.

  Directional consistency between neighboring voxels (and showing successful tract connection) does not guarantee fiber integrity, even if directional consistency and fiber integrity are generally believed to be positively correlated.

- Estimation errors: Maybe the most important limitation of tractography in clinical neuroradiology. All the fiber tracks are only computational estimations based on tensorial information with presence of noise. The errors on step estimation, fiber direction and created by noise are all mutually integrated. It is difficult to isolate their influences independently. These errors accumulate, hence, longer the fiber path, is harder to reconstruct the path accurately. Also, different computers can have different levels of threshold error; therefore fiber tracks results may also be computer dependent.

- Data acquisition limitations (Spatial resolution, SNR, anisotropy misattributions): Limited resolution can affect the result of the tractography. According to Kim et al. [44], undersampling of the voxel size affects widely the distribution of fiber tracks.

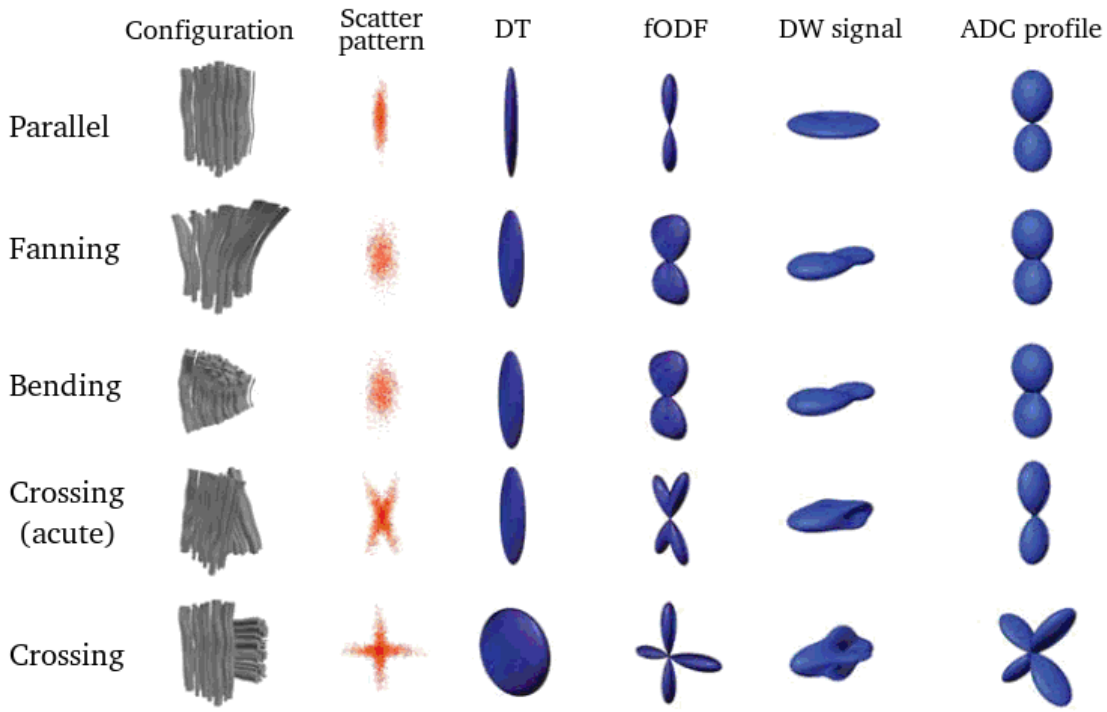

Figure 3.11: ODF estimation for different complex fiber configurations [48].

Usually, there is a exchange between SNR and spatial resolution: increasing spatial resolution results in a reduced SNR, which may affect the FA estimation (since there is a a systematic overestimation of anisotropy as noise increases) [45]. Increasing voxel size results in higher SNR and a reduction of the number of fiber tracts. Meanwhile, areas with low FA can suffer an overestimation, as noise can be interpreted as a random addition of directionality; FA value does not significantly vary along the fiber path due to differents spatial resolutions.

Accuracy of fiber directions is positively correlated with SNR. SNR can be increased at expense of scanning time or spatial resolution. Acquisition with isotropic voxel dimension is preferable for fiber tractography, though not absolutely necessary.

- Lack of validation: For any estimation method, the false-positive and false-negative rates determine the extent to which the method can be clinically useful. Unfortunately, DT MRI tractography results are hard to validate in vivo; hence, false-positive and false-negative rates are both unavailable. Studies with physical or synthetic phantoms and verification with animal experiments, are the only methods to test effectiveness of the estimations. Validation studies are mostly focused on limited aspects only and hence should not be extrapolated to the general situations.

One of the most important ideas that we must remark is that the elements of anatomical connectivity that are poorly known in the human brain are the ones that are challenging for tractography. The tractography main limitation comes from the fact that it is based on an estimation based on reduced anatomical information at voxel level, so often it is difficult to draw any conclusions about the exact cause of error at the cellular level.

The anisotropy is simply a measure of the mean square displacement of water molecules, not a measure of connectivity, but tractography uses it as a mean to obtain structural information. At each voxel, multiple fiber bundles with different orientations contribute to the final signal, and microscopic factors in cellular components may be override by macroscopic factors (for example, crossing fibers within a voxel can lead to isotropic diffusion properties).

Several factors can modulate the anisotropy measures, including the axon diameter distribution, the axon density, the myelination of the fibers, how are the individual axons orientated with respect to each other within

the voxel), and many others. This can lead to paradoxical observations:

Regions with the lowest anisotropy within deep white matter can often contain the largest number of axons: due to their incoherent orientations, diffusion displacements are no longer preferentially hindered along a single axis. In contrast, an elevation of anisotropy can be observed in diseases with selective destruction of one particular fiber orientation.

Another case. When FA is decreased, there can be at least three potential cases: (1) the longest axis of the diffusion ellipsoid is shortened, (2) the shorter axes are elongated, or (3) both of these happen simultaneously. Past studies have shown that myelin loss is correlated with an increase in perpendicular diffusivity, whereas axonal loss is related more to a decrease in the parallel diffusivity [46]. However, there is the possibility that such correlations are specific to the particular disease model used and may not always hold. For instance, histological correlation studies do not support the inverse relationship (e.g., axonal loss may lead to a decrease in the parallel diffusivity, but such a decrease may not necessarily mean axonal loss).

Studying a certain region of the optic nerve, Tuch et al. [49] found a linear correlation between reaction time and FA: higher the anisotropy, the longer the reaction time. This seems to be against the common idea that FA measures alone can provide a measure of efficiency of information transfer, but this anomaly can be explained by the fiber architecture in the vicinity of the region (where two main fiber populations merge at different orientations: from the corpus callosum and from the visual system). If the anisotropy of the visual system fibers is increased, potentially improving efficiency of information transfer, then the result is a reduction in anisotropy in the vicinity.

If this is extremely complicated, the effect of disease can confound matters further. This serves as a very strong argument against the use of voxel-wise measurements of FA to make inferences on connectivity and capacity for information transfer.

Nowadays, with the available data and algorithms, the only information that is calculated on the tractography maps is an estimate of the tangent to the space curve (either from eigenvector or a peak in some other reconstruction from HARDI data) and, for probabilistic tractography, the associated uncertainty. It does not reflect the the number of axonal connections or the capacity to carry information between two points between two points. Some of the challenges for the future of tractography as a tool in the study of the brain are:

- Create a publicly available ground truth for validation. It is difficult to objectively choose among the huge variety of diffusion models, tractography algorithms, and combinations thereof. A number of validation studies have been performed, but each has its drawbacks.
- Finding the exact termination point of a connection, a crucial matter for assessing side-to-side connectivity, both in radial and transversal accuracy. Radial accuracy means determining the cortical layers where a white matter connection ends (which gives information about hierarchical levels of cortical organization [52]). Transverse accuracy refers to the capacity of detecting where a connection first enters in the cortex (which provides a framework to understand functional specializations and interactions of the brain[53]); achieving fine grade transverse accuracy is difficult for two reasons: first because the spatial resolution limits of DTMRI and second because its measures are inherently noisy. In the practice tractography algorithms uses heuristic or macrovoxel termination criteria, so their ending points does not necessarily reflect the end point of a tract.
- Detecting collateral tracts.
- Tracking very dense networks, for example the horizontal intracortical regions.
- Discriminating between afferent and efferent connections.
- Detecting synapses and extract information about axon diameter distribution.

Some of the questions that are of particular interest in neurology, and nowadays cannot be answered by tractography are: Which cortical region send or receives which connections? Does a bundle of axons spreads when it reach the cortex? Do long association tracts send or receive adjunct connections? Is a bundle of axons a continuous long range connection between remote regions or is a succession of short fibers?

Also, it is important to remember that, although the connectivity map can give us a insight of the inner works of the brain, the orientation of a path (via the tangent to the curve) is insufficient to determine the potential to carry information of a connection.

In the next chapters we will try to study the effect of the intrinsic parameters of deterministic and probabilistic tractography in the results and we will explore new methods that can lead to better approximations of the structure of the brain.

Chapter 4

Materials and methods

In this section we will describe the details of the data, methods and processes used for our tractography experiments.

4.1 Materials

4.1.1 Patients and data acquisition

For the present study we have selected six healthy male controls, aged between 23 and 31 (mean age 27 years). All the data sets used in this work have been acquired in a GE Signa 1.5 T MR scanner at the Gregorio Marañon Hospital in Madrid.

Diffusion weighted MR images were acquired using a multi-shot pseudo-3D double spin-echo echo-planar imaging (SE-EPI) sequence with two phase encoding directions and four segments per pseudo-slice. Each patient was scanned nine times with nine different acquisition parameters resulting in a total of one hundred and sixty two scans.

There is no fixed set of parameters optimal for every application; optimization depends on the MR imaging hardware configuration, available scanning time, anatomic coverage needed, and specific anatomic structures to be investigated. The parameters employed are these:

- B-value: Volumes have been acquired with three different b-values: 800,1000 and 1300$\frac{s}{mm^2}$. A *b-value* of $1000s/mm^2$ has become the standard for clinical DWI.
- Spacing: The Field of View of the data spans for three different voxel size: $2 \times 2 \times 2mm^3$, $2.5 \times 2.5 \times 2.5mm^3$ and $3 \times 3 \times 3mm^3$. The matrix sizes varies between $96 \times 96 \times 53$ and $128 \times 128 \times 62$ voxels. The table 4.1 shows all the sizes of each data volume.
- Gradient directions: All the scans have been acquired with 61 gradient directions and one baseline volume. The gradient directions have been specially designed so the tensor volume can be calculated with 61, 40 or just 21 gradient directions. This subsampling technique allows us to measure the effect of the number of gradients in the tensor calculation error with just one data acquisition. Stronger and faster gradients enable stronger diffusion-weighting in a shorter period of time as well as reducing the time required to form an image. This permits DWIs to be acquired at a shorter T_E, which improves SNR and reduces warping artifacts.

The other diffusion acquisition parameters are $TR = 8$, $TE = 1.6ms$.

4.2 Methods

4.2.1 Tensor estimation

Diffusion at each voxel is modeled as a single tensor. More sophisticated and successful diffusion model exists, but the single tensor model is still one of the simplest and most used.

		r2	r2.5	r3
P1	b800	128 128 66	96 96 53	80 80 44
	b1000	128 128 53	96 96 53	80 80 44
	b1300	128 128 66	96 96 53	80 80 44
P2	b800	128 128 66	96 96 53	80 80 44
	b1000	128 128 53	96 96 53	80 80 44
	b1300	128 128 66	96 96 53	80 80 44
P3	b800	128 128 66	128 128 53	128 128 44
	b1000	128 128 66	128 128 53	128 128 44
	b1300	128 128 66	128 128 53	128 128 44
P4	b800	128 128 66	96 96 53	80 80 44
	b1000	128 128 66	96 96 53	80 80 44
	b1300	128 128 66	96 96 53	80 80 44
P5	b800	128 128 66	96 96 53	80 80 44
	b1000	128 128 66	96 96 53	80 80 44
	b1300	128 128 66	96 96 53	80 80 44
P6	b800	128 128 66	96 96 53	80 80 44
	b1000	128 128 66	96 96 53	80 80 44
	b1300	128 128 66	96 96 53	80 80 44

Tabla 4.1: RAS size for the datasets from the Gregorio Marañon

The tensor at each voxel must be estimated from the DWI channels (each channel acquired with a different gradient direction). But, as the acquired data presents a high level of noise, a filter pass is executed before the tensor estimation to improve the quality of the data while preserving the structures of the brain. This filter employs a Linear Minimum Mean Squared Error method (LMMSE). The LMMSE method uses classical linear functions and prior information about the noise distribution to improve the estimation of the signal. In the case of DWI data, the noise is known to have a Rician distribution.

The diffusion tensor (DT) models the diffusion profile in a voxel as a 3D Gaussian with three orthogonal eigenvectors or axis of diffusion (the major, median and minor eigenvector e_1,e_2 and e_3 and their corresponding eigenvalues l_1, l_2 and l_3). The diffusion tensor models the signal S for a diffusion-weighting direction $g = (g_x, g_y, g_z)$ with respect to the baseline weighted image S_0 as:

$$\frac{S}{S_0} = e^{-bg^T Dg} \tag{4.1}$$

The software used for tensor estimation of all the data was the DTItool developed by M. Reisert and V. Kiselev, at the University of Friburg.

4.2.2 Tractography process

Mask computing

Before any computation, the streamline and the global tractography methods require a mask computing step. The mask defines the points that will be used as seeds points.

First, an FA map is created (although a Trace map could also be used), and from a certain threshold value the mask is created. The mask isolates the brain tissue from the background and other non brain structures, such as the skull. This mask can be used to avoid doing computations outside the zones without real value.

Streamline tractography algorithm

The first tractography method used for the study is the Streamline tractography. It is the most simple, uses a fourth order Runge Kutta numeric integrator to create the fiber tracks, starting from a fixed seed point position,

as defined by the mask initiator. The line propagation is initiated for each seedpoint, both in the positive and negative direction of the local primary eigenvector.

The streamline tractography algorithm employed was developed by the LPI in the University of Valladolid.

The parameters used for streamline tractography were:

- Step size: A constant step size of $0.9mm$ was used for RK4 estimation; the tensor at each integration step being calculated using trilinear interpolation of the tensor elements in the neighborhood.
- Start FA limit: The FA value used as minimum threshold for using a voxel as a seed point was 0.35.
- Start Trace limit: The Trace value used as minimum threshold for using a voxel as a seed point was 0.02.
- Stop FA limit: The FA value used as maximum threshold for stopping the tractography process was 0.005.
- Stop Trace limit: The Trace value used as maximum threshold for stopping the tractography process was 0.002.
- Maximum angle between steps: 40
- Minimum number of steps fpr saving a fiber: 25.

4.2.3 Stochastic tractography algorithm

For our experiments, we have used the stochastic tractography method implemented by Friman et al. [38] in Matlab. It does not perform a whole brain tractography and requires a previous step for defining the starting seed points of the tractography. The ROI definition has been done with the DTITool implemented by Reisert et al.

The stochastic tractography algorithm employed was developed by O.Friman from the LMI, Brigham and Women's Hospital, Harvard Medical School, Boston.

From this selected points the tractography is repeated n iterations; and the resulting fibers and the connectivity information are stored. The parameters used for stochastic tractography were:

- Step length: $0.9mm$.
- Anisotropy stopping criteria: The tracking is terminated if the diffusion anisotropy is too low, as below of 0.05.
- Max $\frac{\beta}{\alpha+\beta}$: 0.15. Stopping criteria related to the eigenvalues, the main eigenvector and the estimate of the noise variance obtained from the residuals.
- Number of start positions: 100.
- Number of steps per iterations:120.
- Number of iterations: 1000.

4.2.4 Global tractography parameters

In [56], Reisert et al. suggest two series of parameters: a set of "sparse" parameters and a set of "full" parameters. The latter have far greater computational and memory requirements. For example, the first set can complete a whole brain tractography in four hours; the latter requires at least twelve hours. The tractographies used in our experiments have been generated with a set of "sparse parameters".

The Global algorithm method can be described as similar in spirit of statistical physics. The reconstruction is controlled by two energy terms: one of internal energy (E_{int}) that handles the behavior of line segments and one of external energy (E_{ext}) that expresses the similarity of the model to the data. Maximizing the probability is equivalent to finding the minimum of the total energy. The temperature represents the state of agitation of each particle, how probable is that it could break its connection to form another.

The parameters include the particle shape specifications. The width wi and length l control the maximum fiber curvature, and it is recomended that $l > 2 \times wi$. The weight w is a third parameter that controls the expected number of segments. For low values of w, the reconstruction needs more segments to "explain" the same signal portion than for high values. For higher weights, the segments get very sparsely distributed.

The global tractography algorithm employed was developed by M. Reisert and V. Kiselev, at the U.of Friburg.

The parameters used for global tractography were:

- Start temperature: 0.5.

- Stop temperature: 0.001.
- Number of steps: 50.
- Particle width: 1.5.
- Particle length: 4.5.
- Particle weight: 0.19. The weight is a crucial point in obtaining good results. The algorithm provides a rough estimate for w, in a more or less automatic way, as the standard deviation of the meanless signal (around $0.2 \times std < w = 0.5 \times s$).
- Density penalty: 0.2.
- Probabilities employed: $p_{birth} = 0.25$, $p_{death} = 0.05$, $p_{shift} = 0.15$, $p_{opt} = 0.1$, $p_{fiber} = 0.45$.
- Number of iterations: 5×10^7 iterations.
- Range of allowed fiber length: From 10 to 150 mm.

4.3 Spatial Filtering

The result of the tractography step is usually a big volume of connected fibers. To extract values from this data is necessary to do a previous spatial filtering step. Tracked fibers were filtered by a combination of maximum length, main orientation and logic ROI filtering. Each group of fibers was separated by three ROIs working as an AND filter group.

Regions of interest (ROIs) were drawn as contiguous patches of voxels on coronal and Sagittal slices through the left and right cingulum bundle, the inferior fronto-occipital fasciculus and the corticospinal tract, according to the points suggested by Mori et al. [57] and described in the chapter 2. The software employed for the spatial filtering was the Saturn, developed at the University of Valladolid [64].

All the data has been processed on a Toshiba laptop with four cores i7-740QM, working with an Ubuntu 12.02 OS.

Chapter 5

Software additions to Saturn (Software Application of Tensor Utilities for Research in Neuroimaging)

5.1 Introduction

Saturn (Software Application of Tensor Utilities for Research in Neuroimaging) is a software program developed at the Laboratory of Image Processing at the University of Valladolid specially designed for visualization and quantitative analysis of DT images. It includes a complete set of visualization capabilities to browse and analyze efficiently DTI data, making it a powerful tool for research and diagnostical purposes. Saturn has been presented in several papers and conferences, such as [58, 62, 63], and has been used in several studies of neurological diseases. In [61], Saturn was used to compare robustly fiber bundles affected by tumors with healthy fiber tracts from control subjects and also to quantify the relative state of degeneration between the fiber tracts in the two hemispheres of the same patient. Also, Saturn had been used in [60], to analyze the fiber structures, like the corticospinal tract, in brain white matter to characterize different subjects, either patients or controls. This paper also proposes some measures such as integrity, discontinuity and connectivity of the fiber bundles. For this

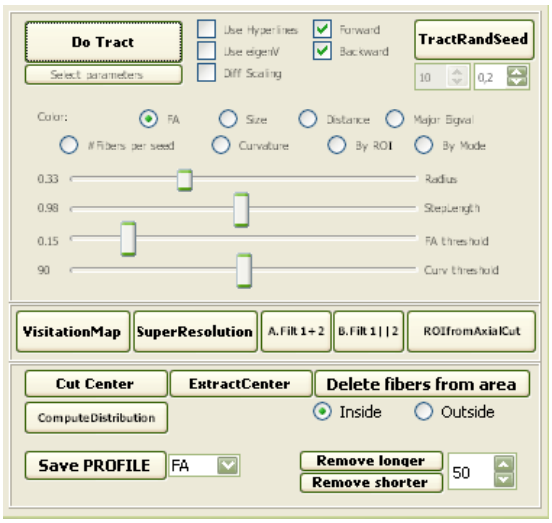

Figure 5.1: Additions to the GUI.

project, new additions have been developed for this software, which have been used for the development of this project. These new methods include improvements in the Graphics User Interface (GUI), new fiber selection and

3d model editing tools, new spatial filtering methods based on regions of interest, a user tool to create visitation maps of tridimensional fiber models, and a random seeding method to create tractographies starting from random positions within a voxel.

These additions have been included in the last version of the SATURN software, available at [64] and are currently used for future DTI research studies.

5.2 Additions in the GUI

The main panels of GUI in the program have been modified for this work, as can be seen in the fig. 5.1. Buttons associated with different functions have been rearranged to facilitate its use. For example, in the figure 5.1 different buttons from different panels used for fiber editing have been arranged together.

Another addition of the GUI are the dialog windows. The dialog in the fig. 5.2 appears each time a new DW dicom image is loaded, and offers the possibility of flip the volume along each one of the three main axes.

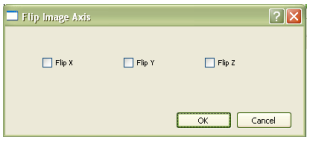

Figure 5.2: Flip DWI loading directions.

5.3 New tools

5.3.1 Fiber selection tool

One of the most useful changes added for this work is the fiber selection tool. This tool work as an interaction method over the 3d viewer window. It can be activated by clicking on a checkbox situated over the viewer, as is shown in fig. 5.3.1.

When is active, this interaction method blocks the camera over the tridimensional scene. Then, to select a single fiber or a bunch of fibers on the display, the user just have to click and drag over them. The selected rectangular area defines six planes between the frustrum of the camera and the infinity. These six planes can be used to select, extract, highlight, delete or enhace the tridimensional data represented on the scene.

This simple tool is useful, quick and precise and can facilitate in great way the user interaction with the data. The next section shows an implementation of a tool that uses this interaction method.

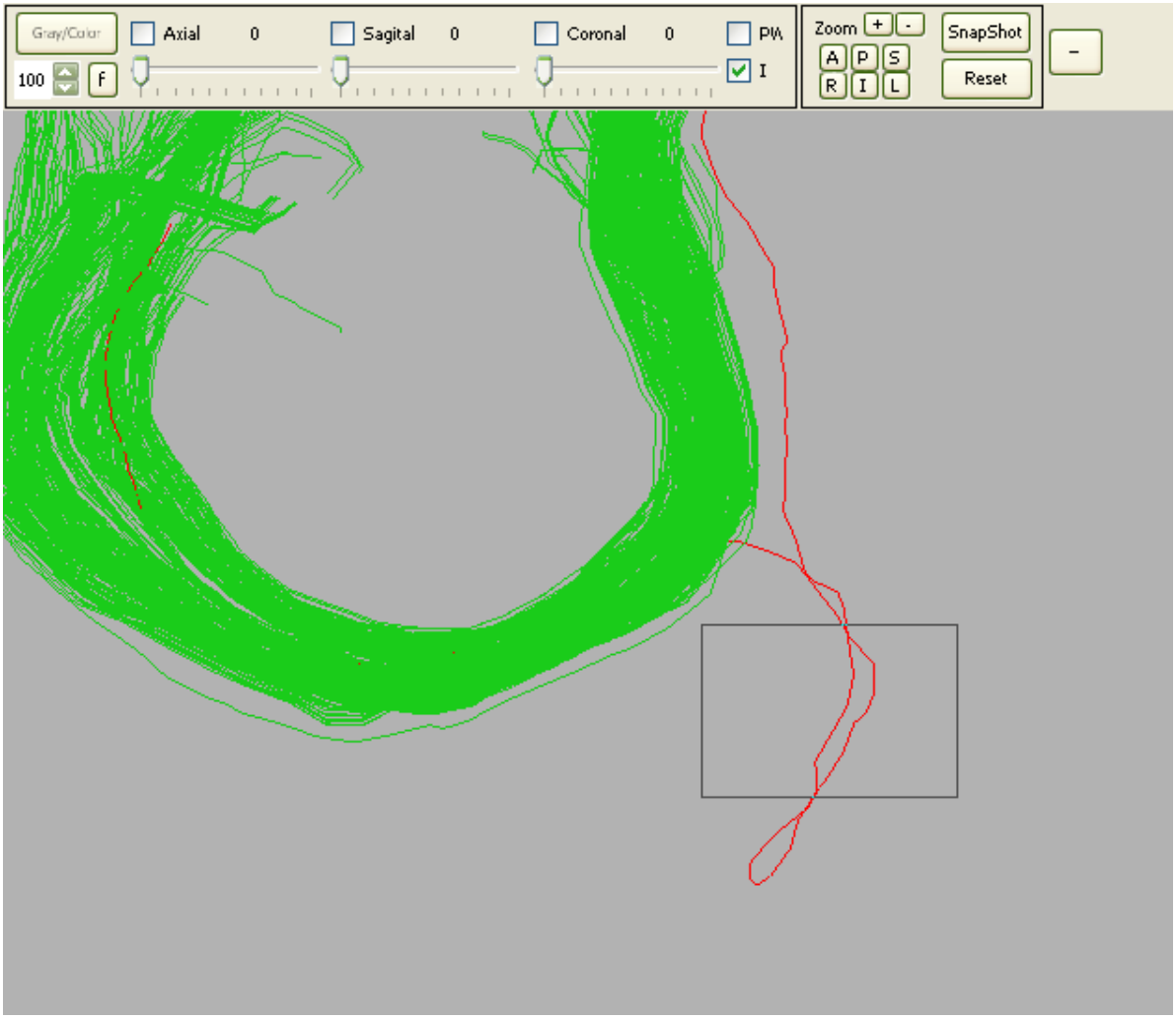

Figure 5.3: Interactive fiber selection.

5.3.2 Fiber deleting tool

For a selected tridimensional area and a tridimensional model, this function goes through every cell in the model. If any point of the cell is located within this area the whole cell is discarded. This method used in conjunction with

Figure 5.4: Delete fiber tool panel.

the method described in the previous section can be used to remove spurious fibers from a tractography. It also can be used with other already implemented deleting tools, for example it can remove only the fibers that have a certain condition, such as remove fibers longer or shorter than the mean fiber length. Other implementation of the same filter uses an absolute metric value to delete those fibers over or below a certain length.

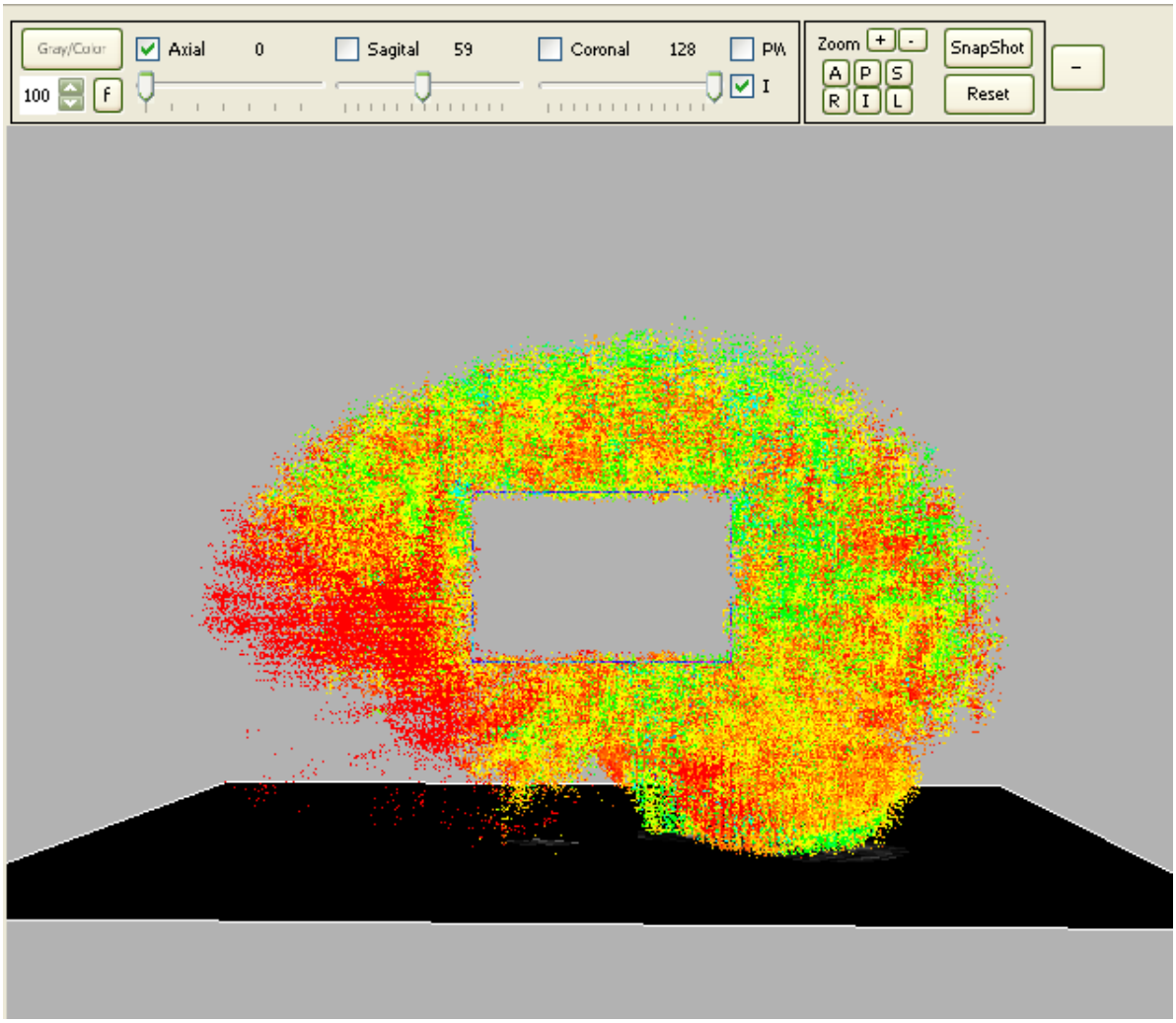

Figure 5.5: Interactive fiber deleting tool.

5.3.3 Deleting fibers by size

This function allows to entirely delete fiber longer or shorter than a given physical distance.

Figure 5.6: Delete fibers by distance panel.

5.3.4 Spatial filtering methods based on ROIs

Removes all the fibers in a tridimensional volume except those that pass through certain regions. These regions are selected by the user by drawing them over the scalar data volume shown in the active 2D viewer of the program. It can be used as a logic filter (AND or OR filter), selecting fibers that pass through at least one of these regions, or at least two or through all the active regions created by the user.

Figure 5.7: Fiber filter by ROI panel.

5.3.5 Fiber visitation map creator

Creates a mask of all the voxels that a fiber model visits and saves the result as a raw volume file. This file can be used as a ROI mask to create new tractographies or a more precise fiber spatial filtering tool (as explained in the previous point).

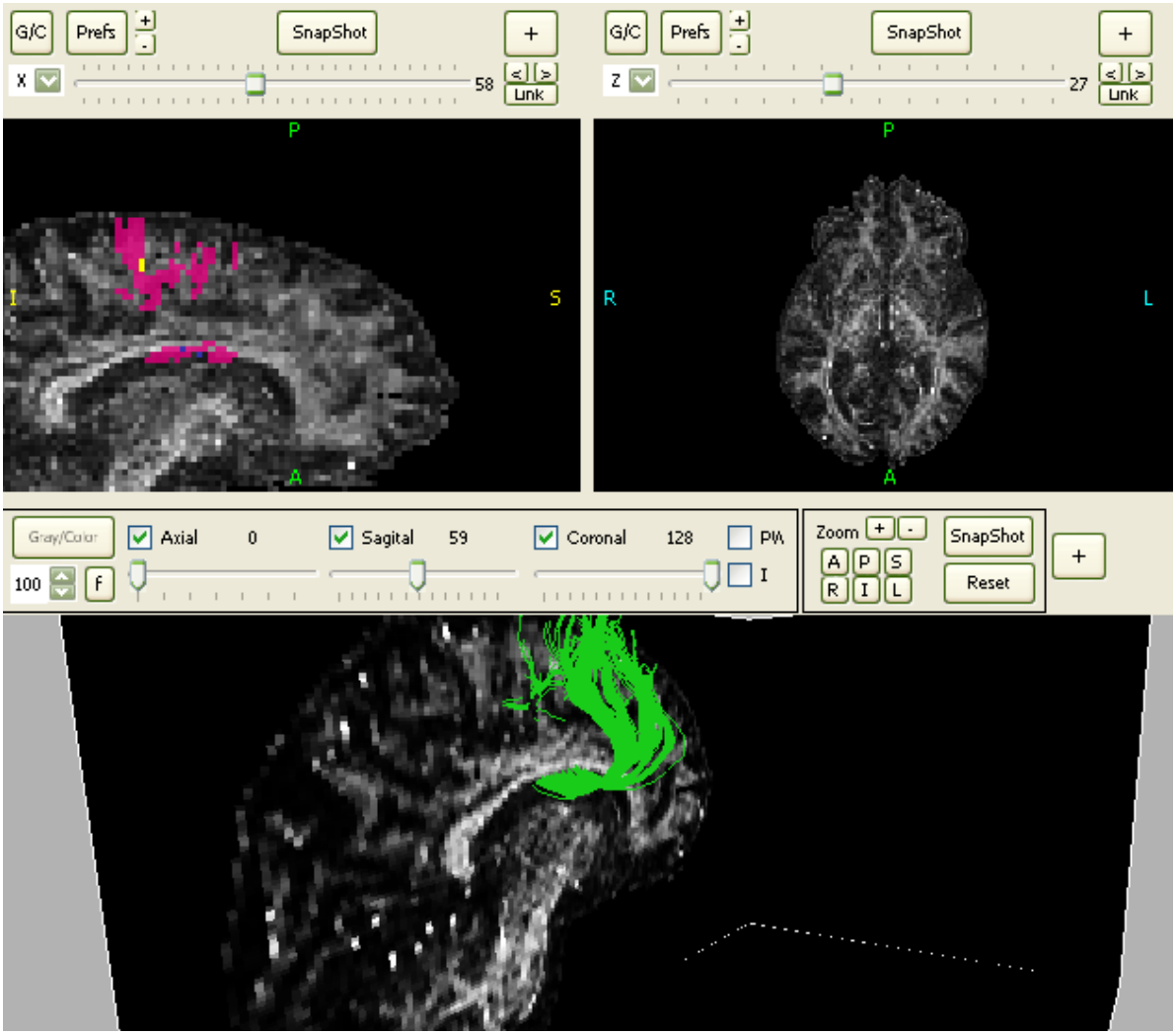

Figure 5.8: Example of fiber visitation map.

For example, this method was used in this work to filter the models of the inferior occipito-frontal fasciculus from a whole brain tractography. First, using the maximum length fiber selection tool and the spatial orientation tool, we could quickly obtain a few fibers that we positively knew were part of this fasciculus.

Then we used these few fibers to create a visitation map, that later was used to separate all the fibers from the whole brain tractography from all the fibers that passed through this region. The result is a precise approximation of the fasciculus; a fiber model that later can be used to extract DT measures and make comparisons between patient groups.

5.3.6 Random seed tractography tool

In the standard Runge-Kutta streamline tractography, each voxel covered by an active ROI mask is used as seed. This seeds works as stringting points for tractography: from the center of each voxel, starts integrating a line from the center of the voxel through the tensorial volume, until certain threshold conditions are reached.

With random seed tractography, each voxel is used as starting point for n fibers; not from the center of the voxel but from random positions within it. The user can select the number n of fibers generated per voxel and the dispersion from the center (in millimeters). The seed placement was implemented in $C++$ and follows a

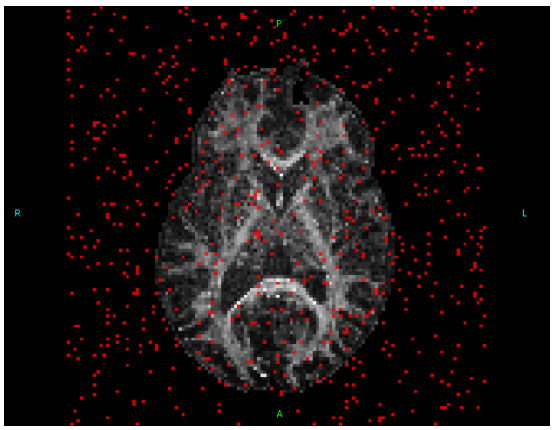

Figure 5.9: Random seed example.

uniform random probability distribution.

Using random seeds helps to visualize the estimation errors created during the numerical integration caused by the different staring points.

5.3.7 Profile extractor for fiber tracks

One of the means used to compare different tractography methods are their DT values along certain fibers. This tool extracts those scalar values, for a previously defined fiber bundle track, and displays them into a bidimensional color map. First, the fiber tract data is used as basis to create a k-dimensional tree data structure which later

Figure 5.10: Profile extractor panel.

will be used for a nearest-neighbour point search. The user must define a series of points that follow the main direction of the fiber track; this rough model is used to create a smoother parametric spline model.

The spline is placed over the fiber track, so each point of it can be used to find all the fiber point within a certain radius, that then are projected over the spline. Different fibers can be in the range of each spline point, so the values are added by rows (each row correspond to a different fiber).

The whole data is exported to Matlab, where the map shown in fig. 5.3.7 is created. The x-axis represents the length of the whole track in millimeters, (in this case the cingulum, from the frontal lobe to the hippocampus), the y-axis represents each one of the fibers tracks calculated. The scalar values are represented by the color, in this example the FA is represented.

5.3.8 Superresolution track density imaging method

Also, for this project we have implemented the Superresolution Track Density Imaging (TDI) proposed by Calamante et al.[55]. If one major limitation of current methods is the spatial scale, this method uses the fiber count visitation map created by random seed tractography to reveal structures beyond the resolution of the acquired imaging voxel. A unique property of these maps is that their spatial resolution and signal-to-noise ratio can be tailored depending on the chosen image resolution and total number of fiber-tracks generated. An example can be seen in the figure 5.3.8.

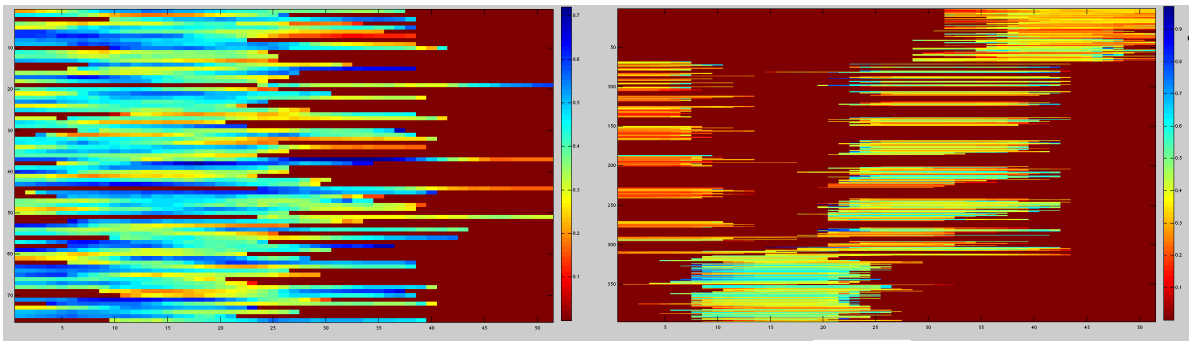

Figure 5.11: Profile map example for two different tractography methods, left -global tract, right -streamline tract.

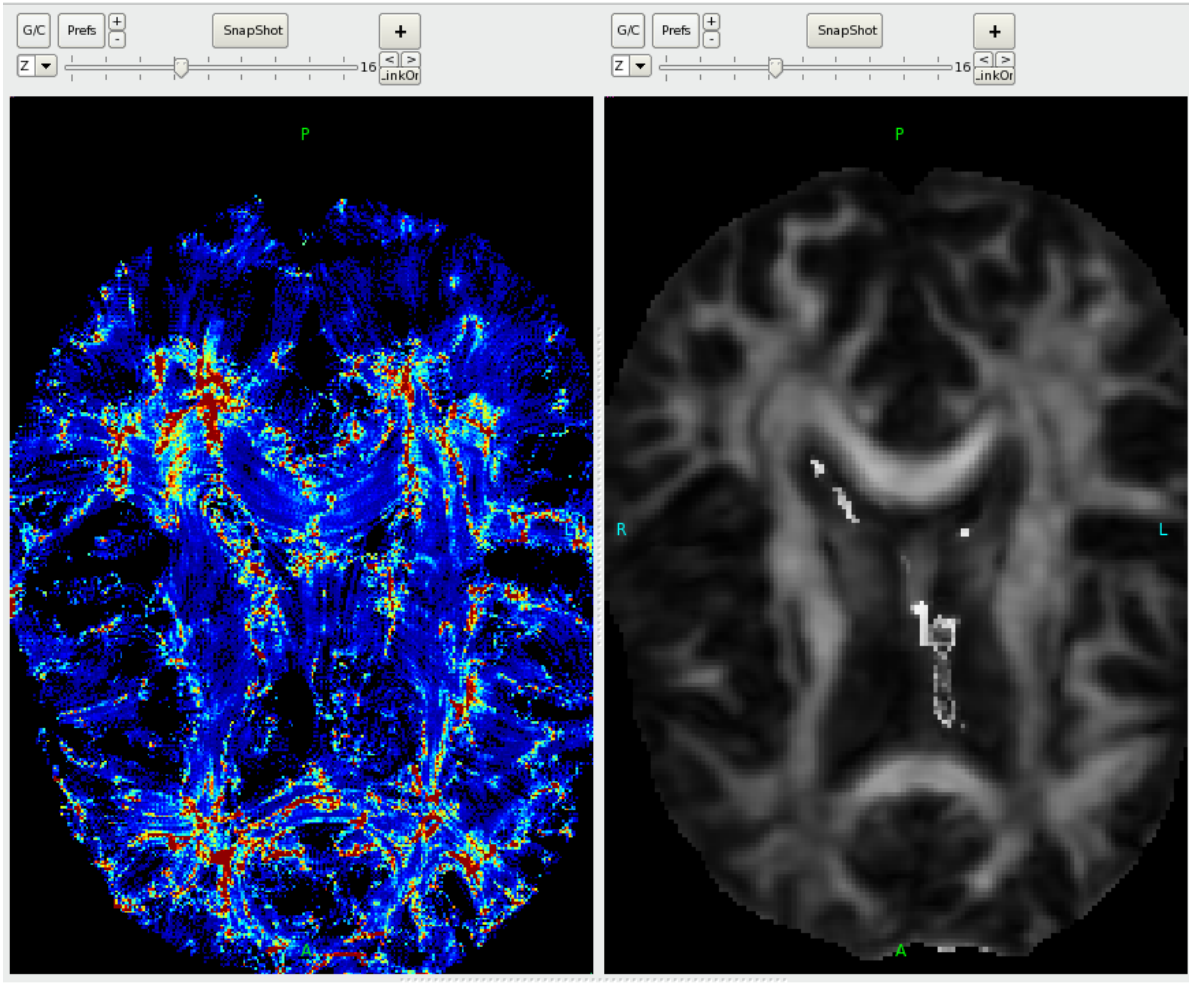

Figure 5.12: Superresolution TDI example.

Chapter 6

Results

This chapter describes the results of the experiments conducted with different acquisition parameters for three different tractography methods: streamline, global and stochastic.

In the fig.6 we can see one example of the reconstructed fibers with Global tractography; while in the fig.6 we can see the results with streamline tractography. The reconstructed tracts are:

- Corpus Callosum, in yellow.
- Left and right Cingulum, in dark red.
- Left and right Corticospinal tract, in green.
- Left and right Inferior Occipito Frontal Fasciculus, in blue.

At first sight, the streamline tractography reconstruction seems more direct and clean while the global tractography seems more disperse and untidy, some of its fibers even follow strange loops. But we must remember that it doesn't exist a real validation process for brain tractography.

We have studied two different kind of data: First, the number of successfully reconstructed fibers and second, the mean and standard deviation of the mean values of FA fiber profiles.

6.1 Reproducibility studies

The number of successfully reconstructed fibers can help us to understand the reproducibility of each tractography method for each acquisition method.

We understand successfully reconstructed fiber as a fiber that goes through three preselected ROIs (as were defined onto chapter 4. To illustrate better the connectivity between the three ROIs we present this value as the normalized scalar R, calculated as the absolute value of the difference between the number of fibers and the maximum number of fibers of that reconstruction. The value of R ranges from zero to one.

$$R = \sqrt{\left(\frac{N_{max} - N_{fibs}}{N_{max}}\right)^2} \tag{6.1}$$

We have grouped the reproducibility values by brain zones and patients into the figures 6.1, 6.1 and 6.1. The full tables of connectivity for all zones and patients can be seen in the Appendix B.

6.1.1 Reproducibility of the Corpus Callosum

In global tractography

The figure 6.1 shows the results for Corpus Callosum. For Global tractography, there are usually low values for higher b-values. For most of the patients, the values seem higher at $b = 800\frac{s}{mm}^2$. There also a clear correlation between the number of gradients and the reproducibility values. For lower number of gradients, more fibers crosses the three ROIs. The lower R results usually appear for $b = 1300\frac{s}{mm}^2$ and spacing of $r = 2.5mm$. Higher values of R appear at $b = 1000\frac{s}{mm}^2$ and $r = 2mm$. There are normally high values for all the $r = 3mm$ cases.

The figure6.1.1 shows the mean and standard deviations of all the patients for the different parameters. Higher b-values get higher variance. The maximum variance appears for $b = 1000\frac{s}{mm}^2$ and $r = 2mm$.

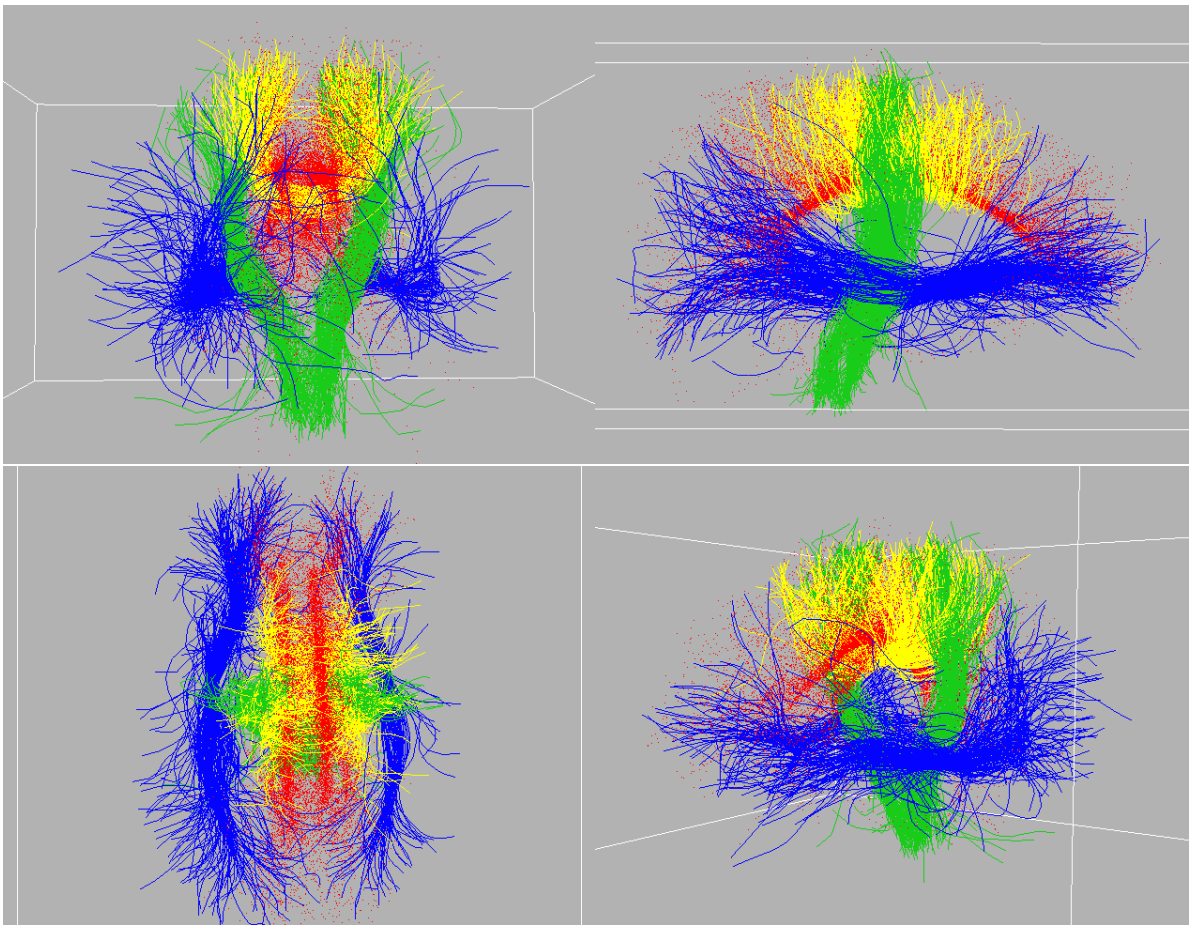

Figure 6.1: Reconstructed fibers with Global tractography.

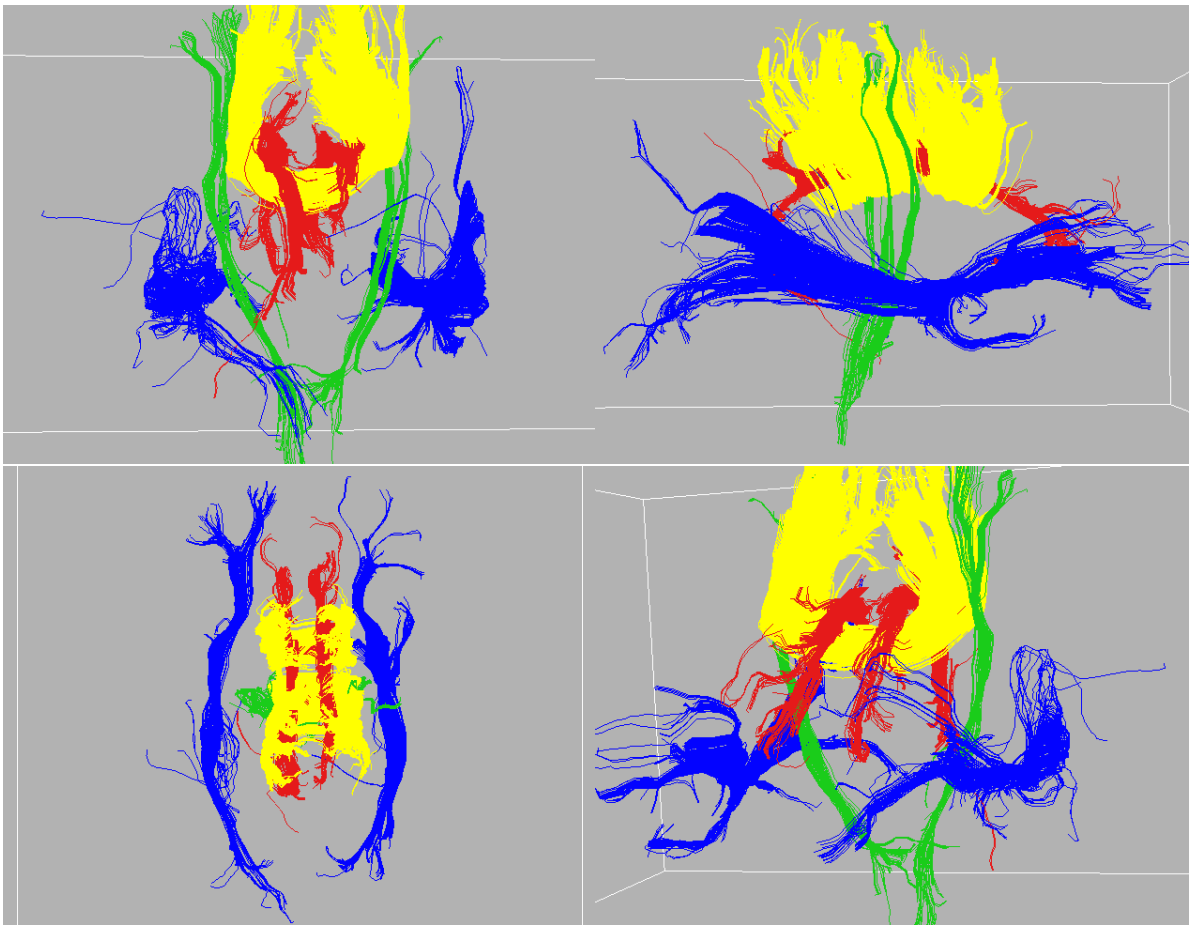

Figure 6.2: Reconstructed fibers with Streamline tractography.

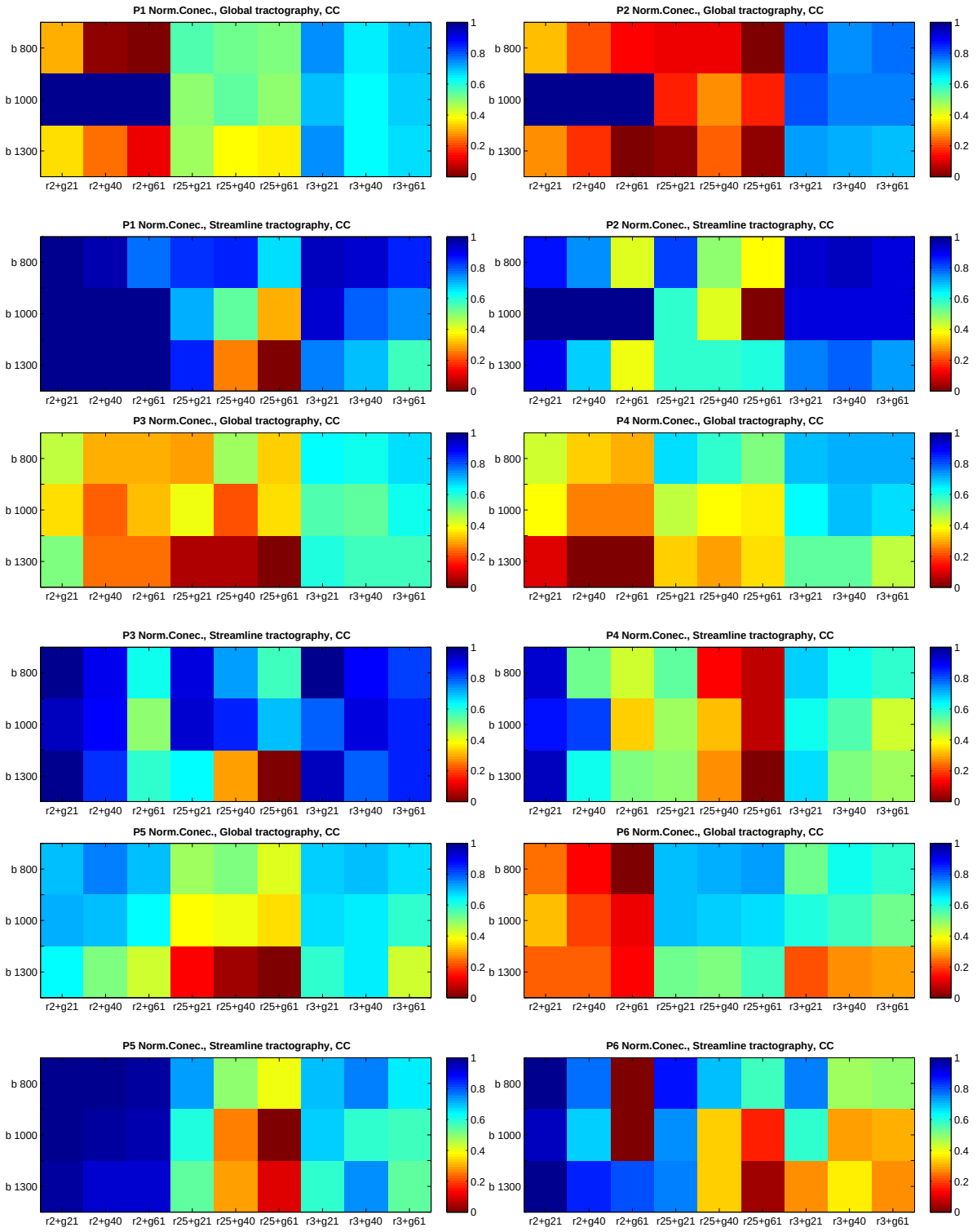

Figure 6.3: Normalized fiber count, Corpus Callosum, for global t.(up) and streamline t.(down).

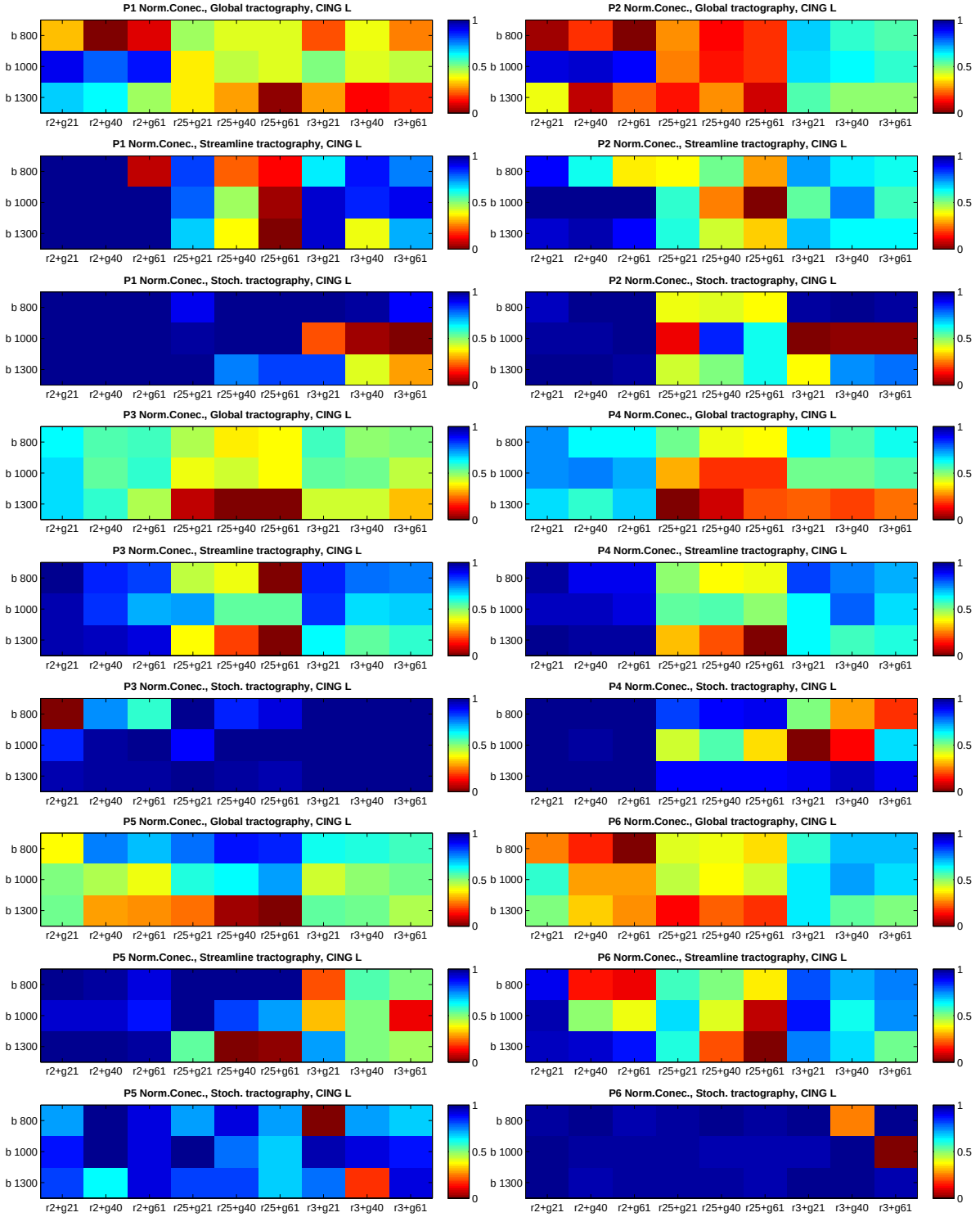

Figure 6.4: Normalized fiber count, Left Cingulum, for global t.(up), streamline t. (middle) and stoch. t.(down).

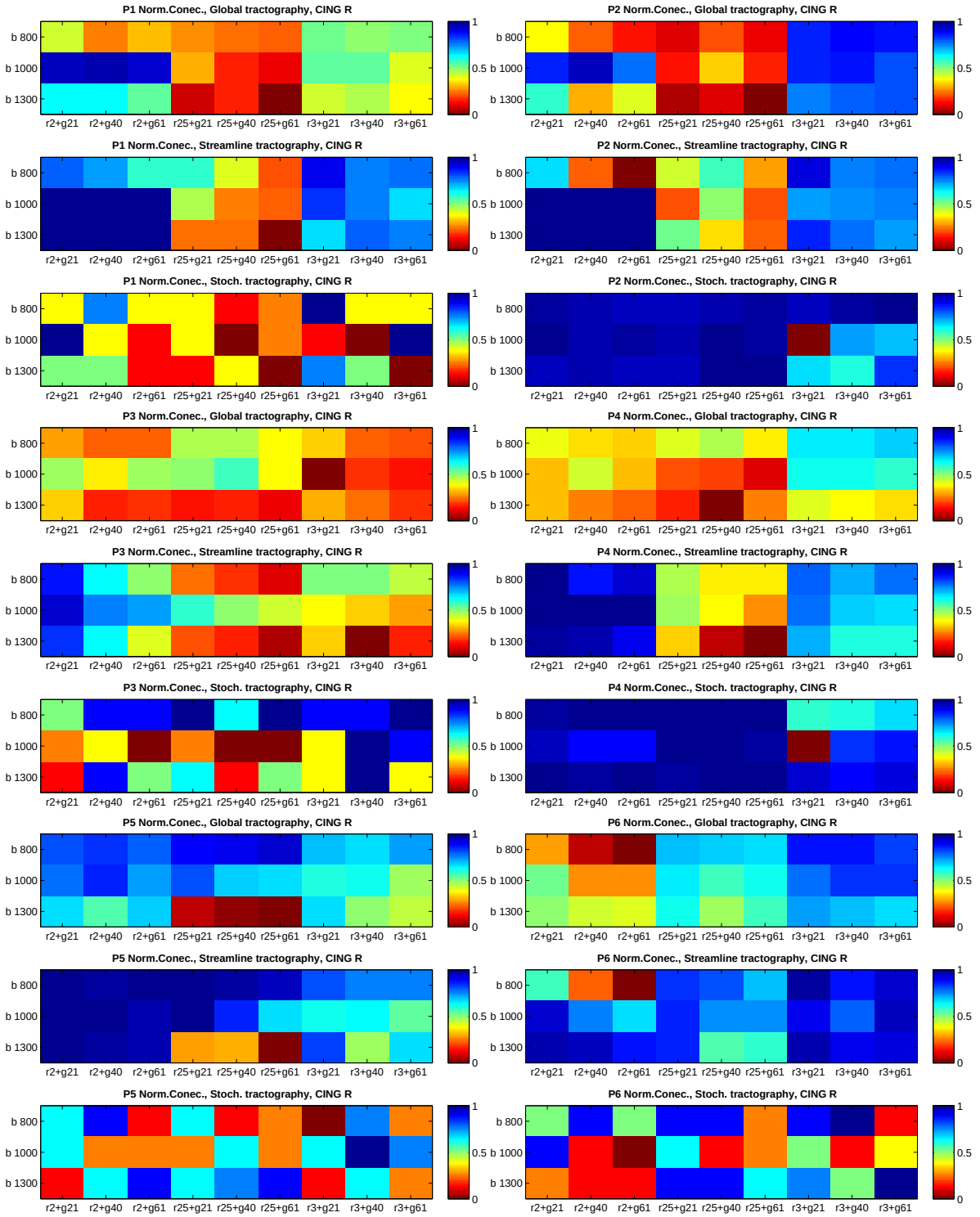

Figure 6.5: Normalized fiber count, Right Cingulum, for global t.(up), streamline t. (middle) and stoch. t.(down).

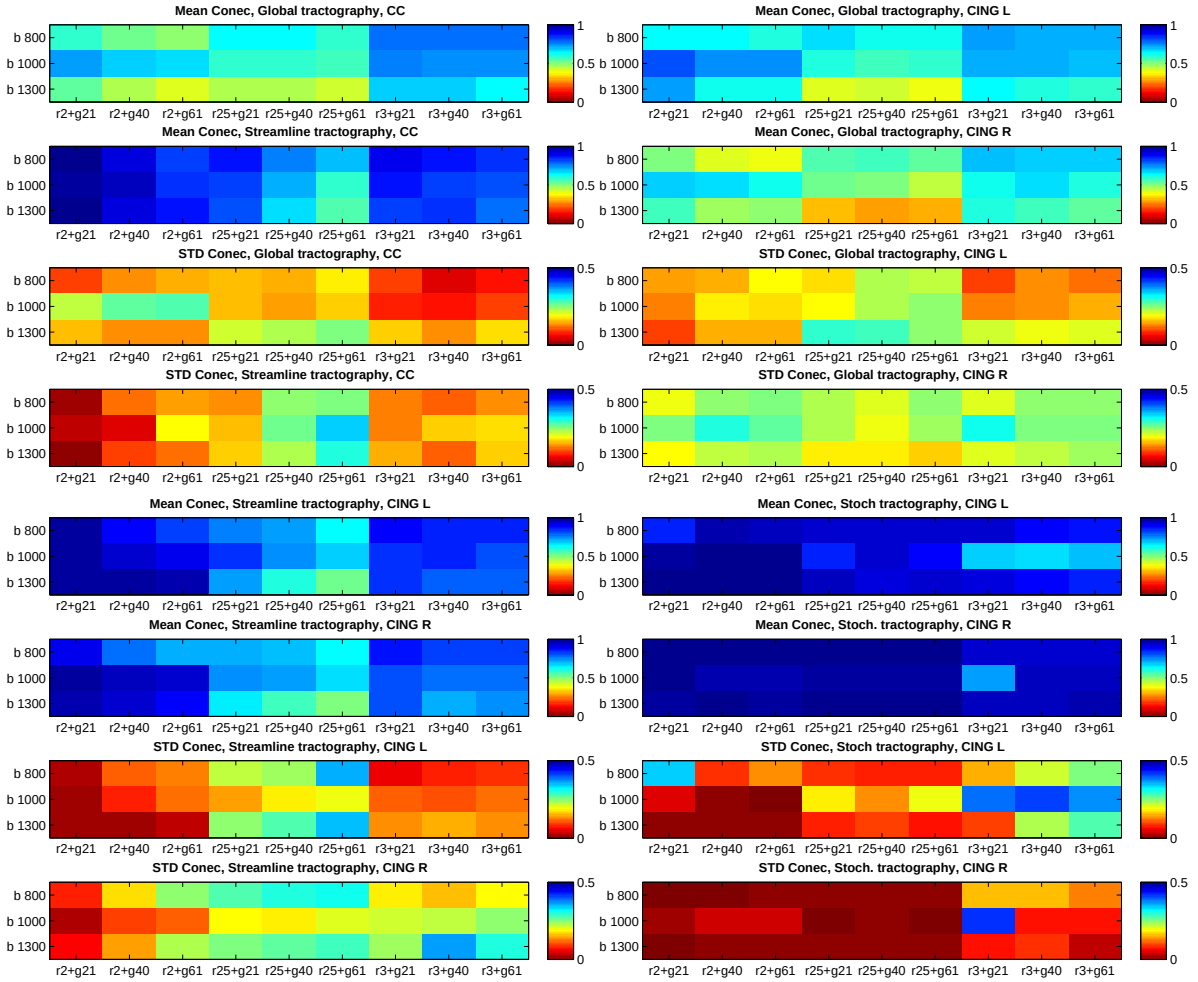

Figure 6.6: Mean and Standard Deviation of the connectivity for Global, Streamline and Stoch. tract., Corpus Callosum, Left and Right Cinglum.

In streamline tractography

For Streamline tractography, also seems to be a correlation between low b-values and high R; and a correlation between low number of gradients and high R. The values at $r = 2.5mm$ seem worse that those calulated with Global tractograhy. It is remarkable that Streamline tractography produces a much higher absolute number of correct ly reconstructed fibers.

The means and standard deviation values of Streamline t. follow the same patterns than the Global t. The variance of the values at $r = 2.5mm$ is higher than those at $r = 3mm$ and those of $r = 2mm$. A high number of gradients also seems to be related with higher variance.

6.1.2 Reproducibility of the Left Cingulum

The figure 6.1 shows the results for the left Cingulum.

In global tractography

Again, the maximum values seem to appear at $b = 1000\frac{s}{mm}^2$ and $r = 2mm$, and the minimum at $b = 1300\frac{s}{mm}^2$ and $r = 2.5mm$. The relation between number of gradients and number of fibers also can be seen here.

The number of R for $b = 800$ is usually higher than for $b = 1300$, but there are exceptions like in patient 5.

This time the maximum variance appears for $b = 1300\frac{s}{mm}^2$ and $r = 2.5mm$ and the minimum variance at $b = 1300\frac{s}{mm}^2$ and $r = 2mm$ and at $b = 800\frac{s}{mm}^2$ and $r = 3mm$.

In streamline tractography

For most of the patients, the R values seem to be higher for b-values of $b = 1000$, slightly lower for $b = 800$ and been lowest for $b = 1300\frac{s}{mm}^2$. For spacing, the R values seem to be higher for $r = 2$, slightly lower for $r = 3$ and been lowest for $r = 2.5mm^3$.

The maximum values appear at $b = 1000\frac{s}{mm}^2$ and $r = 2mm$ and the minimum values at $b = 1300\frac{s}{mm}^2$ and $r = 2.5mm$, which are also the parameters that get the maximum variation. The minimum variation appear at $b = 1300$, $r = 2mm$ and at $b = 800$ and $r = 3mm$.

In stochastic tractography

There does not seem to be clear patterns on the values of stochastic tractography, or at least their values are not consistent with the other two methods. The reproducibility values seem very similar for a few patients and very variable for others.

The mean values of the patients combined are consistently high, and their standard deviation is low for high values of b and very high for $b = 1000$ and $r = 3mm$.

6.1.3 Reproducibility of the Right Cingulum

The figure 6.1 shows the results for the right Cingulum.

In global tractography

As in the previous zones, the maximum values seem to appear at $b = 1000\frac{s}{mm}^2$ and $r = 2mm$, and the minimum at $b = 1300\frac{s}{mm}^2$ and $r = 2.5mm$. The number of gradients again have a inverse relation with the reproducibility value, as like the $b - values$. The spacing seems to affect the R value, as $R_{r=2mm} > R_{r=3mm} > R_{r=2.5mm}$, except for patients six and four.

The standard deviations are higher than those of the left cingulum, but more constant. The maximum variance appears for $b = 1000\frac{s}{mm}^2$ and $r = 2mm$ or $r = 3mm$ and the minimum variance at $b = 1300\frac{s}{mm}^2$ and $r = 2.5mm$.

In streamline tractography

The maximum values are at $b = 1000, 1300\frac{s}{mm}^2$ for $r = 2mm$, and the minimum at $b = 1300\frac{s}{mm}^2$ and $r = 2.5mm$,$g = 61$. The effect of the number of gradients is still shown. In this case, high b-values seem to gt higher reproducibility values.

The maximum variance starts for $r = 2.5$ and $b = 800, 1300$; meanwhile the minimum appears at $b = 1000$ and $r = 2mm$.

In stochastic tractography

Again, it does not seem to be a pattern on the values of stochastic tractography. There is small variance for spacing values of $r = 2, 2.5mm$. The maximum variance appears at $b = 1000$, $r = 3mm$ and $g = 21$.

6.2 Profile comparison studies

From the filtered fibers we have extracted their mean values of FA, as was explained in the chapter 4. These fiber profiles contain the mean and standard deviation of FA per each fiber. Here, in the figure 6.2.2 the standard deviations for all patients and tractography methods are represented.

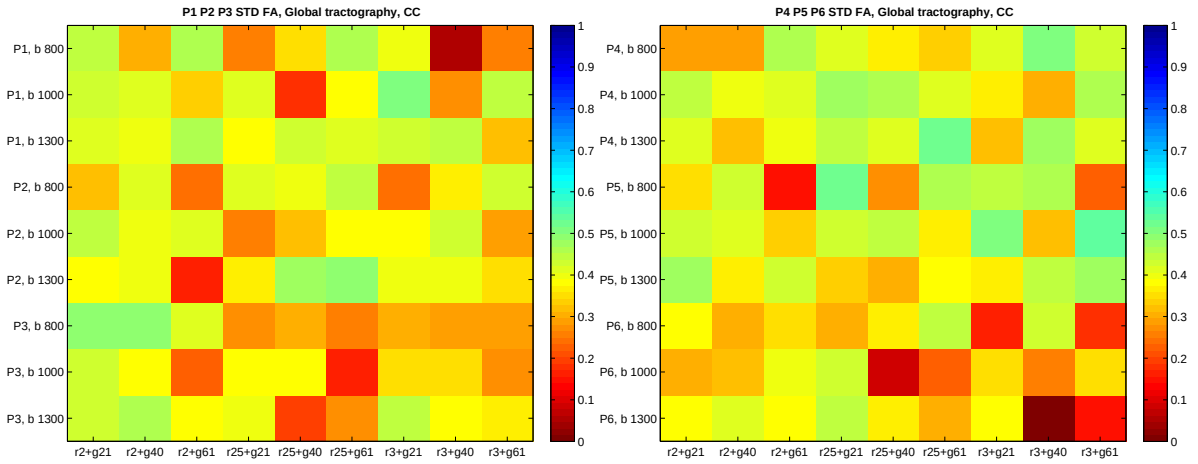

Figure 6.7: Standard Deviation of FA from the fiber profiles separated by patients, Global t., Corpus Callosum.

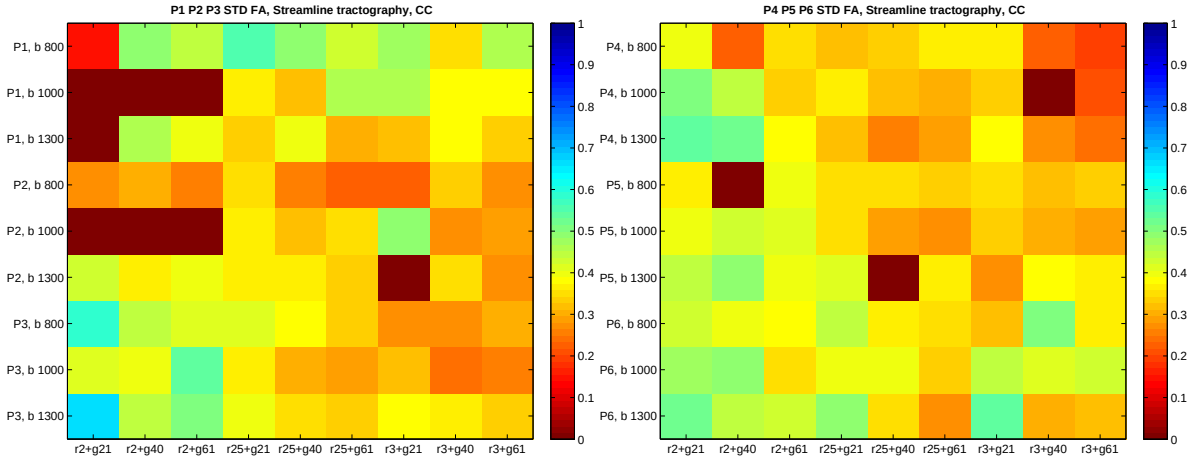

Figure 6.8: Standard Deviation of FA from the fiber profiles separated by patients, Streamline t., Corpus Callosum.

6.2.1 In Corpus Callosum

For both global and streamline tractography there seems to be profile differences caused by the different spacing configurations and number of gradients. Lower values of r have higher deviations and viceversa. Also, tractographies from lower number of gradients $g = 21$, have higher variability than those of high number of gradients $g = 61$.

6.2.2 In Left and Right Cingulum

Our calculations for left cingulum profiles have a lot of null values, so we must be particularly careful in order to interpret the results. The global tractography profiles seem to suggest that a low number of gradients leads to higher variability (like the Corpus Callosum results) and the same happens with lower b-values.

Global tractography seems to have lower variability than Streamline tractography.

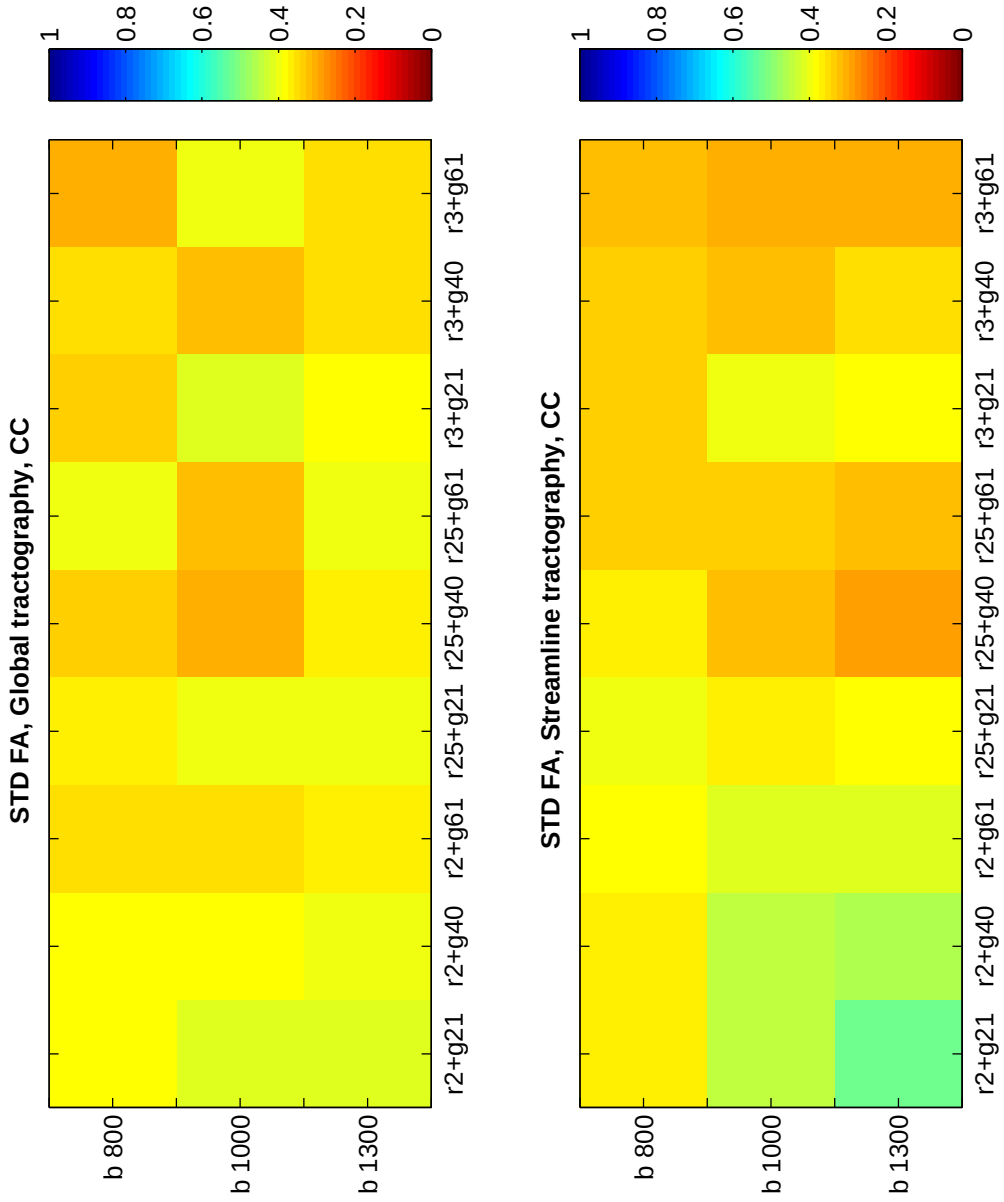

Figure 6.9: Standard Deviation of FA from the fiber profiles, Global(up) and Streamline t.(down), Corpus Callosum.

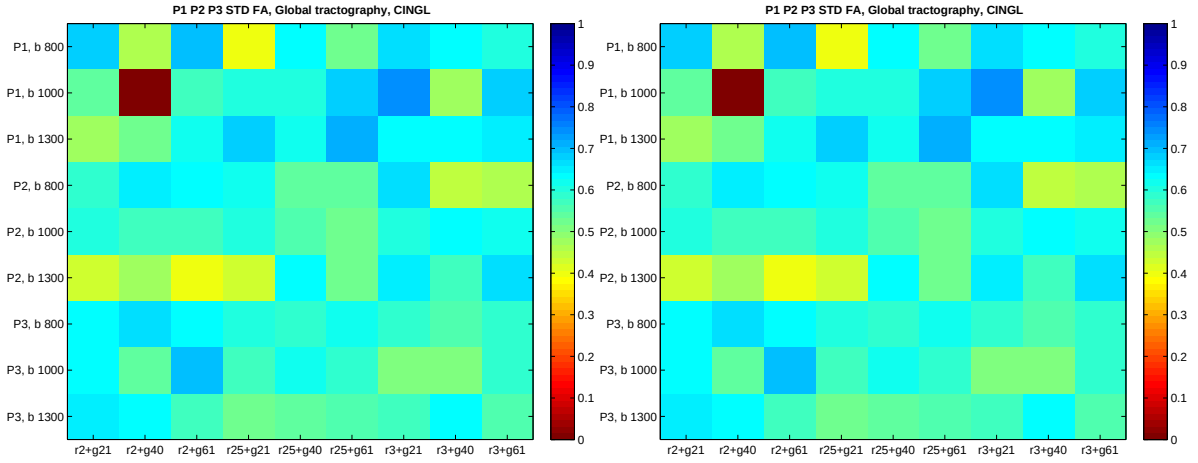

Figure 6.10: Standard Deviation of FA from the fiber profiles separated by patients, Global t., Left Cingulum.

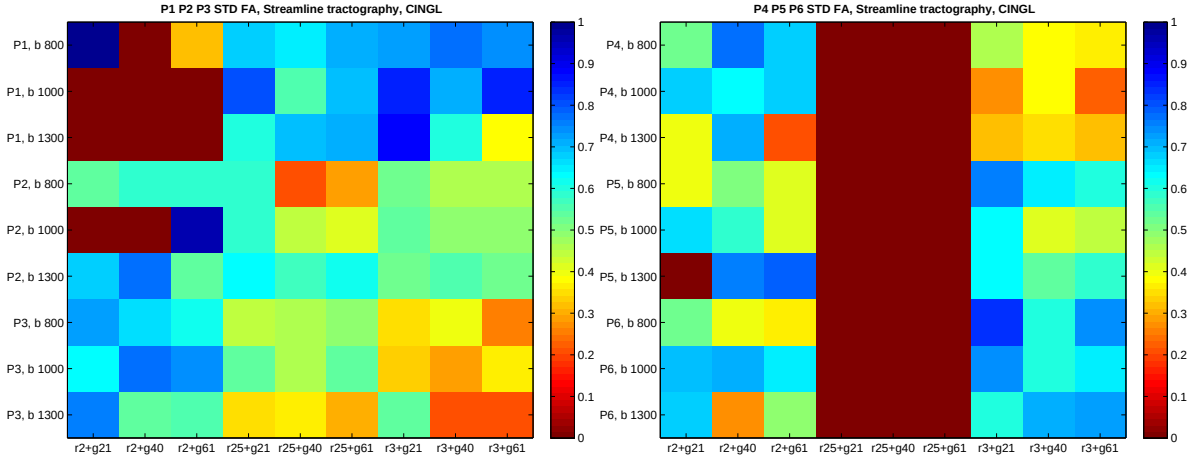

Figure 6.11: Standard Deviation of FA from the fiber profiles separated by patients, Streamline t., Left Cingulum.

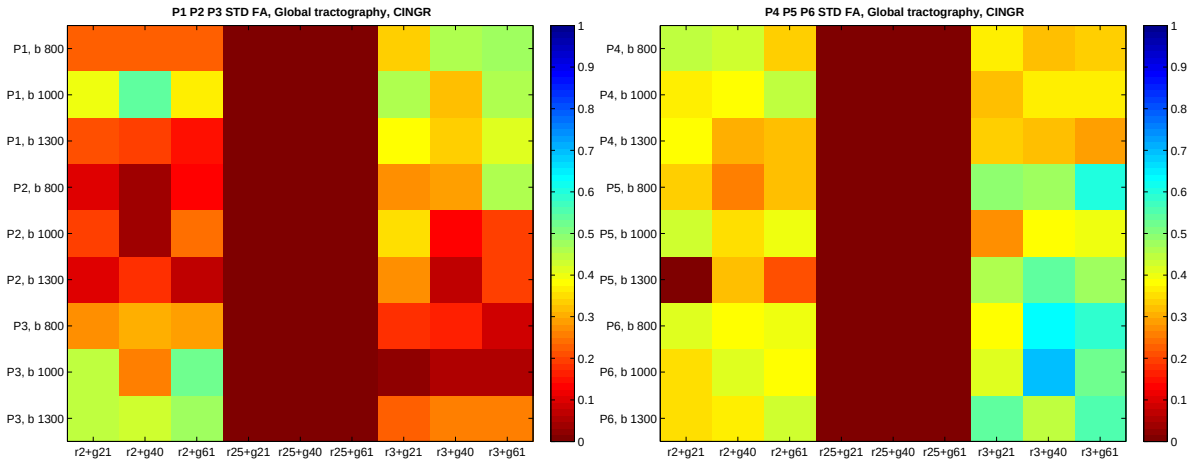

Figure 6.12: Standard Deviation of FA from the fiber profiles separated by patients, Global t., Right Cingulum.

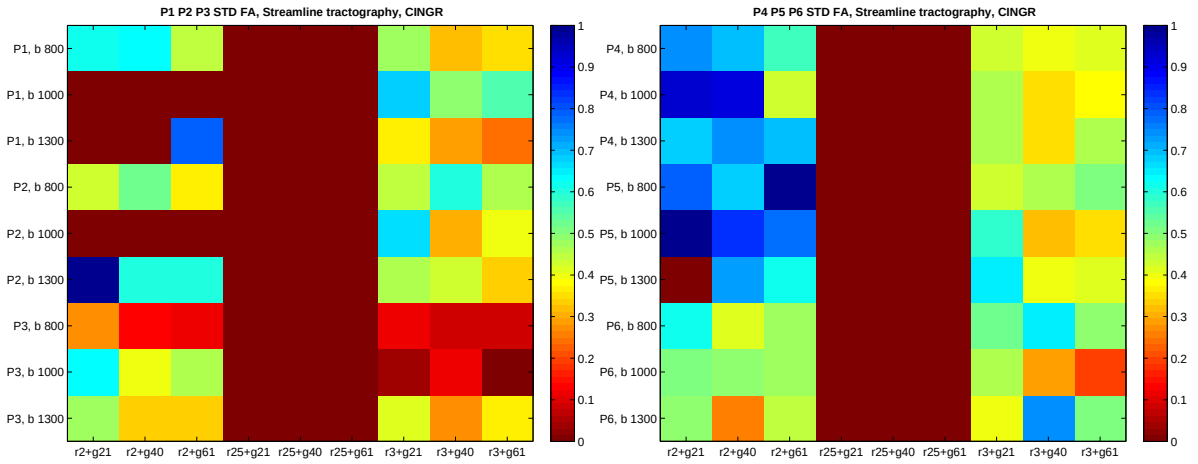

Figure 6.13: Standard Deviation of FA from the fiber profiles separated by patients, Streamline t., Right Cingulum.

6.3 Discussion of the results

The effect of the MR acquisition parameters on the reproducibility of the DTI quantitative measures has been studied by many previous works [74],[75]).

6.3.1 Effects of SNR

The effect of a high and low SNR into DTI measures have been studied in several papers, such as [67], [68]. These studies reveal that imaging parameters do indeed have an effect on DTI measures. It is supposed that higher SNR leads to higher track reproducibility[75]).

According to Jones et al.[47] the FA values exhibit an upward bias at low SNR. Insufficient SNR is undesirable because weak diffusion-weighted signals close to the background noise level bias the estimated diffusion tensor parameters [66]. Very small signals tend to be overestimated by noise, because MR imaging signals are reconstructed as the magnitude of complex values and forced to be non-negative. Overestimation of diffusion signals results in the underestimation of diffusivity and, in anisotropic structures, underestimation of anisotropy (because diffusivities along the directions of fiber bundles are larger and more underestimated)[69]. Highly anisotropic white matter structures, such as those studied here, can be especially vulnerable to insufficient SNR because the lack of restriction of water diffusion along the fiber orientation of the white matter tracts leads to strongly attenuated diffusion-weighted signals.

The overestimation in FA could have effects into the tracking reproducibility, as lower minimum FA thresholds will produce more and longer streamlines, and more spurious (ie, false-positive) fiber tracks. The variance in the anisotropy increases as the added noise increases. However, the mean value remains approximately constant in the white matter, but increases rapidly in the grey matter [47]. This fact can explain the variability that we have noticed into our profile data. Data acquired with less spatial resolution is more prone to partial volume effect.

Partial volume effects occur when multiple fibers cross within a single voxel resulting in a diffusion distribution which is affected by both fiber orientations. Under a single tensor model, partial volume effects result in reduced anisotropy and thus increased uncertainty in the fiber orientation estimate. From our profile data we can see that higher spatial resolution leads to less variance in the fiber profiles FA value.

6.3.2 Variance differences between global and streamline tractography

In global tractography, the observed signal is modeled by an ensemble of non-collinear segments. For example, a high sniotropic region, the group of segments inside a voxel fluctuate around one strong mean direction and the fluctuation leads to a broadening of the predicted signal.

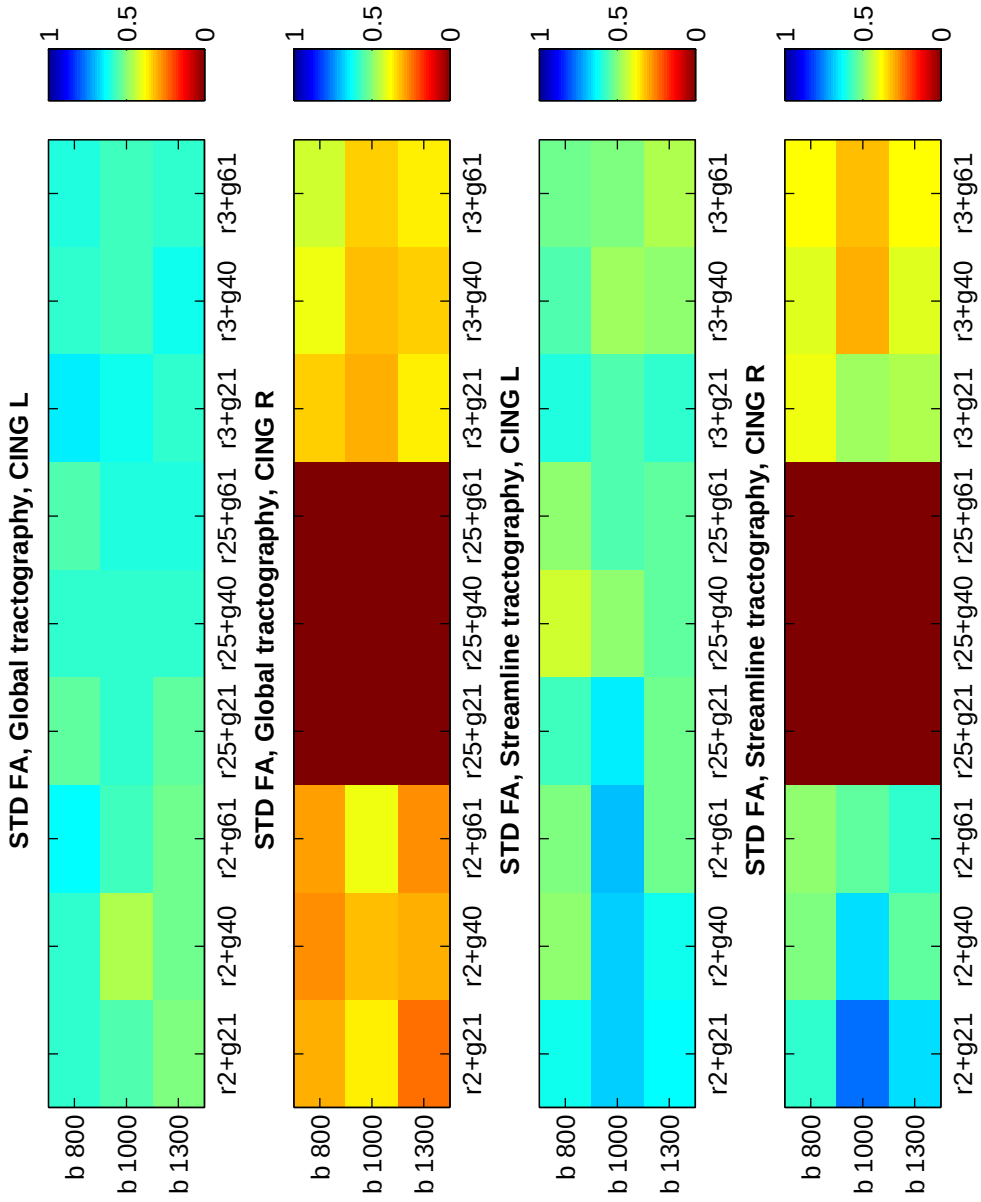

Figure 6.14: Standard Deviation of FA from the fiber profiles, Global and Streamline t., Left and Right Cingulum.

This approach makes the model parameters more or less independent of the b-value of the measurement, because if the width of the measured orientation distribution, for instance, gets smaller (for high *b-values*), the reconstructed fibers just get more aligned to the data.

This could explain the difference of variance in the FA profiles between the global and the streamline methods.

6.3.3 Effect of b-values

Lazar et al.[72] tested a series of experiments with synthetic data and their conclusions were that, in general, the tract dispersion increased with distance and decreased with SNR and anisotropy.

Higher b-values lead to complete dephasing of water molecules and signal loss for faster-moving extra-axonal water. Hence higher b-values make the angular diffusion profile sharper and more senstive to the orientation of the fibers. However, larger b-values also mean larger signal loss and lower SNR. This could explain the variance in our values of reproducibility between b-values in some of the cases, in which lower b-values lead to more correctly reconstructed fibers.

6.3.4 Effect of the number of gradients

To estimate the diffusion tensor, usually is needed with high b-values along at least six noncollinear directions in addition to a low-b DWI image, but for most applications, many more images are usually required. In theory, sampling more directions reduces the orientational dependence and increases the accuracy and precision of diffusion tensor parameters.

In other words, measurement errors will not be as dependent on relative orientation of the measured diffusion tensor compared with the set of diffusion-gradient directions. According to [65] at least 20 unique directions are necessary for a robust estimation of anisotropy, and at least 30 directions are required for a robust estimation of tensor orientation (ie, the primary eigenvector) and mean diffusivity.

Variance in derived indexes can be strongly dependent on the orientation of the structure. For example, according to [65] the lowest variance is found when the fiber is aligned with one of the sampling orientations, and is largest when the fibre is at the greatest angle to the sampling vectors. The orientational dependence becomes more marked as the anisotropy increases.

Our data has been collected from equidistant positions so we did not get high variance results with lower number of gradients; in fact our data suggest that the tracks have higher reproducibility with twenty one gradients that with sixty one. This seems to be an counter intuitive result.

6.3.5 Effects of spatial resolution

Spacing can affect both the reproducibility of the tracking and the degree of partial volume averaging. Larger voxels are more likely to contain more than one fiber tract. The presence of multiple intravoxel fiber populations with different orientations will cause errors in the estimation of fiber direction (this limitation is inherent to the diffusion tensor). The literature recommends using the maximum possible resolution in any case, unless SNR is not sufficiently high. Jones et al.[76] suggest a SNR value higher than $3:1$. If higher resolution leads to lower SNR, this could have had an effect in our experiments but it the values of the variance data tables are inconclusive.

The effects of spatial resolution and the varying degrees of partial volume averaging of complex fiber architecture on the performance of these methods could be investigated.

Chapter 7

Conclusions

Overall, in this thesis we have presented a comparative between tractography methods and acquisition parameters.

The tracking results depend on many factors: the particular tracts of interest, imaging parameters (e.g. SNR, partial volume effect, patient motion, etc.), tracking algorithms and the choice of ROIs and thresholds. Usually the precision of a tracking procedure can be given by repeating the measurement N times for a given tract and reconstruction protocol. After discussing the results of the experiments presented in this Master thesis, we have to take in account that there are two measures for judging the quality of a tractography:

- Precision, or how reproducible the results are. The reproducibility measurement could be one of the most important steps to establish the tractography as a useful research and clinical tool. Even if its accuracy is unknown, if tractography can detect reproducible difference in a specific tract between two groups, this would be an important information to understand disease status or even mechanism.
- Accuracy, or how real or valid the results are. This is not easy to measure because of the lack of a gold standard in tractography. As for accuracy of tracking results, we have chosen tracts that are well documented in previous anatomical studies using anatomical constraints (multiple ROIs) based on a priori knowledge. The macroscopic configuration of these reconstructed tracts are likely to reflect true fiber bundles.

We must also highlight that fiber count should not be considered as a measure of connection strength, but of reproducibility. The uncertainty in fiber orientation depends on the anisotropy. Therefore if we measure the fiber count through a white matter bundle with higher anisotropy, it will naturally exhibit a higher fiber count that a bundle with lower anisotropy, even if both have the same topology.

These reconstructed track estimation are the best possible guesses (in absence of any further information), but any track reconstruction has a big uncertainty attached to them. It is necessary to develop new methods able to compensate for the many existing differences in the tractography reconstruction procedures, from acquisition to reconstruction.

7.1 Future lines of investigation

Here we present some outlines for future continuation of this work:

These techniques rely on the diffusion tensor model to provide an accurate estimate of the white matter fiber orientation. Unfortunately, the diffusion tensor model is not always adequate, particularly in voxels containing contributions from differently oriented fiber bundles (a common occurrence in real neurological data). An obvious line of investigation should be try to reproduce this results using newer and more sophisticated orientation models, such as ODF, DSI or HARDI.

Another point from the literature that could be checked with our data: According to Descoteaux et al.[30], in synthetic data, increasing the b-values reduces the minimal resolvable angle between fibers. A possible method for checking this would be to compare our tractographies reconstruction for the cingulum with different b-values. The number of fibers that correctly complete the reconstruction of the back corner of the cingulum should be smaller in those data set with higher b's.

Another possible line of study will be use the fiber profile data to estimate some index of anatomical integrity between brain regions, using a measure such as those proposed by Cardenes et al.[61]. Also, some metrics like normalized reconstructed volume could be calculated.

Bibliography

[1] Basser P, Mattiello J, Bihan DL. "Estimation of effective self-diffusion tensor from the NMR spin echo". J. Magn. Reson. 1994 103:247-254.

[2] Callaghan P T, "NMR microscopy of dynamic displacements: k-space and q-space imaging". J. Phys. E: Sci. Instrum. 1988 21:820-822.

[3] Horsfield M, Jones D, "Applications of diffusion-weighted and diffusion tensor MRI to white matter diseases. A review" NMR Biomed. 2002;15:570-577.

[4] Mitra PP. "Multiple wave-vector extensions of the NMR pulsed-field-gradient spin-echo diffusion measurement". Phys Rev B Condens Matter 1995;51:15074-15078.

[5] Bar-Shir A, Avram L, Ozarslan E, Basser PJ, Cohen Y. "The effect of the diffusion time and pulse gradient duration ratio on the diffraction pattern and the structural information estimated from q-space diffusion MR: experiments and simulations". J Magn Reson 2008; 194:230-236.

[6] Zhan W, Yang Y. "How accurately can the diffusion profiles indicate multiple fiber orientations? A study on general fiber crossings in diffusion MRI". J Magn Reson 2006;183:193-202.

[7] Canales-Rodriguez EJ, Melie-Garcia L, Iturria-Medina Y. "Mathematical description of q-space in spherical coordinates: exact q-ball imaging". Magn Reson Med 2009;61:1350-1367.

[8] Ozarslan E, Mareci TH. "Generalized diffusion tensor imaging and analytical relationships between diffusion tensor imaging and high angular resolution diffusion imaging". Magn Reson Med 2003;50: 955-965.

[9] Jones DK, Symms MR, Cercignani M, Howard RJ. "The effect of filter size on VBM analyses of DT-MRI data". Neuroimage 2005;26:546-554.

[10] Seunarine K. "Linear persistent angular structure MRI and non-linear spherical deconvolution for diffusion MRI". In: International Society for Magnetic Resonance in Medicine, Seattle, Washington; 2006.

[11] Tuch DS. "Q-ball imaging". Magn Reson Med 2004;52:1358-1372.

[12] Jansons KM, Alexander DC. "Persistent angular structure: new insights from diffusion MRI data". Inf Process Med Imaging 2003;18:672-683.

[13] Beaulieu C. "The basis of anisotropic water diffusion in the nervous system a technical review". NMR Biomed 2002;15:435-455.

[14] Tournier J, Mori S, Leemans A. "Diffusion tensor imaging and beyond"., Magnetic Resonance in Medicine 2011; 65:1532-1556.

[15] Anderson AW. "Measurement of fiber orientation distributions using high angular resolution diffusion imaging". Magn Reson Med 2005; 54:1194-1206.

[16] Tournier JD, Calamante F, Connelly A. "Robust determination of the fibre orientation distribution in diffusion MRI: non-negativity constrained super-resolved spherical deconvolution". Neuroimage 2007; 35:1459-1472.

[17] Conturo TE, Lori NF, Cull TS, Akbudak E, Snyder AZ, Shimony JS, McKinstry RC, Burton H, Raichle ME. "Tracking neuronal fiber pathways in the living human brain". Proc Natl Acad Sci USA 1999;96:10422-10427.

[18] Batchelor PG, Moakher M, Atkinson D, Calamante F, Connelly A. "A rigorous framework for diffusion tensor calculus". Magn Reson Med 2005;53:221-225.

[19] Basser PJ, Pajevic S, Pierpaoli C, Duda J, Aldroubi A. "In vivo fiber tractography using DT-MRI data". Magn Reson Med 2000;44:625-632.

[20] Arsigny V, Fillard P, Pennec X, Ayache N. "Log-Euclidean metrics for fast and simple calculus on diffusion tensors". Magn Reson Med 2006;56:411-421.

[21] Mishra A, Lu Y, Meng J, Anderson AW, Ding Z. "Unified framework for anisotropic interpolation and smoothing of diffusion tensor images". Neuroimage 2006;31:1525-1535.

[22] Mori S, Crain BJ, Chacko VP, van Zijl PC. "Three-dimensional tracking of axonal projections in the brain by magnetic resonance imaging". Ann Neurol 1999;45:265-269.

[23] Weinstein DM, Kindlmann G, Lundberg E. "Tensorlines: advection-diffusion based propagation through diffusion tensor fields". IEEE Vis.00 1999, 40.

[24] Lazar M, Alexander A. "Bootstrap white matter tractography (boot-tract)". Neuroimage 2005;24:524-532.

[25] Fillard P, Descoteaux M, Goh A, Gouttard S, Jeurissen B, Malcolm J, Ramirez-Manzanares A, Reisert M, Sakaie K, Tensaouti F, Yo T, Mangin JF, Poupon C. "Quantitative evaluation of 10 tractography algorithms on a realistic diffusion MR phantom". Neuroimage 2011,56:220-234.

[26] Ramirez-Manzanares A, Rivera M, Vemuri B, Carney P, Mareci T, "Diffusion basis functions decomposition for estimating white matter intravoxel fiber geometry". IEEE Trans.Med.Imaging 2007;26(8):1091-1102.

[27] Malcolm J, Shenton M, Rathi Y. "Filtered multi-tensor tractography". IEEE Trans.Med.Imaging 2010;29: 1664-1675.

[28] Sakaie K. "Fast persistent angular structure based streamline tractography". MICCAI Workshop on Diffusion Modelling and the Fiber Cup (DMFC'09), 2009, London, United Kingdom.

[29] Goh A, Lenglet C, Thompson P, Vidal R. "A nonparametric Riemannian framework for processing high angular resolution diffusion images (HARDI)". IEEE Computer Society Conference on Computer Vision and Pattern Recognition, 2009;2496-2503.

[30] Descoteaux M, Deriche R, Knosche T, Anwander A. "Deterministic and probabilistic tractography based on complex fibre orientation distributions". IEEE Trans. Med. Imaging, 2009;28(2):269-286.

[31] Jeurissen B, Leemans A, Jones DK, Tournier J, Sijbers J. "Probabilistic fiber tracking using the residual bootstrap with constrained spherical deconvolution". Hum. Brain Mapp. 2010;32.

[32] Parker GJ, Haroon HA, Wheeler-Kingshott CA. "A framework for a streamline-based probabilistic index of connectivity (PICo) using a structural interpretation of MRI diffusion measurements". J Magn Reson Imaging 2003;18:242-254.

[33] Jones DK, Pierpaoli C. "Confidence mapping in diffusion tensor magnetic resonance imaging tractography using a bootstrap approach". Magn Reson Med 2005;53:1143-1149.

[34] Jones DK. "Tractography gone wild: probabilistic fibre tracking using the wild bootstrap with diffusion tensor MRI". IEEE Trans Med Imaging 2008;27:1268-1274.

[35] Koch MA, Norris DG, Hund-Georgiadis M. "An investigation of functional and anatomical connectivity using magnetic resonance imaging". Neuroimage 2002;16:241-250.

[36] Tournier JD, Calamante F, Gadian DG, Connelly A. "Diffusion weighted magnetic resonance imaging fibre tracking using a front evolution algorithm". Neuroimage 2003;20:276-288.

[37] Behrens TE, Berg HJ, Jbabdi S, Rushworth MF, Woolrich MW. "Probabilistic diffusion tractography with multiple fibre orientations: what can we gain?". Neuroimage 2007;34:144-155.

[38] Friman O, Farneback G, Westin CF. "A Bayesian approach for stochastic white matter tractography". IEEE Trans Med Imaging 2006; 25:965-978.

[39] Wedeen VJ, Wang RP, Schmahmann JD, Benner T, Tseng WY, Dai G, Pandya DN, Hagmann P, D'Arceuil H, de Crespigny AJ. "Diffusion spectrum magnetic resonance imaging (DSI) tractography of crossing fibers". Neuroimage 2008;41:1267-1277.

[40] Berman JI, Chung S, Mukherjee P, Hess CP, Han ET, Henry RG. "Probabilistic streamline q-ball tractography using the residual bootstrap". Neuroimage 2008;39:215-222.

[41] Reisert M, Mader I, Kiselev V. "Tracking a physical phantom by global fibre reconstruction". MICCAI Workshop on Diffusion Modelling and the Fiber Cup (DMFC'09), 2009, London, United Kingdom.

[42] Parker GJ, Wheeler-Kingshott CA, Barker GJ. "Estimating distributed anatomical connectivity using fast marching methods and diffusion tensor imaging". IEEE Trans Med Imaging 2002;21:505-512.

[43] Hagler DJ, Ahmadi ME, Kuperman J. "Automated white-matter tractography using a probabilistic diffusion tensor atlas: application to temporal lobe epilepsy". Hum Brain Mapp 2009;30:1535-47.

[44] Kim M, Ronen I, Ugurbil K, Kim DS. "Spatial resolution dependence of DTI tractography in human occipito-callosal region". Neuroimage. 2006;32(3):1243-9.

[45] Werring DJ, Clark CA, Parker GJ, Miller DH, Thompson AJ, Barker GJ. "A direct demonstration of both structure and function in the visual system: combining diffusion tensor imaging with functional magnetic resonance imaging". Neuroimage 1999;9:352-361.

[46] Song SK, Yoshino J, Le TQ, Lin SJ, Sun SW, Cross AH, Armstrong RC. "Demyelination increases radial diffusivity in corpus callosum of mouse brain". Neuroimage 2005;26:132-140.

[47] Jones DK. "Challenges and limitations of quantifying brain connectivity in vivo with diffusion MRI". Imaging Med.2010;2:341-355.

[48] Jones DK. "Diffusion MRI: Theory, Methods, and Applications". First. Oxford: Oxford University Press; 2010.

[49] Tuch D, Salat D, Wisco J, Zaleta AK, Hevelone N, Rosas H. "Choice reaction time performance correlates with diffusion anisotropy in white matter pathways supporting visuospatial attention". Proc. Natl Acad. Sci. USA; 2005;102(34):12212-12217.

[50] Pierpaoli C, Barnett A, Pajevic S. "Water diffusion changes in Wallerian degeneration and their dependence on white matter architecture". Neuroimage 2001;13:1174-1185.

[51] Jones DK "Determining and visualizing uncertainty in estimates of fiber orientation from diffusion tensor MRI". Magn. Reson. Med. 2003;49:7-12.

[52] Hagmann P. "Mapping human whole brain structural networks with DTMRI" PLoS ONE,2007;2:e597.

[53] Passingham R, Stephan K, Kotter R. "The anatomical basis of functional localization in the cortex". Nat Rev Neuroci, 2002;2:606-616.

[54] Yo TS, Anwander A, Descoteaux M, Fillard P, Poupon C, Knosche TR. "Quantifying brain connectivity: A comparative tractography study". In: Yang G-Z, Hawkes D, Rueckert D, Noble A, Taylor C. (eds.) MICCAI 2009. LNCS, 5761:886-893. Springer, Heidelberg 2009.

[55] Calamante F, Tournier J, Jackson G, Connelly A. "Track-density imaging (TDI): Super-resolution white matter imaging using whole-brain track-density mapping", NeuroImage. 2010 53(4):1233-1243.

[56] Reisert M, Mader I, Anastasopoulos C, Weigel M, Schnell S, Kiselev V. "Global Fiber Reconstruction Becomes Practical". NeuroImage,2010.54(2):955-962.

[57] Mori S, Wakana S, Nagae-Poetscher LM, van Zijl PCM. MRI atlas of human white matter. Amsterdam: Elsevier; 2005.

[58] Cardenes R, Tristan-Vega A, Cordero-Grande L, Muñoz-Moreno E, Martin-Fernandez M. "UsimagTool: An interactive tool for ultrasound image processing", IEEE 7th Int. Symp. BioInformat. BioEng., 2007, Istambul, Turkey.

[59] Cardenes R, Muñoz-Moreno E, Tristan-Vega A, Martin-Fernandez M. "Una Herramienta para el Procesado y Visualizacion de Imagenes de Resonancia Magnetica de Tensor de Difusion", in Congreso Anual de la Sociedad Española de Ingenieria Biomedica,pp. 9-12, 2008, Valladolid, Spain.

[60] Cardenes R, Argibay-Quiñones D, Muñoz-Moreno E, Martin-Fernandez M. "Characterization of Anatomic Fiber Bundles for Diffusion Tensor Image Analysis", Medical Image Computing and Computer-Assisted Intervention-MICCAI, pp.903-910, 2009, London, UK.

[61] Cardenes R, Muñoz-Moreno E, Sarabia-Herrero R, Rodriguez-Velasco M, Fuertes-Alija JJ, Martin-Fernandez M. "Analysis of the pyramidal tract in tumor patients using diffusion tensor imaging", NeuroImage 2010; 50(1):27-39.

[62] Cardenes R, Muñoz-Moreno E, Tristan-Vega A, Martin-Fernandez M. "Saturn: a software application of tensor utilities for research in neuroimaging", Comput. Methods Programs Biomed. 2010;97:264-279.

[63] Barrio-Arranz G, Aja-Fernandez S, Alberola-Lopez C, Martin-Fernandez M. "Saturn2: an improved software tool for Diffusion Imaging", in Congreso Anual de la Sociedad Española de Ingenieria Biomedica,pp. 3-7, 2011, Caceres, Spain.

[64] Web page. http://lpi.tel.uva.es/saturn. Home page of Saturn. Last visit:September 2012.

[65] Jones DK. "The effect of gradient sampling schemes on measures derived from diffusion tensor MRI: a Monte Carlo study". Magn Reson Med. 2004;51:807-15

[66] Jones DK, Basser PJ. "Squashing peanuts and smashing pumpkins: how noise distorts diffusion-weighted MR data". Magn Reson Med 2004;52:979-93.

[67] Marenco S, Rawlings R, Rohde GK. "Regional distribution of measurement error in diffusion tensor imaging". Psychiatry Res 2006; 147: 69-78.

[68] Pfefferbaum A, Adalsteinsson E, Sullivan EV. "Replicability of diffusion tensor imaging measurements of fractional anisotropy and trace in brain". J Magn Reson Imaging. 2003;18:427-433.

[69] Mukherjee P, Chung SW, Berman JI, Hess CP, Henry RG. "Diffusion tensor MR imaging and fiber tractography: technical considerations". AJNR 2008; 29:843-852.

[70] Landman BA, Farrell JA, Jones CK. "Effects of signal-to-noise ratio on the accuracy and reproducibility of diffusion tensor imaging-derived fractional anisotropy, mean diffusivity, and principal eigenvector measurements at 1.5T" Neuroimage. 2007;36:1123-38.

[71] Wakana S, Caprihan A, Panzenboeck MM, Fallon JH, Perry M, Gollub RL, Hua K, Zhang J, Jiang H, Dubey P, "Reproducibility of quantitative tractography methods applied to cerebral white matter" NeuroImage. 2007;36:630-644.

[72] Lazar M, Alexander AL. "An error analysis of white matter tractography methods: synthetic diffusion tensor field simulations". Neuroimage 2003;20:1140-1153.

[73] Zhan L, Franc D, Patel V, Jahanshad N, Yan Jin, Mueller BA, Bernstein M, Borowski B, Jack C, Toga AW, Lim KO, Thompson PM. "How do spatial and angular resolution affect brain connectivity maps from diffusion MRI?". 9th IEEE International Symposium on Biomedical Imaging (ISBI12), Barcelona, Spain, May 2012.

[74] Heiervang E, Behrens TE, Mackay CE, Robson MD, Johansen-Berg H. "Between session reproducibility and between subject variability of diffusion MR and tractography measure". NeuroImage. 2006;33:867-877

[75] Huang H, Zhang J, van Zijl P, Mori S. "Analysis of noise effects on DTI-based tractography using the brute-force and multi-ROI approach". Magn. Reson. Med. 2004;52(3):1522-2594

[76] Jones DK, Knosche T, Turner R. "White matter integrity, fiber count, and other fallacies: The do's and don'ts of diffusion MRI" NeuroImage, In Press, 2012. $http://dx.doi.org/10.1016/j.neuroimage.2012.06.081$

Appendix A

Publications of this Master thesis

Barrio-Arranz G, "Estudio de los efectos de los parámetros de adquisición en la tractografía global", *Congreso Anual de la Sociedad Española de Ingeniería Biomédica, 2012. CASEIB.* vol. XX, pp. XX-XX, 2012. (enviado)

Estudio de los efectos de los parámetros de adquisición en la tractografía global

G. Barrio-Arranz
Laboratorio de Procesado de Imagen, Universidad de Valladolid, Valladolid, Spain, *gbararr@lpi.tel.uva.es*

Abstract

La tractografía es el proceso que se emplea para estimar la estructura de las fibras nerviosas del interior del cerebro in vivo *a partir de datos de Resonancia Magnética (MR).*

Los métodos de tractografía global, al contrario que los métodos locales, intentan reconstruir todas las estructuras neuronales a la vez, buscando una configuración que mejor se ajusta a los datos proporcionados.

Dichos métodos globales han demostrado ser más precisos y fiables que los métodos de tractografía local, para datos sintéticos. Sin embargo hasta la fecha no hay estudios que definan la relación entre los parámetros de adquisición de la MR y los resultados de tractografía global con datos reales.

Este artículo pretende mostrar la influencia de ciertos parámetros de adquisición como el factor de difusión de las secuencias de adquisición (b-value) o el número de gradientes en la variabilidad de las tractografías obtenidas.

1 Introducción

DTI (*Diffusion Tensor Imaging*) es una modalidad de MRI (*Magnetic Resonance Imaging*) que se emplea para estudiar las características internas del cerebro y las conexiones que existen entre ellas. Esta técnica se basa en medir la cantidad y la dirección principal de difusión de las moléculas de agua dentro de los tejidos vivos al aplicarles una serie de fuertes pulsos magnéticos. Dentro del cerebro los tejidos limitan las direcciones de difusión, el agua contenida dentro de ellas tiende a difundirse más a lo largo de los axones que perpendicular a ellos; por tanto conociendo la dirección principal dentro de cada voxel podemos estimar las estructuras de las fibras nerviosas que forman el cerebro [1].

Los distintos parámetros con los que se realiza la adquisición de la resonancia magnética como el factor de difusión de las secuencias de imáganes (*b-value*), el tiempo entre pulsos (T_E), el espaciado entre muestras (r), el número de gradientes (g) acaban teniendo gran importancia durante la estimación del tensor y en los resultados finales de tractografía.

La tractografía es un proceso diseñado para estimar los tractos de fibras cerebrales a partir de la información de difusión. Existen varios métodos tractográficos: los más comunes son los métodos locales que reconstruyen cada fibra de manera independiente, cada fibra estimada no influye sobre el resto. La reconstrucción se realiza a través de una serie de pequeños pasos sucesivos.

- La tractografía *"streamline"* emplea un estimador numérico (Euler o Runge-Kutta) para seguir la dirección principal de difusión desde un punto semilla a lo largo de varios voxels hasta que se cumple algún tipo de condición de umbral (angular, medida de difusión, etc.)[2]. Algunas de las principales ventajas de este método es su simplicidad y su bajo coste computacional. Uno de los inconvenientes es que no proporciona información sobre la reproducibilidad del tracto generado.

- La tractografía estocástica o probabilística intenta solucionar dicha limitación modelando explícitamente la incertidumbre en la orientación de la fibra durante la estimación. Existen varias implementaciones de algoritmos probabilísticos; Jones et al.[3] emplean combinaciones aleatorias creadas a partir de una serie de datos redundantes con métodos *streamline*. En cambio, Friman et al.[4] o Jbabdi et al. [5] emplean modelos Bayesianos para generar una distribución posterior de posibles orientaciones en cada paso. Puesto que existen múltiples posibles caminos, deben generarse múltiples tractos para obtener una idea de la probabilidad de que un tracto alcance una determinada región.

A pesar de su simplicidad, los métodos locales se ven afectados por su falta de exactitud: los pequeños errores producidos al determinar cada nuevo paso pueden acumularse y afectar significativamente al resultado final. Para minimizar este tipo de error surgen los métodos globales.

Los métodos globales intentan reconstruir todas las fibras simultáneamente, buscando una configuración que mejor describe los datos proporcionados.

Las fibras se reconstruyen mediante pequeños segmentos que se unen, desunen y recombinan (en orientación y número)durante la fase de optimización. Su comportamiento está gobernado por la interacción entre dichos segmentos y la maximización del acople con los

datos. El mayor problema de este tipo de métodos es su largo tiempo de computación.

El algoritmo empleado en este artículo es el desarrollado por Reisert et al.[6]. Este algoritmo resultó el mejor puntuado en la comparación entre distintos algoritmos de tractografía que se llevó a cabo en congreso MICCAI en 2010[7].

La zona del cerebro que hemos elegido como base de las medidas es el cíngulo, una colección de fibras de materia blanca que se extienden desde el giro cíngulado hasta el cortex entorrinal. Hay varias razones para esta elección: se trata de una región muy estudiada; con altos valores de anosotropía (lo que facilita la estimación de la tractografía) y relativamente estrecha por lo que a la hora de extraer los perfiles de las fibras podemos asumir una distancia máxima de la que tomar la media de los valores tensoriales.

Recientemente otros artículos, como el de Zhan et al.[8] han estudiado como los parámetros de resolución espacial y el número de gradientes afectan a la "conectividad" en varias zonas de materia blanca del cerebro empleando tractografía streamline. sin embargo, no existe literatura sobre como estos parámetros pueden afectar a los métodos de tractografía global.

En este artículo intentamos entender como los distintos parámetros de adquisición como el valor de b afectan al resultado de la tractografía global del cíngulo, estudiando su variabilidad en número de fibras que completan con éxito la reconstrucción y los valores medios de los perfíles de las fibras. En la sección 2 describiremos los detalles y características de los volúmenes de datos que empleamos en nuestros experimentos. A continuación en la sección 3 hablaremos de las medidas calculadas y discutiremos las posibles deducciones a partir de ellas. Finalmente en la sección 4 cerraremos con las conclusiones y futuras líneas de trabajo.

2 Materiales y métodos

En esta sección describiremos los detalles de los datos empleados en nuestros experimentos de tractografía.

2.1 Adquisición

Para este estudio hemos seleccionado a seis pacientes control saludables, hombres de entre 23 y 31 años (con edad media de 27 años). Todos los datos fueron adquiridos en un escáner GE Signa de 1.5 Teslas en el Hospital Gregorio Marañon de Madrid.

Cada paciente fue escaneado nueve veces con nueve distintas combinaciones de parámetros:

- $B-value$: Los volúmenes se adquirieron con tres valores diferentes de b: 800,1000 y $1300 \frac{s}{mm^2}$.
- Espaciado: La matriz de datos posee un tamaño de voxel de $2 \times 2 \times 2mm^3$. El número de índices de las matrices de datos es de $128 \times 128 \times 62$ voxels.
- Direcciones de gradientes: Todos los volúmenes se adquirieron con 61 gradientes y un volumen *baseline*. Las direcciones se diseñaron para que los datos pudieran ser submuestreados a 40 o 21 gradientes fácilmente. El submuestreo nos permite medir el efecto del número de gradientes en el cálculo tensorial con una sola adquisición.

Otros parámetros son: tiempo de repetición $T_R = 8$, tiempo entre pulsos $T_E = 1.6ms$.

2.2 Procesado de datos

Los valores tensoriales de cada voxel se estiman a partir de los múltiples gradientes. Para disminuir el nivel de ruido primero se ejecutó una etapa de filtrado mediante un método de mínimo error cuadrático medio lineal (LMMSE).

Luego, a partir de un cierto valor umbral de anisotropía se creó una máscara sobre la que se ejecutó el algoritmo de tractografía global de Reisert et al. desarrollado en la Universidad de Friburgo.

2.3 Filtrado espacial

Una vez realizada la tractografía de todo el cerebro se definieron tres regiones de interés (ROIs) sobre el cíngulo de acuerdo con los puntos propuestos por Mori et al. [10]. Se eliminaron todas las fibras que no atravesaban las tres ROIs. El filtrado se realizó por medio del software Saturn [9] desarrollado por la Universidad de Valladolid.

2.4 Extracción de los perfiles de las fibras

Una de las formas de comparar diferentes grupos de fibras es midiendo sus valores tensoriales a lo largo de la fibra, generalmente se comparan valores escalares como el índice de anisotropía fraccional (FA). Para extraer valores consistentes de los tensores y evitar los efectos de volumen parcial (contaminación de valores cercanos a la fibra) creamos un método extractor de perfiles.

En primer lugar, a partir de las ROIs definidas se crea un esqueleto promedio sobre el que luego se proyectarán los valores tensoriales de cada punto de las fibras. Los puntos de este esqueleto se suavizan para formar una curva *spline* parámetrica.

En segundo lugar, los puntos de las fibras se ordenan según una estructura de árbol k-dimensional, empleada para poder realizar una busqueda de puntos cercanos.

Para cada punto de la curva spline se buscan los puntos de las fibras situados dentro de un radio de $2mm$ de distancia y se proyectan sus valores sobre ella para cada fibra por separado. Finalmente se calculan las medias y varianzas de cada fibra proyectada y de todas las fibras proyectadas.

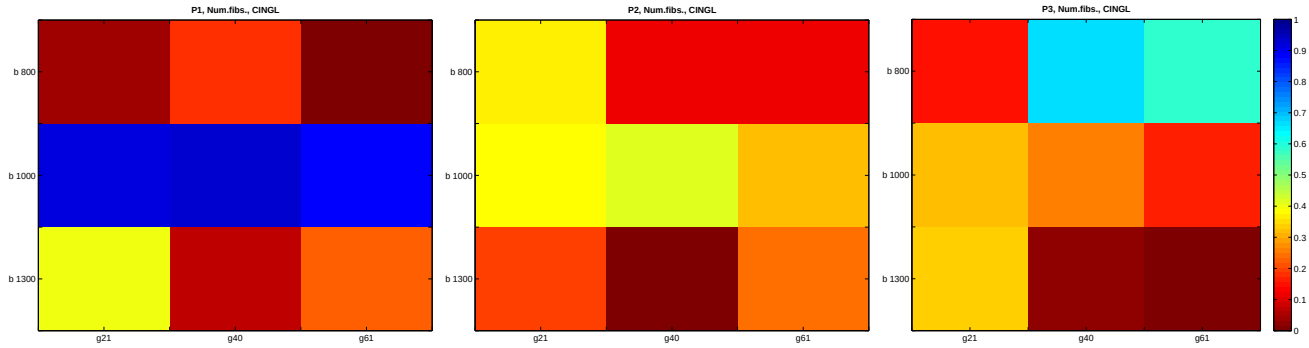

Figure 3. *Número de fibras reconstruídas para los tres pacientes para varios valores de b y g.*

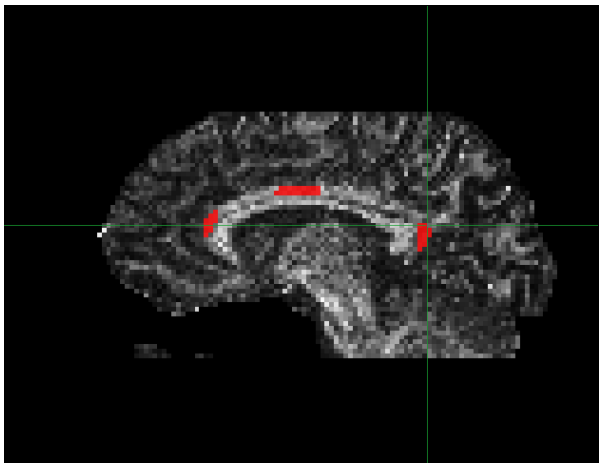

Figure 1. *ROIs usadas para filtado espacial.*

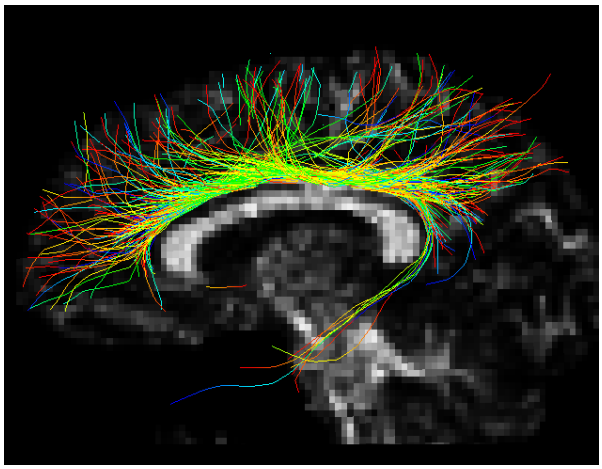

Figure 2. *Cíngulo reconstruído con la tractografía global.*

3 Resultados

En esta sección presentamos los resultados de los experimentos. Una vez computados las fibras que forman el cíngulo para todos los volúmenes de datos, tomamos dos medidas como base: el número de fibras que completan el recorrido con éxito entre las tres ROIs y los perfiles de FA de dichas fibras. La FA es una medida comúnmente usada en los estudios neurológicos de DTI [1]. En la fig. 3 se muestra el número de fibras que completan el recorrido normalizado por el número máximo de fibras de cada reconstrucción:

$$Val = \sqrt{\left(\frac{N_{max} - N_{fibs}}{N_{max}}\right)^2} \quad (1)$$

El valor resultante, situado entre cero y uno, nos permite tener una idea de como los valores de b y el número de gradientes afectan al resultado tractográfico. Los valores que obtienen resultados más reproducibles son para b intermedios ($b = 1000$).

Sin embargo, no parece haber un patrón claro entre los valores de b. De acuerdo con Lazar et al.[12] un aumento de los valores de b hace que los valores de difusión sean más sensibles a la orientación de las fibras a cambio de una perdida de SNR. En teoría, un mayor valor de b conlleva una reducción de SNR y una mayor dispersión en las fibras. Esta diferencia con nuestros datos podría ser causado por la naturaleza del algoritmo de reconstrucción global. El número de fibras no parece ser una buena medida para comparar el efecto de los parámetros de adquisición.

La figura 4 representa los valores de la media de FA de los perfiles, y la figura 5 representa la desviación estándar para cada conjunto de fibras estimado. De esta forma podemos observar la variabilidad de las medidas de los perfiles. Para valores de b de entre 800 y 1300 la desviación de los valores es muy pequeña. Esto nos sugiere que es posible emplear valores de b más pequeños sin afectar en gran medida a la reconstrucción de grandes grupos de fibras. No podemos discutir los efectos de los grupos de fibras más pequeños y dispersos, como aquellas cercanas al cortex.

El número de gradientes afecta tanto a la media como a la desviación estándar. Un menor número de gradientes aumenta los valores medios y la desviación estándar, especialmente para valores altos de b. Esto puede ser explicado por el hecho de que valores altos de b conducen a una subestimación de los valores de FA [11] en los voxels más anisotrópicos.

4 Conclusiones

Los resultados de la tractografía dependen de muchos factores: las regiones de interés, los parámetros de adquisición, las fuentes de variación (por ejemplo, la

SNR, el efecto de volumen parcial, movimiento del paciente, etc.), los algoritmos de reconstrucción empleados y la elección de umbrales.

Si bien podemos medir la precisión de un método (cómo de reproducibles son sus resultados), no existe un "golden-standard" sobre la exactitud de una reconstrucción tractográfica. Uno de los objetivos de este trabajo es sentar las bases para computar la influencia de los parámetros de adquisición, de forma que puedan tenerse en cuenta en futuros modelos capaces de validar los resultados de tractografías sobre tejidos *in-vivo*.

Para este artículo hemos estudiado tractos bien documentados en estudios anatómicos previos, por lo que es probable que al menos la configuración macroscópica de estos tractos sea exacta.

Entre las futuras líneas de investigación de este trabajo esta el estudiar la influencia del espaciado entre voxels para este tipo de algoritmos de tractografía.

También hay que destacar que estos datos se basan en el modelo de tensor de difusión para estimar la orintación de la fibra en materia blanca. Sin embargo, el modelo de tensor de difusión no siempre es adecuado, particularmente en voxels que contienen varias fibras. Una posible forma de avanzar sería emplear modelos de orientación más sofisticados como ODF, DSI o HARDI que han demostrado ser capaces de resolver mejor cruces de fibras en datos sintéticos.

Agradecimientos

Este artículo ha sido financiado por .También agradecemos a M. Reisert y a V. Kiselev de la Universidad de Friburgo permitirmos utilizar su código de tractografía global.

References

[1] Le Bihan D, Mangin JF, Poupon C, Clark CA, Pappata S, Molko N,Chabriat H "Diffusion tensor imaging: concepts and applications". J Magn Reson Imaging 2001; 13:534-546

[2] Mori S, Crain BJ, Chacko VP, van Zijl PC. "Three-dimensional tracking of axonal projections in the brain by magnetic resonance imaging". Ann Neurol 1999; 45:265-269.

[3] Jones DK, "Tractography gone wild: probabilistic fibre tracking using the wild bootstrap with diffusion tensor MRI" IEEE Transactions on Medical Imaging. 2008; 27:1268-1274.

[4] Friman O, Farneback G, Westin CF "A Bayesian approach for stochastic white matter tractography". IEEE Trans Med Imaging. 2006; 25:965-978.

[5] Jbabdi S, Woolrich MW, Andersson JLR, Behrens TE. "A Bayesian framework for global tractography". NeuroImage. 2007;37:116-29.

[6] Reisert M, Mader I, Anastasopoulos C, Weigela M, Schnella S, Kiseleva V. "Global fiber reconstruction becomes practical". Neuroimage. 2011;54:955-962.

[7] Fillard P, Descoteaux M, Goh A, Gouttard S, Jeurissen B, Malcolm J, Ramirez-Manzanares A, Reisert M, Sakaie K, Tensaouti F, Yo T, Mangin JF, Poupon C. "Quantitative evaluation of 10 tractography algorithms on a realistic diffusion MR phantom". Neuroimage. 2011;56:220-234.

[8] Zhan L, Franc D, Patel V, Jahanshad N, Yan Jin, Mueller BA, Bernstein M, Borowski B, Jack C, Toga AW, Lim KO, Thompson PM. "How do spatial and angular resolution affect brain connectivity maps from diffusion MRI?". 9th IEEE International Symposium on Biomedical Imaging (ISBI12), Barcelona, Spain, May 2012.

[9] Barrio-Arranz G, Aja-Fernández S, Alberola-López C, Martín-Fernández M, "SATURN2: An Improved Software Tool for Neuroimaging Analysis" Congreso Anual de la Sociedad Española de Ingeniería Biomédica - CASEIB2011, Cáceres, España, Nov. 2011.

[10] Mori S, Wakana S, Nagae-Poetscher LM, van Zijl PCM. MRI atlas of human white matter. Amsterdam: Elsevier; 2005.

[11] Jones DK, Cercignani M. "Twenty-five pitfalls in the analysis of diffusion MRI data". NMR in Biomedicine. 2010; 23(7):803-820.

[12] Lazar M, Alexander AL. "An error analysis of white matter tractography methods: synthetic diffusion tensor field simulations". Neuroimage 2003;20:1140-1153.

Appendix B

Connectivity data tables

	P1	P2	P3	P4	P5	P6
b800,r2,g21	124	158	109	154	107	193
b800,r2,g40	173	184	136	182	86	223
b800,r2,g61	177	202	136	188	104	255
b800,r25,g21	80	206	140	93	178	77
b800,r25,g40	85	206	103	114	171	75
b800,r25,g61	88	232	129	135	201	69
b800,r3,g21	47	37	71	82	113	120
b800,r3,g40	61	62	76	77	106	96
b800,r3,g61	54	52	66	78	114	106
b1000,r2,g21	0	0	126	166	102	175
b1000,r2,g40	2	1	151	202	105	205
b1000,r2,g61	1	0	134	202	125	224
b1000,r25,g21	89	196	119	150	212	79
b1000,r25,g40	82	169	155	167	207	83
b1000,r25,g61	89	196	126	171	223	85
b1000,r3,g21	54	47	87	98	116	101
b1000,r3,g40	65	55	91	84	123	109
b1000,r3,g61	58	55	75	93	141	121
b1300,r2,g21	114	169	96	244	127	199
b1300,r2,g40	135	193	148	271	171	199
b1300,r2,g61	157	234	148	267	196	221
b1300,r25,g21	94	227	186	178	297	120
b1300,r25,g40	110	181	184	192	333	127
b1300,r25,g61	112	229	196	177	345	109
b1300,r3,g21	46	65	78	124	143	200
b1300,r3,g40	65	67	84	126	122	185
b1300,r3,g61	60	73	83	152	196	182

Tabla B.1: Connectivity table for Global tractography, Corpus Callosum

	P1	P2	P3	P4	P5	P6
b800,r2,g21	3	297	4	478	18	5
b800,r2,g40	143	577	405	3595	5	740
b800,r2,g61	879	1320	1446	4244	242	3233
b800,r25,g21	627	389	336	3485	2998	421
b800,r25,g40	576	1132	1049	6583	5522	999
b800,r25,g61	1342	1374	1646	7041	6502	1384
b800,r3,g21	197	145	22	2419	3279	802
b800,r3,g40	278	138	429	2856	2646	1715
b800,r3,g61	612	204	675	3105	3800	1679
b1000,r2,g21	0	0	195	1033	4	185
b1000,r2,g40	0	0	429	1389	272	1043
b1000,r2,g61	0	0	1936	4990	364	3261
b1000,r25,g21	1137	939	268	3951	4319	866
b1000,r25,g40	1814	1319	573	5121	8049	2142
b1000,r25,g61	2745	2246	1128	7034	10746	2735
b1000,r3,g21	284	209	787	2916	3403	1375
b1000,r3,g40	800	183	322	3391	4498	2318
b1000,r3,g61	995	209	535	4243	4697	2244
b1300,r2,g21	0	229	58	405	216	33
b1300,r2,g40	22	726	640	2914	685	480
b1300,r2,g61	18	1364	1546	3722	835	625
b1300,r25,g21	602	914	1396	3825	4938	784
b1300,r25,g40	2890	947	2677	5451	7620	2183
b1300,r25,g61	3935	912	3768	7534	9695	3128
b1300,r3,g21	947	541	221	2580	4499	2344
b1300,r3,g40	1196	479	769	3704	2721	2072
b1300,r3,g61	1710	609	568	3952	5001	2381

Tabla B.2: Connectivity table for Streamline tractography, Corpus Callosum

	P1	P2	P3	P4	P5	P6
b800,r2,g21	26	87	56	36	54	72
b800,r2,g40	38	74	67	50	21	80
b800,r2,g61	34	91	65	50	26	96
b800,r25,g21	20	66	83	66	20	57
b800,r25,g40	22	79	97	83	12	58
b800,r25,g61	22	74	95	85	13	63
b800,r3,g21	30	29	66	51	33	40
b800,r3,g40	23	37	78	60	35	30
b800,r3,g61	28	40	76	53	38	29
b1000,r2,g21	4	8	52	35	43	40
b1000,r2,g40	8	6	70	33	47	68
b1000,r2,g61	5	10	64	39	53	68
b1000,r25,g21	24	67	91	95	34	54
b1000,r25,g40	21	78	86	113	32	60
b1000,r25,g61	22	75	94	113	24	55
b1000,r3,g21	19	31	70	65	49	34
b1000,r3,g40	22	34	72	65	44	26
b1000,r3,g61	21	37	84	61	41	32
b1300,r2,g21	12	55	51	46	42	47
b1300,r2,g40	14	85	64	57	62	64
b1300,r2,g61	20	70	82	43	63	70
b1300,r25,g21	24	78	141	137	66	84
b1300,r25,g40	27	66	150	125	83	75
b1300,r25,g61	37	83	152	108	87	79
b1300,r3,g21	27	41	86	106	40	34
b1300,r3,g40	33	46	86	110	42	44
b1300,r3,g61	32	46	104	103	47	48

Tabla B.3: Connectivity table for Global tractography, Left Cingulum

	P1	P2	P3	P4	P5	P6
b800,r2,g21	1	180	2	50	7	90
b800,r2,g40	3	565	384	209	16	768
b800,r2,g61	229	915	479	219	61	805
b800,r25,g21	45	905	1448	1094	0	398
b800,r25,g40	191	692	1588	1302	2	452
b800,r25,g61	213	1028	2602	1287	5	580
b800,r3,g21	85	388	371	373	532	171
b800,r3,g40	31	518	591	528	305	269
b800,r3,g61	59	554	633	607	333	227
b1000,r2,g21	0	0	100	101	50	29
b1000,r2,g40	0	0	421	122	52	460
b1000,r2,g61	0	2	761	169	87	544
b1000,r25,g21	51	596	706	989	5	306
b1000,r25,g40	127	1088	1200	937	122	539
b1000,r25,g61	238	1457	1218	1071	184	849
b1000,r3,g21	17	662	451	795	459	118
b1000,r3,g40	36	342	870	434	332	351
b1000,r3,g61	26	634	852	726	596	232
b1300,r2,g21	0	109	117	20	0	51
b1300,r2,g40	0	62	162	42	5	58
b1300,r2,g61	0	161	226	64	11	120
b1300,r25,g21	78	583	1604	1446	310	364
b1300,r25,g40	153	841	2113	1689	677	719
b1300,r25,g61	246	965	2624	2124	656	910
b1300,r3,g21	18	444	946	792	181	221
b1300,r3,g40	149	536	1194	906	330	304
b1300,r3,g61	73	528	1096	851	352	433

Tabla B.4: Connectivity table for Streamline tractography, Left Cingulum

	P1	P2	P3	P4	P5	P6
b800,r2,g21	5	20	801	3	6	5
b800,r2,g40	6	1	210	7	0	1
b800,r2,g61	3	0	330	6	2	6
b800,r25,g21	95	200	0	132	6	4
b800,r25,g40	4	194	114	84	2	1
b800,r25,g61	14	205	68	75	6	3
b800,r3,g21	5	6	0	368	22	2
b800,r3,g40	23	5	3	534	6	128
b800,r3,g61	107	7	0	622	7	2
b1000,r2,g21	0	7	125	5	3	0
b1000,r2,g40	0	8	24	20	0	5
b1000,r2,g61	5	0	7	3	2	3
b1000,r25,g21	26	295	97	427	0	3
b1000,r25,g40	1	51	2	337	5	7
b1000,r25,g61	2	129	5	492	7	6
b1000,r3,g21	766	334	2	752	1	8
b1000,r3,g40	924	325	2	651	2	0
b1000,r3,g61	963	325	1	251	3	174
b1300,r2,g21	5	4	34	4	4	2
b1300,r2,g40	8	4	25	6	8	7
b1300,r2,g61	1	8	24	6	2	4
b1300,r25,g21	5	191	1	83	4	3
b1300,r25,g40	235	163	18	90	4	4
b1300,r25,g61	176	129	35	85	7	6
b1300,r3,g21	176	207	5	75	5	0
b1300,r3,g40	562	88	4	40	18	1
b1300,r3,g61	681	78	6	80	2	6

Tabla B.5: Connectivity table for Probabilistic tractography, Left Cingulum

	P1	P2	P3	P4	P5	P6
b800,r2,g21	64	72	109	92	21	95
b800,r2,g40	83	91	117	101	18	125
b800,r2,g61	76	100	118	102	23	134
b800,r25,g21	82	105	82	91	13	40
b800,r25,g40	86	93	82	83	11	42
b800,r25,g61	88	103	93	98	7	44
b800,r3,g21	53	18	101	55	33	17
b800,r3,g40	58	14	117	55	36	18
b800,r3,g61	56	16	119	49	30	24
b1000,r2,g21	7	18	80	104	24	63
b1000,r2,g40	4	6	97	87	16	97
b1000,r2,g61	8	26	80	105	30	98
b1000,r25,g21	78	99	78	122	22	47
b1000,r25,g40	94	77	66	124	35	57
b1000,r25,g61	99	98	95	138	37	51
b1000,r3,g21	52	18	152	59	44	31
b1000,r3,g40	52	16	124	59	41	22
b1000,r3,g61	66	22	129	64	57	23
b1300,r2,g21	41	49	102	104	37	69
b1300,r2,g40	41	81	128	114	49	77
b1300,r2,g61	52	68	125	118	35	78
b1300,r25,g21	104	110	130	128	102	52
b1300,r25,g40	95	106	128	154	106	71
b1300,r25,g61	113	117	134	115	109	58
b1300,r3,g21	64	29	106	90	36	37
b1300,r3,g40	61	25	116	95	56	41
b1300,r3,g61	70	22	125	99	60	45

Tabla B.6: Connectivity table for Global tractography, Right Cingulum

	P1	P2	P3	P4	P5	P6
b800,r2,g21	258	612	414	23	7	606
b800,r2,g40	334	1454	1167	316	24	1071
b800,r2,g61	489	1862	1618	148	1	1389
b800,r25,g21	487	1063	2420	1273	11	237
b800,r25,g40	708	789	2660	1490	16	262
b800,r25,g61	945	1321	2898	1477	52	420
b800,r3,g21	121	154	1574	507	189	43
b800,r3,g40	281	441	1571	674	234	175
b800,r3,g61	270	422	1771	535	243	104
b1000,r2,g21	0	0	203	2	1	104
b1000,r2,g40	0	0	780	11	8	342
b1000,r2,g61	0	1	886	27	42	460
b1000,r25,g21	645	1465	1358	1230	8	215
b1000,r25,g40	885	937	1631	1452	150	356
b1000,r25,g61	921	1457	1834	1710	326	361
b1000,r3,g21	190	506	1993	538	378	137
b1000,r3,g40	293	489	2144	753	365	286
b1000,r3,g61	401	449	2286	795	451	75
b1300,r2,g21	0	2	548	45	1	53
b1300,r2,g40	0	14	1159	104	20	68
b1300,r2,g61	5	12	1870	220	31	184
b1300,r25,g21	911	890	2523	1564	703	209
b1300,r25,g40	914	1219	2697	2177	683	624
b1300,r25,g61	1196	1430	3031	2345	979	577
b1300,r3,g21	409	264	2144	665	174	45
b1300,r3,g40	260	430	3219	925	510	147
b1300,r3,g61	296	499	2689	920	332	124

Tabla B.7: Connectivity table for Streamline tractography, Right Cingulum

	P1	P2	P3	P4	P5	P6
b800,r2,g21	5	5	4	5	3	4
b800,r2,g40	2	6	1	2	1	1
b800,r2,g61	5	8	1	0	7	4
b800,r25,g21	5	8	0	4	3	1
b800,r25,g40	7	6	3	3	7	1
b800,r25,g61	6	5	0	1	6	6
b800,r3,g21	0	8	1	126	8	1
b800,r3,g40	5	5	1	122	2	0
b800,r3,g61	5	0	0	103	6	7
b1000,r2,g21	0	1	6	15	3	1
b1000,r2,g40	5	7	5	36	6	7
b1000,r2,g61	7	4	8	38	6	8
b1000,r25,g21	5	7	6	4	6	3
b1000,r25,g40	8	1	8	3	3	7
b1000,r25,g61	6	4	8	6	6	6
b1000,r3,g21	7	170	5	308	3	4
b1000,r3,g40	8	46	0	51	0	7
b1000,r3,g61	0	53	1	41	2	5
b1300,r2,g21	4	8	7	4	7	6
b1300,r2,g40	4	6	1	7	3	7
b1300,r2,g61	7	8	4	4	1	7
b1300,r25,g21	7	8	3	6	3	1
b1300,r25,g40	5	1	7	0	2	1
b1300,r25,g61	8	1	4	4	1	3
b1300,r3,g21	2	58	5	23	7	2
b1300,r3,g40	4	67	0	36	3	4
b1300,r3,g61	8	28	5	26	6	0

Tabla B.8: Connectivity table for Probabilistic tractography, Right Cingulum

Appendix C

Fiber FA profiles data tables

	P1		P2		P3		P4		P5		P6	
	Mean	Std	Mean	Std	Mean	Std	Mean	Std	Mean	Std	Mean	Std
b800,r2,g21	0.569589	0.097521	0.566618	0.120881	0.575407	0.089724	0.576293	0.125957	0.555953	0.114572	0.509676	0.122316
b800,r2,g40	0.538903	0.122765	0.553428	0.102102	0.568467	0.088599	0.593588	0.125245	0.572229	0.100571	0.514757	0.114341
b800,r2,g61	0.540605	0.094900	0.556457	0.134565	0.523514	0.103418	0.573763	0.095815	0.535277	0.149614	0.486304	0.122495
b800,r25,g21	0.488991	0.132141	0.514069	0.103488	0.558398	0.129447	0.559472	0.103836	0.539624	0.085228	0.478885	0.112437
b800,r25,g40	0.495472	0.114816	0.500996	0.106213	0.538630	0.122363	0.565594	0.112396	0.499171	0.129106	0.495881	0.097116
b800,r25,g61	0.481969	0.095580	0.507922	0.098563	0.504597	0.131486	0.549592	0.115977	0.506658	0.094264	0.494995	0.147160
b800,r3,g21	0.481184	0.106705	0.539885	0.133834	0.495153	0.122234	0.498522	0.103319	0.522266	0.097693	0.459252	0.100431
b800,r3,g40	0.549632	0.166955	0.489119	0.111130	0.507675	0.124793	0.527164	0.087690	0.520423	0.094309	0.479444	0.145575
b800,r3,g61	0.481702	0.131827	0.521868	0.100532	0.497095	0.124061	0.517949	0.100179	0.558726	0.136394	0.546799	0.123193
b1000,r2,g21	NaN	NaN	NaN	NaN	0.582912	0.100329	0.598617	0.097296	0.576622	0.100708	0.523527	0.120236
b1000,r2,g40	NaN	NaN	0.453949	0.000000	0.512356	0.109257	0.577044	0.105850	0.561138	0.103402	0.521296	0.105145
b1000,r2,g61	NaN	NaN	NaN	NaN	0.575480	0.136012	0.564415	0.102983	0.547507	0.118125	0.511324	0.101541
b1000,r25,g21	0.525222	0.102778	0.569941	0.131142	0.531153	0.109227	0.547905	0.093550	0.533550	0.100073	0.505579	0.162605
b1000,r25,g40	0.528644	0.145483	0.529829	0.119236	0.544960	0.109040	0.534858	0.096132	0.525990	0.097921	0.475786	0.136661
b1000,r25,g61	0.510147	0.108266	0.513103	0.107800	0.480250	0.147023	0.540508	0.102091	0.520775	0.111517	0.455909	0.113258
b1000,r3,g21	0.460691	0.087844	0.493188	0.108279	0.479073	0.113764	0.557815	0.110346	0.512782	0.086336	0.447478	0.130771
b1000,r3,g40	0.460279	0.129193	0.515506	0.100081	0.464666	0.115405	0.499282	0.121653	0.483653	0.119639	0.437736	0.114781
b1000,r3,g61	0.493915	0.097419	0.477642	0.125783	0.480448	0.128446	0.515261	0.095609	0.513129	0.082599	0.536990	0.108634
b1300,r2,g21	0.541883	0.104186	0.548393	0.109555	0.554458	0.099313	0.573947	0.102264	0.565332	0.092613	0.517564	0.103517
b1300,r2,g40	0.523175	0.104999	0.550099	0.107080	0.518448	0.096363	0.560944	0.119786	0.542124	0.098298	0.500955	0.108733
b1300,r2,g61	0.516215	0.095938	0.548702	0.147224	0.494972	0.107907	0.549455	0.106490	0.522925	0.100833	0.524369	0.098067
b1300,r25,g21	0.515721	0.108734	0.516256	0.112296	0.529915	0.107117	0.538829	0.097429	0.539871	0.117124	0.490567	0.111745
b1300,r25,g40	0.498692	0.101573	0.501417	0.092294	0.493781	0.142892	0.545677	0.102214	0.482348	0.122306	0.489155	0.122989
b1300,r25,g61	0.505219	0.104595	0.492080	0.088932	0.496446	0.128172	0.547757	0.083787	0.527902	0.108892	0.450510	0.107864
b1300,r3,g21	0.487850	0.100744	0.494671	0.106800	0.493892	0.098294	0.532130	0.121093	0.506492	0.110432	0.515682	0.176433
b1300,r3,g40	0.487161	0.096523	0.494671	0.106800	0.499089	0.109669	0.504583	0.093193	0.509797	0.097112	0.462631	0.151157
b1300,r3,g61	0.464026	0.119010	0.490502	0.114306	0.487480	0.111030	0.496527	0.103033	0.473608	0.092449	0.432431	0.141451

Tabla C.1: FA profiles mean and std. dev. values, for Global Tractography, Corpus Callosum

	P1		P2		P3		P4		P5		P6	
	Mean	Std	Mean	Std	Mean	Std	Mean	Std	Mean	Std	Mean	Std
b800,r2,g21	0.483115	0.198202	0.474394	0.167192	0.508265	0.097752	0.474073	0.138067	0.486991	0.146941	0.417940	0.133645
b800,r2,g40	0.431986	0.118133	0.452481	0.160973	0.420260	0.128406	0.474040	0.179992	0.491188	NaN	0.461453	0.138853
b800,r2,g61	0.435563	0.127953	0.437963	0.173715	0.413712	0.134638	0.444259	0.149717	0.472988	0.138917	0.410777	0.144895
b800,r25,g21	0.560224	0.104163	0.587995	0.150989	0.648737	0.137796	0.616275	0.157269	0.618420	0.149158	0.609235	0.129166
b800,r25,g40	0.562055	0.116448	0.570753	0.170507	0.549995	0.144040	0.555572	0.153993	NaN	0.149949	0.512363	0.147342
b800,r25,g61	0.527093	0.133736	0.544757	0.178426	0.501064	0.154881	0.559418	0.148695	0.526932	0.152382	0.510824	0.150760
b800,r3,g21	0.523155	0.120290	0.540552	0.180391	0.502180	0.167122	0.531895	0.147290	0.527640	0.152223	0.446726	0.156758
b800,r3,g40	0.481673	0.151247	0.496592	0.154369	0.478031	0.168461	0.510978	0.179845	0.489072	0.159342	0.477743	0.114978
b800,r3,g61	0.454822	0.123782	0.479302	0.167383	0.466148	0.160684	0.502138	0.186094	0.383061	0.154348	0.419980	0.145913
b1000,r2,g21	0.472948	NaN	0.471706	NaN	0.438387	0.136592	0.502979	0.114415	0.480015	0.139756	0.429018	0.120791
b1000,r2,g40	0.432431	NaN	0.482328	NaN	0.463742	0.140049	NaN	0.128665	0.454574	0.132838	0.379589	0.116623
b1000,r2,g61	0.429014	NaN	0.492068	NaN	0.449339	0.108122	0.447926	0.152940	0.460262	0.134356	0.418321	0.149073
b1000,r25,g21	NaN	0.145632	NaN	0.145950	0.591639	0.146670	0.641650	0.147188	0.667390	0.151980	0.619805	0.140608
b1000,r25,g40	NaN	0.158839	NaN	0.157773	0.527075	0.161731	0.589802	0.156062	0.557366	0.165250	0.573830	0.138575
b1000,r25,g61	NaN	0.125653	NaN	0.152222	0.525366	0.164395	0.555632	0.159845	0.559646	0.168556	0.497095	0.154438
b1000,r3,g21	0.474404	0.125372	0.554634	0.119575	0.476569	0.158635	0.539355	0.153242	0.522236	0.153217	0.486471	0.130497
b1000,r3,g40	0.469239	0.142955	0.491844	0.169372	0.485789	0.175394	0.502404	NaN	0.492130	0.163134	0.458715	0.134984
b1000,r3,g61	0.475403	0.144063	0.498939	0.164943	0.443911	0.170470	0.496284	0.182169	0.471061	0.165189	0.443513	0.130796
b1300,r2,g21	0.472936	NaN	NaN	0.131553	0.467525	0.078007	0.664714	0.107403	0.480983	0.128270	0.448564	0.111763
b1300,r2,g40	0.458512	0.124931	0.464301	0.147385	0.455941	0.128694	0.482353	0.108998	0.459213	0.116528	0.409544	0.130521
b1300,r2,g61	0.427370	0.141285	0.473043	0.140573	0.478479	0.113148	0.472669	0.144067	0.435877	0.140223	0.394969	0.133189
b1300,r25,g21	NaN	0.155525	0.615514	0.147794	0.657780	0.139751	0.611108	0.156585	0.625501	0.136911	0.620092	0.118631
b1300,r25,g40	0.575802	0.140074	0.573401	0.147525	0.532326	0.150608	0.589920	0.171741	0.601552	0.232125	0.551008	0.150651
b1300,r25,g61	0.559193	0.160309	0.570839	0.155649	0.510872	0.153350	0.548901	0.166209	0.554167	0.147884	0.520914	0.167680
b1300,r3,g21	0.483005	0.159197	0.495171	NaN	0.498349	0.144353	0.501068	0.142475	0.520964	0.168630	0.523151	0.106612
b1300,r3,g40	0.471903	0.142318	0.497868	0.152224	0.462064	0.145483	0.503770	0.170236	0.350729	0.142852	0.467155	0.159845
b1300,r3,g61	0.442356	0.153753	0.465023	0.167453	0.460446	0.155320	0.490584	0.177393	0.493659	0.148062	0.442695	0.157730

Tabla C.2: FA profiles mean and std. dev. values, for Streamline Tractography, Corpus Callosum

	P1		P2		P3		P4		P5		P6	
	Mean	Std	Mean	Std	Mean	Std	Mean	Std	Mean	Std	Mean	Std
b800,r2,g21	0.598023	0.054506	0.569530	0.067855	0.624955	0.060097	0.642690	0.091553	0.558134	0.073016	0.557867	0.073099
b800,r2,g40	0.553894	0.089512	0.540887	0.072469	0.593563	0.055736	0.583075	0.081952	0.456699	0.066621	0.505492	0.060643
b800,r2,g61	0.537487	0.049646	0.497353	0.072641	0.571199	0.060856	0.578375	0.071828	0.475325	0.080330	0.487293	0.051957
b800,r25,g21	0.479732	0.099341	0.507518	0.063046	0.528935	0.065730	NaN	NaN	NaN	NaN	NaN	NaN
b800,r25,g40	0.505067	0.061173	0.507601	0.075881	0.527864	0.068548	NaN	NaN	NaN	NaN	NaN	NaN
b800,r25,g61	0.491495	0.078554	0.492008	0.077453	0.515420	0.063706	NaN	NaN	NaN	NaN	NaN	NaN
b800,r3,g21	0.474145	0.056453	0.485158	0.055614	0.516549	0.069390	0.525081	0.072116	0.437285	0.045498	0.388468	0.049203
b800,r3,g40	0.460023	0.061627	0.471640	0.092347	0.478043	0.073961	0.510297	0.085966	0.433375	0.048638	0.393491	0.052265
b800,r3,g61	0.459373	0.065317	0.459988	0.089709	0.492913	0.068498	0.527290	0.077383	0.421769	0.055243	0.378262	0.041376
b1000,r2,g21	0.463383	0.076231	0.507155	0.117992	0.587455	0.061755	0.601446	0.091647	0.587088	0.107235	0.555039	0.066457
b1000,r2,g40	0.489880	0.166898	0.473075	0.085691	0.549193	0.077476	0.560019	0.067034	0.537049	0.104085	0.518781	0.057560
b1000,r2,g61	0.460481	0.070505	0.463723	0.099786	0.536545	0.052002	0.580992	0.069816	0.493322	0.085360	0.492653	0.050578
b1000,r25,g21	0.508683	0.067565	0.481120	0.067070	0.521517	0.070962	NaN	NaN	NaN	NaN	NaN	NaN
b1000,r25,g40	0.504186	0.065497	0.499770	0.074424	0.527824	0.064665	NaN	NaN	NaN	NaN	NaN	NaN
b1000,r25,g61	0.494382	0.052440	0.473029	0.080563	0.529881	0.070278	NaN	NaN	NaN	NaN	NaN	NaN
b1000,r3,g21	0.435784	0.043407	0.463790	0.066792	0.509463	0.081083	0.518620	0.093038	0.441530	0.062660	0.415687	0.043219
b1000,r3,g40	0.421467	0.088113	0.439779	0.061971	0.492013	0.082327	0.521300	0.085660	0.418880	0.066309	0.403554	0.038896
b1000,r3,g61	0.398788	0.053279	0.433783	0.064880	0.496169	0.069661	0.497558	0.104095	0.439979	0.073528	0.389795	0.060122
b1300,r2,g21	0.524057	0.086487	0.551895	0.064497	0.590343	0.058065	0.546630	0.100420	0.518815	0.088128	0.535849	0.050081
b1300,r2,g40	0.499977	0.079168	0.516100	0.059345	0.536401	0.062157	0.533435	0.095305	0.519477	0.093879	0.480851	0.045413
b1300,r2,g61	0.514968	0.064036	0.503247	0.060961	0.520487	0.072334	0.525387	0.094904	0.467466	0.111362	0.451791	0.058110
b1300,r25,g21	0.528632	0.053400	0.483007	0.094646	0.536020	0.079262	NaN	NaN	NaN	NaN	NaN	NaN
b1300,r25,g40	0.506574	0.064721	0.465709	0.062327	0.519958	0.078119	NaN	NaN	NaN	NaN	NaN	NaN
b1300,r25,g61	0.493483	0.048117	0.450425	0.079414	0.515429	0.073287	NaN	NaN	NaN	NaN	NaN	NaN
b1300,r3,g21	0.452879	0.061326	0.470033	0.058814	0.510811	0.071250	0.506224	0.100942	0.451063	0.067651	0.399011	0.057060
b1300,r3,g40	0.434151	0.061394	0.452396	0.072724	0.489564	0.060702	0.494261	0.079612	0.400694	0.056108	0.407209	0.058139
b1300,r3,g61	0.436216	0.057997	0.456945	0.055010	0.484779	0.075065	0.500321	0.097344	0.374899	0.068464	0.412504	0.055363

Tabla C.3: FA profiles mean and std. dev. values, for Global Tractography, Left Cingulum

	P1		P2		P3		P4		P5		P6	
	Mean	Std	Mean	Std	Mean	Std	Mean	Std	Mean	Std	Mean	Std
b800,r2,g21	0.400860	0.000000	0.579522	0.070103	0.625511	0.041479	0.691520	0.071746	0.729951	0.090519	0.526280	0.071480
b800,r2,g40	0.631334	0.151200	0.548438	0.061907	0.583797	0.049989	0.612224	0.033887	0.565827	0.073401	0.517948	0.091699
b800,r2,g61	0.427014	0.101765	0.520935	0.061853	0.574018	0.057915	0.619827	0.048232	0.644789	0.088147	0.521691	0.095632
b800,r25,g21	0.576081	0.047499	0.553635	0.062878	0.576060	0.084472	NaN	NaN	NaN	NaN	NaN	NaN
b800,r25,g40	0.554908	0.054155	0.522959	0.119504	0.562858	0.081496	NaN	NaN	NaN	NaN	NaN	NaN
b800,r25,g61	0.548235	0.044130	0.492002	0.107476	0.521677	0.077918	NaN	NaN	NaN	NaN	NaN	NaN
b800,r3,g21	0.547983	0.040774	0.466201	0.071269	0.538291	0.098921	0.575271	0.082673	0.457544	0.036808	0.409064	0.024334
b800,r3,g40	0.527754	0.033289	0.466999	0.081490	0.505045	0.090849	0.538732	0.092440	0.455005	0.052788	0.391684	0.059353
b800,r3,g61	0.527021	0.039374	0.449588	0.082145	0.518320	0.112407	0.540681	0.096847	0.444355	0.061356	0.412538	0.038872
b1000,r2,g21	NaN	NaN	NaN	NaN	0.558748	0.054689	0.702507	0.047259	0.577615	0.050605	0.621991	0.045143
b1000,r2,g40	NaN	NaN	NaN	NaN	0.534711	0.033319	0.614962	0.054435	0.565681	0.062884	0.534899	0.043088
b1000,r2,g61	NaN	NaN	0.435891	0.006752	0.508602	0.039219	0.622770	0.047460	0.528668	0.088455	0.526884	0.054271
b1000,r25,g21	0.588230	0.028574	0.549854	0.061471	0.583541	0.070649	NaN	NaN	NaN	NaN	NaN	NaN
b1000,r25,g40	0.568055	0.067150	0.519387	0.083214	0.574280	0.080859	NaN	NaN	NaN	NaN	NaN	NaN
b1000,r25,g61	0.568494	0.046446	0.482528	0.088540	0.558088	0.069244	NaN	NaN	NaN	NaN	NaN	NaN
b1000,r3,g21	0.464435	0.023345	0.478040	0.069459	0.489123	0.100545	0.524743	0.111018	0.470572	0.055767	0.423168	0.039369
b1000,r3,g40	0.443185	0.044849	0.460083	0.075875	0.471839	0.106643	0.554981	0.092283	0.469131	0.089536	0.414834	0.059146
b1000,r3,g61	0.454367	0.022029	0.424641	0.076653	0.479091	0.095379	0.505762	0.117761	0.456094	0.083697	0.424190	0.053879
b1300,r2,g21	NaN	NaN	0.549541	0.048794	0.549722	0.035892	0.572394	0.091216	NaN	NaN	0.452953	0.047932
b1300,r2,g40	NaN	NaN	0.544972	0.034961	0.522935	0.068963	0.581595	0.043589	0.675211	0.036228	0.478764	0.110112
b1300,r2,g61	NaN	NaN	0.488229	0.070277	0.514581	0.066410	0.644804	0.119804	0.721639	0.032609	0.505604	0.076939
b1300,r25,g21	0.544174	0.059792	0.547455	0.055422	0.584315	0.098906	NaN	NaN	NaN	NaN	NaN	NaN
b1300,r25,g40	0.572668	0.046503	0.512419	0.064790	0.561376	0.094635	NaN	NaN	NaN	NaN	NaN	NaN
b1300,r25,g61	0.571230	0.043434	0.523792	0.058104	0.534842	0.105591	NaN	NaN	NaN	NaN	NaN	NaN
b1300,r3,g21	0.364078	0.018178	0.444979	0.071447	0.581537	0.070104	0.546672	0.101666	0.452609	0.054765	0.418155	0.059858
b1300,r3,g40	0.469504	0.059920	0.484601	0.067202	0.535585	0.119152	0.517875	0.098336	0.393216	0.069257	0.429135	0.044697
b1300,r3,g61	0.411293	0.093716	0.462157	0.072858	0.537061	0.119675	0.521021	0.102297	0.346951	0.062161	0.433372	0.041252

Tabla C.4: FA profiles mean and std. dev. values, for Streamline Tractography, Left Cingulum

	P1		P2		P3		P4		P5		P6	
	Mean	Std	Mean	Std	Mean	Std	Mean	Std	Mean	Std	Mean	Std
b800,r2,g21	0.597507	0.090452	0.611494	0.106059	0.603688	0.086335	0.674423	0.065154	0.580444	0.078513	0.593819	0.069062
b800,r2,g40	0.553031	0.090410	0.574791	0.113155	0.558451	0.082665	0.645502	0.067312	0.554525	0.087156	0.561056	0.072589
b800,r2,g61	0.545346	0.091288	0.565079	0.102039	0.543079	0.083315	0.634937	0.078105	0.546777	0.079824	0.543296	0.070752
b800,r25,g21	NaN	NaN	NaN	NaN	NaN	NaN	NaN	NaN	NaN	NaN	NaN	NaN
b800,r25,g40	NaN	NaN	NaN	NaN	NaN	NaN	NaN	NaN	NaN	NaN	NaN	NaN
b800,r25,g61	NaN	NaN	NaN	NaN	NaN	NaN	NaN	NaN	NaN	NaN	NaN	NaN
b800,r3,g21	0.490701	0.078521	0.599776	0.085414	0.540320	0.097138	0.562111	0.074456	0.498782	0.060118	0.398278	0.073276
b800,r3,g40	0.467119	0.063742	0.564865	0.083814	0.526296	0.098596	0.558973	0.079571	0.487984	0.061833	0.423087	0.043424
b800,r3,g61	0.479472	0.061630	0.543685	0.064136	0.515756	0.107441	0.572031	0.078791	0.460172	0.046807	0.412275	0.049255
b1000,r2,g21	0.501304	0.070395	0.504903	0.095576	0.635870	0.066035	0.644026	0.075525	0.577837	0.068125	0.577371	0.076033
b1000,r2,g40	0.470634	0.054914	0.517644	0.113075	0.591854	0.087413	0.610276	0.073631	0.520673	0.076913	0.556012	0.069711
b1000,r2,g61	0.430383	0.074844	0.468148	0.090196	0.590548	0.056305	0.611693	0.065936	0.523057	0.071106	0.549992	0.072357
b1000,r25,g21	NaN	NaN	NaN	NaN	NaN	NaN	NaN	NaN	NaN	NaN	NaN	NaN
b1000,r25,g40	NaN	NaN	NaN	NaN	NaN	NaN	NaN	NaN	NaN	NaN	NaN	NaN
b1000,r25,g61	NaN	NaN	NaN	NaN	NaN	NaN	NaN	NaN	NaN	NaN	NaN	NaN
b1000,r3,g21	0.480333	0.063786	0.519196	0.077283	0.530139	0.115350	0.552013	0.080727	0.483789	0.085255	0.433289	0.068907
b1000,r3,g40	0.477707	0.079918	0.564726	0.102382	0.530479	0.111852	0.551342	0.075341	0.465987	0.072763	0.419460	0.035775
b1000,r3,g61	0.459772	0.063395	0.523554	0.095229	0.524799	0.111746	0.542886	0.074244	0.473690	0.071220	0.415616	0.056221
b1300,r2,g21	0.526695	0.092777	0.570238	0.106831	0.593604	0.066312	0.581363	0.072323	0.559621	0.117941	0.534844	0.076265
b1300,r2,g40	0.494467	0.094870	0.570664	0.096445	0.564193	0.068079	0.557696	0.081215	0.512121	0.080952	0.540190	0.073837
b1300,r2,g61	0.494062	0.099842	0.552334	0.110270	0.557852	0.062506	0.544172	0.081033	0.503495	0.092993	0.519615	0.068176
b1300,r25,g21	NaN	NaN	NaN	NaN	NaN	NaN	NaN	NaN	NaN	NaN	NaN	NaN
b1300,r25,g40	NaN	NaN	NaN	NaN	NaN	NaN	NaN	NaN	NaN	NaN	NaN	NaN
b1300,r25,g61	NaN	NaN	NaN	NaN	NaN	NaN	NaN	NaN	NaN	NaN	NaN	NaN
b1300,r3,g21	0.466904	0.072628	0.588421	0.086568	0.531749	0.090944	0.531789	0.079026	0.493827	0.062951	0.425187	0.054985
b1300,r3,g40	0.455885	0.077513	0.557726	0.109546	0.525948	0.088190	0.529584	0.079680	0.501140	0.054508	0.427224	0.064822
b1300,r3,g61	0.465091	0.068796	0.540250	0.094209	0.528501	0.087339	0.525034	0.084499	0.460737	0.062131	0.414072	0.051635

Tabla C.5: FA profiles mean and std. dev. values, for Global Tractography, Right Cingulum

	P1		P2		P3		P4		P5		P6	
	Mean	Std	Mean	Std	Mean	Std	Mean	Std	Mean	Std	Mean	Std
b800,r2,g21	0.638618	0.056812	0.566461	0.083917	0.515846	0.107390	0.634192	0.039003	0.549188	0.031345	0.616833	0.057389
b800,r2,g40	0.618116	0.054528	0.618010	0.070493	0.528650	0.129340	0.624401	0.046471	0.531898	0.047039	0.568288	0.087992
b800,r2,g61	0.593036	0.083032	0.552300	0.093234	0.498591	0.131810	0.556890	0.063234	0.582193	0.000000	0.528238	0.078363
b800,r25,g21	NaN	NaN	NaN	NaN	NaN	NaN	NaN	NaN	NaN	NaN	NaN	NaN
b800,r25,g40	NaN	NaN	NaN	NaN	NaN	NaN	NaN	NaN	NaN	NaN	NaN	NaN
b800,r25,g61	NaN	NaN	NaN	NaN	NaN	NaN	NaN	NaN	NaN	NaN	NaN	NaN
b800,r3,g21	0.388231	0.078507	0.514667	0.082160	0.561721	0.132249	0.564369	0.085293	0.465218	0.085843	0.345517	0.070838
b800,r3,g40	0.371404	0.101907	0.550128	0.059037	0.516191	0.136196	0.545406	0.089005	0.455956	0.080682	0.458445	0.052917
b800,r3,g61	0.383557	0.096194	0.530819	0.080144	0.521118	0.135944	0.542194	0.087754	0.434380	0.074021	0.419387	0.076089
b1000,r2,g21	NaN	NaN	NaN	NaN	0.629252	0.054741	0.616823	0.010067	0.615985	0.000000	0.564614	0.073221
b1000,r2,g40	NaN	NaN	NaN	NaN	0.588577	0.090631	0.621522	0.013377	0.563108	0.024049	0.519921	0.075261
b1000,r2,g61	NaN	NaN	NaN	NaN	0.567486	0.080012	0.662482	0.084941	0.537266	0.034769	0.495692	0.077373
b1000,r25,g21	NaN	NaN	NaN	NaN	NaN	NaN	NaN	NaN	NaN	NaN	NaN	NaN
b1000,r25,g40	NaN	NaN	NaN	NaN	NaN	NaN	NaN	NaN	NaN	NaN	NaN	NaN
b1000,r25,g61	NaN	NaN	NaN	NaN	NaN	NaN	NaN	NaN	NaN	NaN	NaN	NaN
b1000,r3,g21	0.454155	0.048107	0.592175	0.049373	0.517878	0.143165	0.534771	0.080384	0.487066	0.061726	0.454073	0.081055
b1000,r3,g40	0.432083	0.075042	0.552281	0.103381	0.510938	0.132159	0.543332	0.096725	0.453997	0.100459	0.441903	0.106593
b1000,r3,g61	0.439955	0.065726	0.548546	0.089423	0.489936	0.148804	0.538956	0.092978	0.451840	0.096730	0.399404	0.119555
b1300,r2,g21	NaN	NaN	0.385046	0.000000	0.619074	0.077758	0.465601	0.047947	NaN	NaN	0.584317	0.076035
b1300,r2,g40	NaN	NaN	0.503944	0.058772	0.571572	0.097727	0.606464	0.037474	0.375551	0.040868	0.482862	0.110501
b1300,r2,g61	0.556460	0.031908	0.397400	0.059542	0.552273	0.098868	0.573475	0.044981	0.373026	0.056245	0.502076	0.081794
b1300,r25,g21	NaN	NaN	NaN	NaN	NaN	NaN	NaN	NaN	NaN	NaN	NaN	NaN
b1300,r25,g40	NaN	NaN	NaN	NaN	NaN	NaN	NaN	NaN	NaN	NaN	NaN	NaN
b1300,r25,g61	NaN	NaN	NaN	NaN	NaN	NaN	NaN	NaN	NaN	NaN	NaN	NaN
b1300,r3,g21	0.485907	0.093653	0.554725	0.080317	0.577313	0.087881	0.559685	0.079828	0.513633	0.051449	0.497706	0.090544
b1300,r3,g40	0.436781	0.106065	0.523922	0.085986	0.533075	0.108524	0.552249	0.096330	0.465352	0.089596	0.469892	0.039450
b1300,r3,g61	0.460724	0.113616	0.526996	0.098646	0.548218	0.094212	0.547593	0.080461	0.415420	0.087804	0.479766	0.073789

Tabla C.6: FA profiles mean and std. dev. values, for Streamline Tractography, Right Cingulum